



Mobility & Vehicle Mechanics

*International Journal for Vehicle Mechanics, Engines and
Transportation Systems*

ISSN 1450 - 5304

UDC 621 + 629(05)=802.0

Pál Hansággy Ferenc Palásti Péter Gerse Balázs Ádám László Tóth	UV AGING EXAMINATION OF WINDSHIELD HOLDER RUBBER	1-10
Miroslav Demić Mikhail P. Malinovsky	INVESTIGATION OF TORSIONAL VIBRATIONS OF THE STEERING SHAFT FROM THE ASPECT OF MINIMAL DRIVER-HAND FATIGUE IN HEAVY MOTOR VEHICLES	11-22
Isak Karabegović Ermin Husak Edina Karabegović Mehmed Mahmić	DEVELOPMENT AND IMPLEMENTATION OF ADVANCED ROBOTICS IN THE AUTOMOTIVE AND ELECTRO-ELECTRONIC INDUSTRY OF CHINA	23-36
Vasko Changoski Igor Gjurkov Vase Janushevska	HANDLING AND STABILITY ANALYSIS OF AN AUTOMATED VEHICLE WITH INTEGRATED FOUR-WHEEL INDEPENDENT STEERING (4WIS)	37-60
Miloš Maljković Ivan Blagojević Branko Miličić Dragan Stamenković	TOWARDS AN ENERGY EFFICIENT OPERATION OF A SUPERCAPACITOR ELECTRIC BUS	61-75



M V M

Mobility Vehicle Mechanics

Editor: Prof. dr Jovanka Lukić

MVM Editorial Board
University of Kragujevac
Faculty of Engineering
Sestre Janjić 6, 34000 Kragujevac, Serbia
Tel.: +381/34/335990; Fax: + 381/34/333192

Prof. Dr **Belingardi Giovanni**
Politecnico di Torino,
Torino, ITALY

Dr Ing. **Ćučuz Stojan**
Visteon corporation,
Novi Jicin,
CZECH REPUBLIC

Prof. Dr **Demić Miroslav**
University of Kragujevac
Faculty of Engineering
Kragujevac, SERBIA

Prof. Dr **Fiala Ernest**
Wien, OESTERREICH

Prof. Dr **Gillespie D. Thomas**
University of Michigan,
Ann Arbor, Michigan, USA

Prof. Dr **Glišović Jasna**
University of Kragujevac
Faculty of Engineering
Kragujevac, SERBIA

Prof. Dr **Knapezyk Josef**
Politechniki Krakowskiej,
Krakow, POLAND

Prof. Dr **Krstić Božidar**
University of Kragujevac
Faculty of Engineering
Kragujevac, SERBIA

Prof. Dr **Mariotti G. Virzi**
Universita degli Studidi Palermo,
Dipartimento di Meccanica ed
Aeronautica,
Palermo, ITALY

Prof. Dr **Miloradović Danijela**
University of Kragujevac
Faculty of Engineering
Kragujevac, SERBIA

Prof. Dr **Pešić Radivoje**
University of Kragujevac
Faculty of Engineering
Kragujevac, SERBIA

Prof. Dr **Petković Snežana**
University of Banja Luka
Faculty of Mech. Eng.
Banja Luka
REPUBLIC OF SRPSKA

Prof. Dr **Radonjić Rajko**
University of Kragujevac
Faculty of Engineering
Kragujevac, SERBIA

Prof. Dr **Spentzas Constantinos**
N. National Technical University,
GREECE

Prof. Dr **Todorović Jovan**
Faculty of Mech. Eng. Belgrade,
SERBIA

Prof. Dr **Toliskyj Vladimir E.**
Academician NAMI,
Moscow, RUSSIA

Prof. Dr **Teodorović Dušan**
Faculty of Traffic and Transport
Engineering,
Belgrade, SERBIA

Prof. Dr **Veinović Stevan**
University of Kragujevac
Faculty of Engineering
Kragujevac, SERBIA

For Publisher: Prof. dr Slobodan Savić, dean, University of Kragujevac, Faculty of Engineering

*Publishing of this Journal is financially supported from:
Ministry of Education, Science and Technological Development, Republic Serbia*

Mobility &

Motorna

Vehicle

Volume 50
Number 2
2024.

Vozila i

Mechanics

Motori

Pál Hansághy
Ferenc Palásti
Péter Gerse
Balázs Ádám
László Tóth

UV AGING EXAMINATION OF
WINDSHIELD HOLDER RUBBER

1-10

Miroslav Demić
Mikhail P. Malinovsky

INVESTIGATION OF TORSIONAL
VIBRATIONS OF THE STEERING
SHAFT FROM THE ASPECT OF
MINIMAL DRIVER-HAND FATIGUE IN
HEAVY MOTOR VEHICLES

11-22

Isak Karabegović
Ermin Husak
Edina Karabegović
Mehmed Mahmić

DEVELOPMENT AND
IMPLEMENTATION OF ADVANCED
ROBOTICS IN THE AUTOMOTIVE AND
ELECTRO-ELECTRONIC INDUSTRY OF
CHINA

23-36

Vasko Changoski
Igor Gjurkov
Vase Janushevska

HANDLING AND STABILITY ANALYSIS
OF AN AUTOMATED VEHICLE WITH
INTEGRATED FOUR-WHEEL
INDEPENDENT STEERING (4WIS)

37-60

Miloš Maljković
Ivan Blagojević
Branko Miličić
Dragan Stamenković

TOWARDS AN ENERGY EFFICIENT
OPERATION OF A SUPERCAPACITOR
ELECTRIC BUS

61-75

Mobility &

Vehicle

Mechanics

Motorna

Vozila i

Motori

Volume 50
Number 2
2024.

Pál Hansághy Ferenc Palásti Péter Gerse Balázs Ádám László Tóth	ISTRAŽIVANJE STARENJA GUME DRŽAČA VETROBRANSKOG STAKLA ZBOG UV ZRAČENJA	1-10
Miroslav Demić Mikhail P. Malinovsky	PRILOG ISTRAŽIVANJU TORZIONIH VIBRACIJA OSOVINE UPRAVLJAČA SA ASPEKTA MINIMALNOG ZAMORA RUKU VOZAČA TERETNIH MOTORNIH VOZILA	11-22
Isak Karabegović Ermin Husak Edina Karabegović Mehmed Mahmić	RAZVOJ I IMPLEMENTACIJA NAPREDNE ROBOTIKE U AUTOMOBILSKOJ I ELEKTRO- ELEKTRONSKOJ INDUSTRIJI KIN	23-36
Vasko Changoski Igor Gjurkov Vase Janushevska	ANALIZA UPRAVLJANJA I STABILNOSTI AUTOMATIZOVANOG VOZILA SA INTEGRISANIM NEZAVISNIM UPRAVLJANJEM NA SVA ČETIRI TOČKA (4WIS)	37-60
Miloš Maljković Ivan Blagojević Branko Miličić Dragan Stamenković	KA ENERGETSKI EFIKASNOM RADU SUPERKONDENZATORISKOG ELEKTRIČNOG AUTOBUSA	61-75



UV AGING EXAMINATION OF WINDSHIELD HOLDER RUBBER

Pál Hansághy^{1*}, Ferenc Palásti², Péter Gerse³, Balázs Ádám⁴, László Tóth⁵

Received in August 2024

Accepted in October 2024

RESEARCH ARTICLE

ABSTRACT: The aim of this research is to examine the UV aging properties of windshield holder rubber materials used in public transportation vehicles, with a particular focus on the structural changes induced by UV light and their effects on mechanical properties. During the research, various rubber compounds were prepared, and their mechanical properties were measured in both fresh and UV-aged terms. The mechanical tests included measurements of tensile strength, elongation at break, modulus at 100% elongation (M100), and Shore A hardness. Based on the results, it was determined that UV aging significantly impacts the mechanical properties of the rubbers. UV exposure leads to a decrease in tensile strength and elongation at break, while the Shore A hardness increases. These changes can be attributed to free radical formation and the modification of polymer cross-links within the material structure. Comparison of different compounds revealed that some rubber blends exhibit better resistance to UV-induced aging, thereby possessing a longer lifespan. These findings contribute to the development and manufacture of sunlight-resistant rubber products and are beneficial for professionals working in rubber manufacturing and material testing. In summary, UV aging studies help to better understand the long-term behavior of windshield holder rubbers and provide opportunities for optimizing products against the effects of UV light.

© 2024 Published by University of Kragujevac, Faculty of Engineering

KEY WORDS: *UV aging, Windshield holder rubber, Mechanical properties, Rubber compounds, Public transportation vehicles*

¹Pál Hansághy, Department of Innovative Vehicles and Materials, GAMF Faculty of Engineering and Computer Science, John von Neumann University, H-6000 Kecskemét, Hungary, hansaghy.pal@nje.hu, 

²Ferenc Palásti, Department of Innovative Vehicles and Materials, GAMF Faculty of Engineering and Computer Science, John von Neumann University, H-6000 Kecskemét, Hungary, palasti.ferenc@nje.hu, 

³Péter Gerse, Department of Innovative Vehicles and Materials, GAMF Faculty of Engineering and Computer Science, John von Neumann University, H-6000 Kecskemét, Hungary, gerse.peter@nje.hu, 

⁴Balázs Ádám, Department of Innovative Vehicles and Materials, GAMF Faculty of Engineering and Computer Science, John von Neumann University, H-6000 Kecskemét, Hungary, adam.balazs@nje.hu, 

⁵László Tóth PhD, Department of Innovative Vehicles and Materials, GAMF Faculty of Engineering and Computer Science, John von Neumann University, H-6000 Kecskemét, Hungary, toth.laszlo@nje.hu, ; * Corresponding author

ISTRAŽIVANJE STARENJA GUME DRŽAČA VETROBRANSKOG STAKLA ZBOG UV ZRAČENJA

REZIME: Cilj ovog istraživanja je da se ispituju karakteristike gumenih materijala za držače vetrobrana koji se koriste u vozilima javnog prevoza, sa posebnim fokusom na strukturne promene izazvane starenjem usled UV zračenja i njihov uticaj na mehanička svojstva. Tokom istraživanja pripremljena su različita jedinjenja gume i merena su im mehanička svojstva kako nove tako i ostarele gume usled UV zračenja. Mehanička ispitivanja su obuhvatila merenja: zatezne čvrstoće, izduženja pri lomu, modula elastičnosti pri 100% izduženju (M100) i tvrdoće po Šoru A. Na osnovu rezultata utvrđeno je da starenje izazvano UV zračenjem značajno utiče na mehanička svojstva gume. Izlaganje UV zračenju dovodi do smanjenja zatezne čvrstoće i izduženja pri prekidu, dok se tvrdoća po Šoru A povećava. Ove promene se mogu pripisati formiranju slobodnih radikala i modifikaciji polimernih poprečnih veza unutar strukture materijala. Poređenje različitih jedinjenja otkrilo je da neke mešavine gumene pokazuju bolju otpornost na starenje izazvano UV zračenjem, čime imaju duži životni vek. Ova otkrića doprinose razvoju i proizvodnji gumenih proizvoda otpornih na sunčevu svetlost i korisna su za profesionalce koji rade u proizvodnji gume i ispitivanju materijala. Ukratko, studije starenja zbog UV zračenja pomažu da se bolje razume dugoročno ponašanje gume za držače vetrobrana i pružaju mogućnosti za optimizaciju proizvoda koji sprečavaju staranje usled UV zračenja.

KLJUČNE REČI: *starenje usled UV zračenja, guma za držač vetrobrana, mehaničke karakteristike, mešavina gume, vozila javnog prevoza*

UV AGING EXAMINATION OF WINDSHIELD HOLDER RUBBER

Pál Hansággy, Ferenc Palásti, Péter Gerse, Balázs Ádám, László Tóth

INTRODUCTION

The Ethylene propylene diene monomer rubber (EPDM) is composed of ethylene and propylene monomers, with a small percentage of a diene monomer incorporated into the polymer, retaining one of its double bonds even after polymerization. Since EPDM rubbers contain three monomers, they carry the favorable properties of all three materials. Polyethylene is suitable for producing elastomers with low internal friction, but it is highly crystalline due to its regular structure. This regularity can be disrupted by the presence of methyl groups from the polypropylene chain, which face outward. This is typically achieved with a propylene content of 30-40% by weight, though other proportions can also be used. For sulfur vulcanization to be at least partially feasible, the role of the double bond from the diene monomer is crucial. Despite this, vulcanization is predominantly performed with peroxides, following a radical mechanism that does not require the presence of double bonds. Nevertheless, since EPDM rubbers contain double bonds, traditional sulfur vulcanization is also possible.[1]

In the production of EPDM rubber, the ethylene, propylene, and difunctional monomer are most often polymerized using solution polymerization in aliphatic hydrocarbons (typically pentane or hexane) with a Ziegler-Natta catalyst composed of vanadium chloride and alkyl-aluminum. After the polymerization process, the difunctional monomer groups present in small percentages are randomly and statistically distributed throughout the polymer.[1]

The most important advantage of EPDM rubber is its chemical resistance, which is due to the predominance of strong carbon-carbon and carbon-hydrogen sigma bonds, requiring high energy to break. As a result, EPDM rubbers exhibit excellent resistance to chemicals, heat, light, and ozone, and their highly non-polar nature ensures exceptional water resistance. On the other hand, this non-polarity also means that EPDM rubbers have weak resistance to organic solvents, and their mechanical properties are inferior to those of NR rubbers due to the lack of polysulfide bridges in peroxide vulcanization. Additionally, unlike CR rubbers, EPDM rubbers are not flame-resistant and cannot be used in fire-hazardous environments.[1]

When using vulcanizates made from EPDM rubber, we primarily take advantage of their resistance to ozone, chemicals, heat, and light. This makes them ideal for use in the automotive industry, for example, in windshield wipers and bumpers, as well as in the cable industry due to their good insulating properties. They are also widely used as raw materials for compensators, pipes, and other insulating materials.[1]

The most important application of EPDM rubbers is in the production of sealing materials, especially for securing windows in buses, trains, and passenger vehicles. In this application, the vulcanizate must withstand both high and low temperatures, as well as UV light from the sun and the resulting ozone concentration in the atmosphere. EPDM rubbers are excellently suited for manufacturing such materials, offering significantly longer lifespans than similar products made from other types of rubber.[2]

1 PHYSICAL TESTING METHODS FOR VULCANIZATES

Rubber is often described as a "black box" by rubber industry professionals, as identifying root causes after a failed production process is not an easy task. The challenge lies in the

difficulty, or rather impossibility, of measuring the molecular structure of cross-linked rubber. This is because the cross-linked molecule cannot be dissolved (liquid chromatography methods are not applicable), and it does not possess a regular crystalline structure (X-ray diffraction methods are also ruled out). Nevertheless, the process of vulcanizing rubber compounds, as well as the physical testing of fully vulcanized rubber, can provide valuable insights. When performed correctly, these tests offer significant information about the quality of the finished products and any changes in their properties. In this chapter, we will focus on these physical testing methods.[1]

1.1 Tensile Test

One of the most important physical tests in the rubber industry is the tensile strength test. In this test, after cutting the appropriate test specimen (usually a dumbbell-shaped form, but it can also be a ring-shaped one) from a vulcanized sheet, the ends of the specimen are fixed in the grips of a load cell. The lower grip remains stationary, while the upper one moves at a constant speed, stretching the specimen longitudinally. As a result, the specimen elongates and eventually breaks. The modulus required for breaking is called the tensile strength, usually expressed in MPa, calculated by dividing the force required to break the specimen (in newtons) by the cross-sectional area at the point of fracture (in mm²). This variable accurately indicates the amount of force or modulus that the vulcanizate can withstand, which simulates the resistance of products made from the vulcanizate to tensile and stretching forces. To achieve high tensile strength, a sufficient amount of additives (e.g., carbon black, silica) must be incorporated, as unfilled vulcanizates typically exhibit very low tensile strength.[1]

In addition to measuring tensile strength, elongation at break can also be determined, which indicates how much the specimen has stretched, as a percentage of its original length, until the point of breakage.[1] Extensometers are required to monitor the distance between the grips, ensuring precise measurement of displacement. Elongation at break provides insight into how much a given vulcanizate can be stretched before it ruptures.[3]

When rubber is stretched, internal stress develops within the material, causing it to break at its weakest point. This rupture occurs due to the inhomogeneous distribution of the material and the formation of weak surfaces, primarily caused by the uneven distribution of compound components and the irregular, statistical nature of the rubber's cross-linked structure. Remarkably, the elongation at break in rubbers can often reach several hundred percent. This is because vulcanized rubber, as a cross-linked polymer, has an extremely high molecular weight, resulting in a wide temperature range for its hyperelastic state. This state is largely characterized by viscoelasticity, which enables part of the force applied to the material to be absorbed and the remainder to be elastically reflected after the material deforms. Consequently, even after significant deformational force, the deformation of the material is partially reversible, allowing the specimen to nearly regain its original shape even after being stretched with considerable force.[1]

Tensile strength testing of rubbers is typically performed according to ISO 37, which accepts both ring-shaped and dumbbell-shaped test specimens. In our case, we used dumbbell-shaped specimens, with a schematic drawing shown in Figure 1. The advantage of the dumbbell shape is that the narrow part of the specimen experiences relatively uniform deformation, leading to reproducible results. According to the standard, the length of the specimen (denoted as part 1 in Figure 1.) should be 20 ± 0.5 mm or 25 ± 0.5 mm, and if these lengths are not possible, a length of 10 ± 0.5 mm can be used, with a thickness of 2.0 ± 0.2 mm. For smaller specimens, a thickness of 1.0 ± 0.1 mm is also acceptable. The test

specimen is typically vulcanized directly from the rubber compound in a laboratory vulcanizing press, where cross-linking occurs according to the formulation at a given temperature and duration.[9] It is essential to wait at least 16 hours after vulcanization before performing the test, as prescribed by ISO 23529, to allow the vulcanizate to relax and reach its final molecular structure at room temperature. To obtain reliable results in accordance with the standard, at least three tests must be conducted.[4]

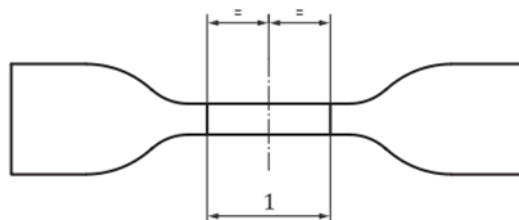


Figure 1. ISO 37 test specimen shape for tensile testing of elastomers – 1. The gauge length of the specimen [5].

Considering that the tensile strength of ebonite, which has a dense sulfur cross-linked structure, significantly exceeds that of soft rubber, it can be stated that the tensile strength of a vulcanizate increases with the increase in cross-link density.[1]

1.2 Hardness Testing

For hardness measurement, both in industry and laboratories, there are various methods available (such as Mohs, Rockwell, Brinell scales, etc.), but in the plastics and rubber industry, Shore hardness is the most widely used, specifically Shore A and Shore D, which operate on a scale from 0 to 100. In Shore hardness testing, a needle is pressed into the specimen, and the depth of penetration determines the Shore hardness. The harder the material, the more it resists the needle, resulting in a higher Shore hardness value.[1] Generally, it is noted that Shore scales are most accurate in the mid-range, while measurements near the extremes (close to 0 or 100) are less reliable (according to the ISO 48-4 standard, below 20 and above 90), and in such cases, switching to another scale is recommended. For the best reproducibility in the plastics and rubber industry, Shore hardness testing is typically conducted in accordance with the ISO 48-4 standard. According to this standard, Shore A and D measurements are usually performed on a solid vulcanized disc with a minimum thickness of 6 mm.[6]

In the rubber industry, Shore A hardness measurement is most commonly performed, using a truncated cone-shaped indenter, meaning the tip of the needle is flat. When testing the hardness of rubber, the Shore A reading should be taken after 3 seconds, as the elastic rubber can continue to deform if more time passes, potentially skewing the results. It is worth noting that 1 unit of Shore hardness corresponds to a spring force of 75 mN.[6]

2 AGING OF RUBBER DUE TO LIGHT EXPOSURE

As is well known, a significant portion of the light coming from the sun falls within the UV range. According to the electromagnetic spectrum of light, the wavelength of UV light (100-380 nm) is shorter than that of visible light (~380-780 nm), which means it carries more energy than visible light. The energy of UV light reaches a level sufficient to break primary chemical bonds, a process also observed in polymers and rubber. As a result, high-energy UV radiation acts as an initiator for various unwanted reactions, leading to the breaking of

carbon-carbon, sulfur-sulfur, and carbon-sulfur bonds. Depending on the composition of the mixture, this can cause the vulcanizate to soften and become sticky, or it may harden and crack, taking on a texture similar to that of elephant skin. Unfortunately, the exact molecular structural changes are difficult to determine because cross-linked polymers cannot be analyzed using classical or instrumental analytical methods. The light resistance of rubber can be significantly improved by adding various additives. One of the best and most commonly used materials for this purpose is carbon black, which has excellent light-absorbing properties. Carbon black absorbs the incoming light and disperses it evenly, reducing the light's intensity and thereby increasing the UV resistance of the compound.[1]

The effect of sunlight can be measured in several ways. One option is to expose the vulcanized test specimen to natural sunlight, but a more efficient and reproducible method is to use UV chambers. In such equipment, the wavelength range and intensity of the applied light can be adjusted, and by increasing the intensity, the exposure time can be shortened. The applied irradiation time can then be converted, using literature data, into an equivalent amount of sunlight exposure, taking into account specific climatic conditions.[1]

2.1 Energy of Solar Radiation

To model the energy and effects of UV light from the sun, we will use UV lamps operating at specific wavelengths and intensities. The energy per square meter (energy density) can be calculated as a function of exposure time. The obtained value can then be compared with data from the literature, using two locations with different geographical characteristics as a reference. In this case, we will consider Hungary (humid continental climate) and Florida in the United States (subtropical climate). According to the literature, one year of solar radiation in Hungary corresponds to an energy density of 2015 kJ/m², while in Florida, it reaches 2800 kJ/m² [7].

2.2 Compounds Used

The manufacturer provided us with four different EPDM rubber-based vulcanizate compositions, the exact formulations of which were not disclosed due to business confidentiality. However, we do know that the EPDM rubber-based compounds are suitable for the production of sealing materials. To differentiate between the formulations, we labeled them as I., II., III., and IV.

2.3 Equipment Used

For the sunlight simulation tests, we utilized UV lamps, exposing rubber test specimens for 0, 400, 800, 1200, and 1600 hours for each compound type. The exposure process was conducted using an ATLAS Material Testing Solutions LLC UV Test device. The chamber temperature was kept constant at 50 °C, with an irradiation intensity of 1.5 W/m². The device was equipped with eight UVA-340 fluorescent tubes, and the wavelength of the irradiation was 340 nm.

For tensile strength tests, we used an Instron 4482 R5900 machine, equipped with a video extensometer. The test specimens were cut in a dumbbell shape according to the ISO 37 standard, with a gauge length of 25 mm for the extensometer. During the test, the crosshead speed was 500 mm/min, and the preloading was conducted with a force of 1 N at 10 mm/min. The grip distance was set to 50 mm. The test was performed under controlled laboratory conditions at a temperature of 23 °C ± 2 °C.

For Shore A hardness measurements, we used a Zwick Shore A hardness tester mounted on a stand.

3 TENSIL TEST RESULT

The measurements were performed after 0, 400, 800, 1200, and 1600 hours of UV exposure, and the data were recorded. During the evaluation, the average of the measurements was considered. Standard deviation values were also taken into account in the assessment of the measurement results. The width of the vulcanized and die-cut test specimens was fixed at 6 mm, while the thickness was measured each time.

Table 1 Tensile test results

Sample	UV	Modulus M100 [MPa]	Tensile stress at Maximum Load [MPa]	Tensile strain [%]
	[h]			
I.	0	3.8	10.7	329
	400	4.4	10.9	283
	800	4.6	10.8	266
	1200	4.4	10.1	258
	1600	4.8	10.2	239
II.	0	3.0	8.0	310
	400	3.2	8.1	302
	800	3.3	8.1	295
	1200	3.5	8.4	294
	1600	3.5	8.0	267
III.	0	7.3	12.0	199
	400	7.8	11.6	173
	800	8.7	11.6	150
	1200	7.8	10.8	155
	1600	8.5	10.7	136
IV.	0	6.2	7.4	127
	400	7.0	8.3	124
	800	6.6	7.6	121
	1200	6.7	7.8	120
	1600	7.3	8.0	114

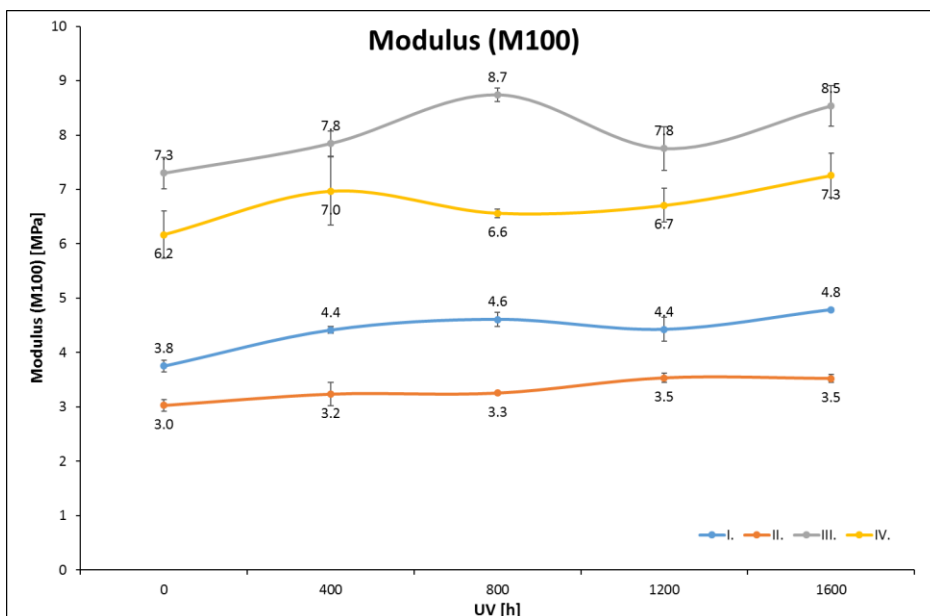


Figure 2. Modulus (M100)

In the case of the modulus, we observed an increasing trend for all samples as a result of aging. The largest percentage difference between the averages was found in Sample I, with an increase of 27.5%, while Samples II, III, and IV showed increases of 16-17%.

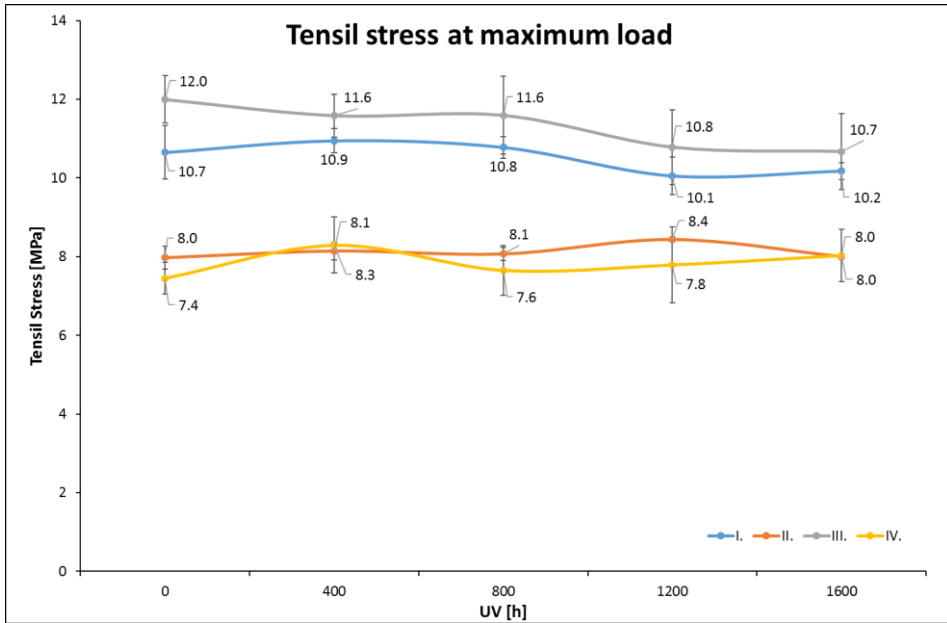


Figure 3 Tensile stress at maximum load

When examining the average values of the tensile stress corresponding to the maximum force, considering the standard deviation, no clear difference or trend can be identified.

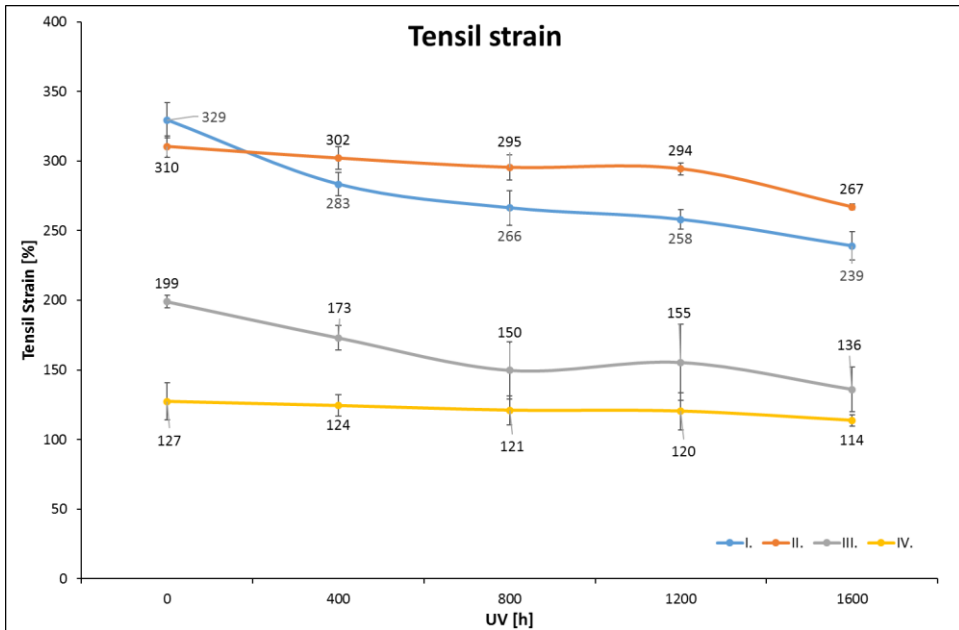


Figure 4. Tensile strain

The elongation at break values show a decreasing trend, with Sample I exhibiting a 27% decrease and Sample III a 32% decrease. For Samples IV and II, the decreases were 11% and 14%, respectively.

Table 2 Shore A

Sample	UV [h]	Shore A	
		Value	Standard deviation
I.	0	70.3	0.5
	400	71.1	0.7
	800	71.6	0.5
	1200	71.8	0.4
	1600	72.5	0.5
II.	0	67.3	0.7
	400	67.6	0.5
	800	68.1	0.3
	1200	68.0	0.0
	1600	68.7	0.5
III.	0	83.6	0.5
	400	83.8	0.4
	800	84.2	0.4
	1200	84.4	0.5
	1600	85.0	0.0
IV.	0	84.2	0.4
	400	85.2	0.4
	800	86.0	0.0
	1200	86.0	0.0
	1600	86.2	0.4

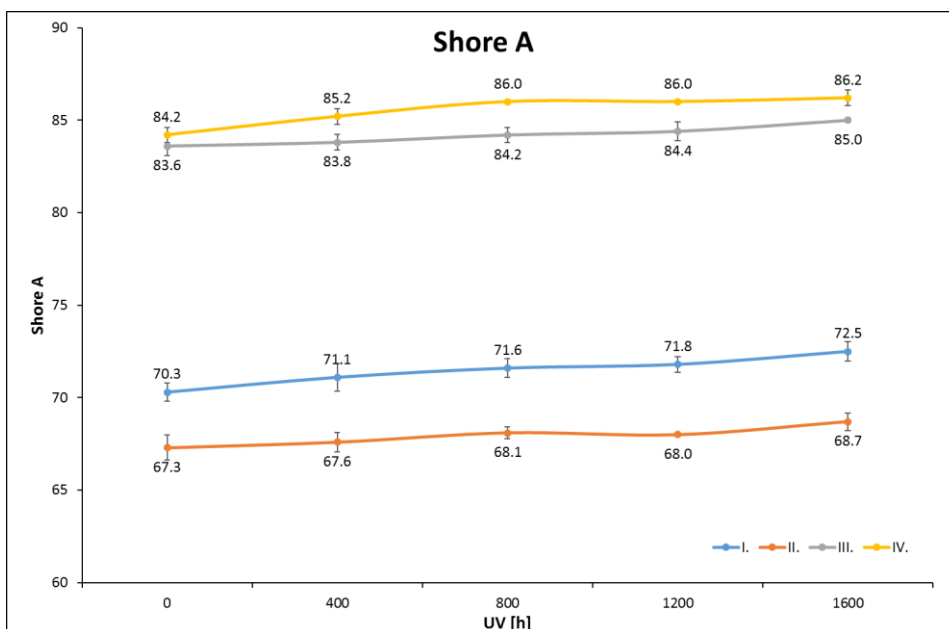


Figure 5. Shore A

The Shore A hardness values across the different compounds showed an increase ranging from 1.5% to 3.2%. This increase is acceptable for future applications.

4 CONCLUSIONS

During the 1600-hour UV aging process, we conducted mechanical tests on samples taken at various time intervals. Our goal was to assess how resistant each compound is to UV radiation and to what extent they change. Samples I and III were the most sensitive to UV radiation, while Samples II and IV were less affected. We recommend further development of the formulation used in Samples II and IV for the windshield sealing material.

Overall, this study demonstrates the varying levels of UV resistance among the tested rubber compounds. By identifying the compounds that show greater resilience, manufacturers can focus on optimizing these formulations for enhanced durability in real-world applications. The findings also highlight the importance of continuous testing and material development to ensure the longevity of rubber materials exposed to UV radiation in transportation settings.

REFERENCES

- [1] Dr. Bartha Zoltán: Gumiipari kézikönyv, Taurus-OMIKK, Budapest,
- [2] A. Mukhopadhyay: Some Triological Characterization of “EPDM” Rubber, *Tribology in Industry* 36(2), 2014 june: pp 109-116
- [3] Roger Brown: *Physical Testing of Rubber*, Springer, New York, 2006
- [4] ISO 23529:2016, Rubber - General procedures for preparing and conditioning test pieces for physical test methods
- [5] ISO 37:2017 Rubber, Vulcanized or Thermoplastic – Determination of tensile stress-strain properties
- [6] Rubber, vulcanized or thermoplastic – Determination of hardness; Part 4: Indentation hardness by durometer method (Shore hardness) 2018
- [7] W. Yang, H. Yu, W. Liang, Y. Wang: Rapid Fabrication of Hydrogel Microstructures Using UV-Induced Projection Printing, *Micromachines* 6(12), 2015 December: pp 1903-1913.



INVESTIGATION OF TORSIONAL VIBRATIONS OF THE STEERING SHAFT FROM THE ASPECT OF MINIMAL DRIVER-HAND FATIGUE IN HEAVY MOTOR VEHICLES

Miroslav Demić ^{1*}, Mikhail P. Malinovsky ²

Received in July 2024

Accepted in August 2024

RESEARCH ARTICLE

ABSTRACT: Local hand vibrations can cause occupational diseases in drivers of heavy motor vehicles, such as white finger syndrome.

In this study, a method has been developed to check the diameter of the steering shaft from the aspect of hand fatigue due to the action of tangential vibrations of the steering wheel, as tangential accelerations occur in it due to torsional vibrations, as an elastic system. By applying the method of “stochastic parametric optimization”, the diameter of the steering shaft was calculated from the aspect of minimizing tangential accelerations. Based on this value, the tangential vibrations of the steering wheel were calculated and compared with the ISO 5349/DIS criteria. Since the obtained values of analyzed accelerations are lower than the mentioned criteria, the calculated diameter of the steering shaft can be used for further analysis. More precisely, it should be compared with the one on the derived steering mechanism and, as authoritative, adopt the larger one.

KEY WORDS: *Steering shaft, torsional vibrations, tangential accelerations of the steering wheel, optimization*

© 2024 Published by University of Kragujevac, Faculty of Engineering

¹Miroslav Demić, University of Kragujevac, Faculty of Engineering Kragujevac, Sestre Janjić 6, Kragujevac, Serbia, demic@kg.ac.rs,  <https://orcid.org/0000-0003-2168-1370>

²Mikhail P. Malinovsky, Moscow Automobile and Road Construction State Technical University (MADI), Moscow, , Russia, ntbmadi@gmail.com,  <https://orcid.org/0000-0001-7812-5653>

PRILOG ISTRAŽIVANJU TORZIONIH VIBRACIJA OSOVINE UPRAVLJAČA SA ASPEKTA MINIMALNOG ZAMORA RUKU VOZAČA TERETNIH MOTORNIH VOZILA

REZIME Lokalne vibracije ruku mogu izazvati profesionalna oboljenja kod vozača teretnih motornih vozila, poput sindroma belih prstiju. U ovom radu je razvijena metoda za proveru prečnika osovine upravljača sa aspekta zamora ruku usled dejstva tangencijalnih vibracija točka upravljača, jer se kod nje usled torzionih vibracija, kao elastičnog sistema, javljaju tangencijalna ubrzanja. Primenom metode stohastičke parametarske optimizacije izračunat je prečnik osovine upravljača sa aspekta minimizacije tangencijalnih ubrzanja. Na osnovu te vrednosti izračunate su tangencijalne vibracije točka upravljača i upoređene sa kriterijumima ISO 5349. Kako su dobijene vrednosti analiziranih ubrzanja niže od pomenih kriterijuma, izračunati prečnik osovine upravljača se može koristiti tokom daljih analiza. Preciznije rečeno, isti treba uporediti sa onim na izvedenom upravljačkom mehanizmu i, kao merodavan, usvojiti veći.

KLJUČNE REČI: *Osovina upravljača, torzione vibracije, tangencijalna ubrzanja točka upravljača, optimizacija*

INVESTIGATION OF TORSIONAL VIBRATIONS OF THE STEERING SHAFT FROM THE ASPECT OF MINIMAL DRIVER-HAND FATIGUE IN HEAVY MOTOR VEHICLES

Miroslav Demić, Mikhail P. Malinovsky

INTRODUCTION

The heavy motor vehicle defined by the project task is elaborated in further design phases [1]. The conceptual design represents the first concretization of the project task, and its main goal is to define the parameters of the driver's ergo-sphere and the external dimensions, mass, and performance of the heavy vehicle, as well as its stylistic indicators necessary for further work on the project [1].

In this paper, there will be more words about the aspect of minimal driver hand fatigue during free driving of a heavy motor vehicle, and as a basis, the author uses the principles set in [2], for the automatic design of elastic systems in cargo motor vehicles.

The assumption is that the project task defines a cargo motor vehicle with a total mass of 11000, kg, with a useful load capacity of 4000, kg, dimensions (length * width * height, mm): 6400*2500*3600, with a short cab. The engine position is front, and the drive is on the rear wheels.

The steering axle (column, shaft-hereinafter referred to as the shaft), in addition to other elements of the steering system, must also provide minimal driver-hand fatigue due to local vibrations on the steering wheel.

For this purpose, a simplified axle model will be used, as well as a stochastic parametric optimization procedure based on the Hooke-Jeeves method.

It is pointed out that the choice of the steering shaft diameter can be made [1]:

- theoretically, using mathematical models and dynamic simulations,
- experimentally, and
- combined.

It should be noted that experimental research is expensive, and often not applicable in the initial phase of vehicle design. Therefore, the procedure of theoretical optimization was accepted here, which required modeling of the steering shaft.

Considering the goal of this paper, it was considered appropriate to compare the tangential accelerations of the steering wheel, which are the result of torsional vibrations of the shaft, with international standards ISO 5349/DIS, which are, for illustration, shown in Figure 1 [3]. They define permissible hand vibration loads for exposure to vibrations lasting 4-8 hours. From Figure 1, it can be seen that the approximate permissible hand accelerations are constant up to 16 Hz, and with further increase in frequency, they linearly increase.

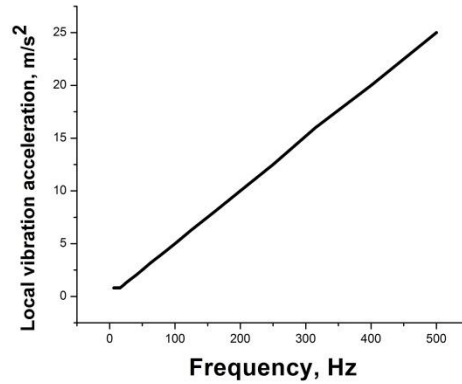


Figure 1. ISO 5349/DIS (1979) Local hand vibrations for exposure to local vibrations lasting 4-8 hours

In practice, there are several characteristic concepts of servo steering systems, which will not be further discussed here, as they are described in detail in [4].

Considering that the goal of this paper is the development of a method for analyzing torsional vibrations of the shaft, from the aspect of minimizing tangential accelerations of the steering wheel, it was considered appropriate to illustrate it on the concept shown in Figure 2a).

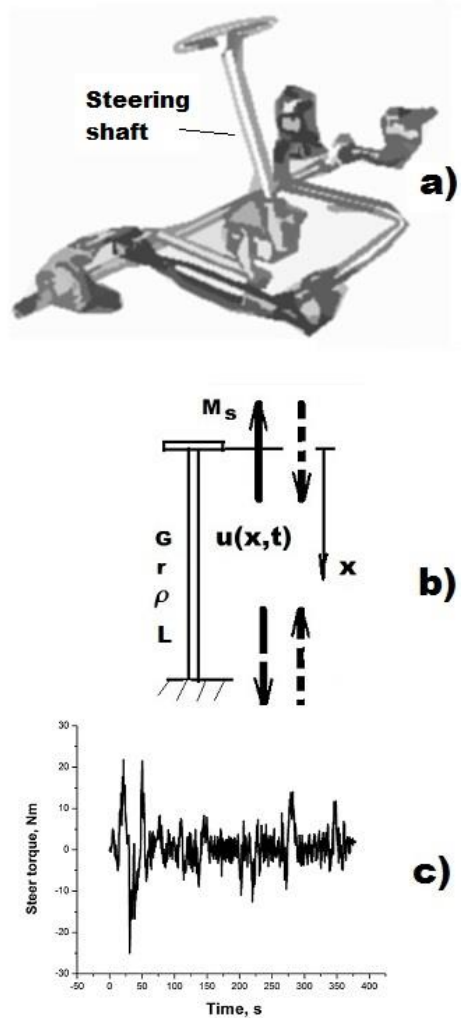


Figure 2. Observed concept of servo steering a), idealized model of the steering shaft b) and experimental torque on the steering wheel c)

It should be noted that the delivered servo steering system has a defined shaft diameter, but it was considered appropriate to calculate it from the conditions of minimal tangential accelerations and compare it with the existing one. The larger one should be adopted as the relevant one.

1 METHOD

As already mentioned, this paper aims to explore the torsional vibrations of the steering shaft from the aspect of minimal driver fatigue due to tangential accelerations of the steering wheel. In doing so, the influences of other oscillatory loads of the vehicle as a whole, or its systems, are neglected.

It should be noted that in the conceptual design phase of the steering system of a commercial motor vehicle, its parameters are usually defined by calculation from the

conditions of the moment of rotation in place, or movement at low speeds [4]. Based on this, the selection of a power steering system is made, which already has a defined shaft diameter.

For the research of torsional vibrations of the shaft, it was considered appropriate to idealize it and observe it as a homogeneous rod of adopted length (from ergonomic conditions [1], and unknown diameter [4], (Figure 2b). The shaft undergoes torsional vibrations under the action of a disturbing torque. The torque at the steering wheel point registered in operational conditions [2] was used in the work. For illustration, a depiction of its temporal change during the free ride of an analog vehicle on an asphalt road is shown in Figure 2c.

By applying the method of stochastic parametric optimization, the diameter of the steering shaft was calculated from the aspect of minimizing tangential accelerations. Based on this value, the tangential vibrations of the steering wheel were calculated and compared with ISO 5349/DIS criteria.

2 STEERING SHAFT MODEL

When defining a model that describes the torsional vibrations of an elastic steering shaft, the following assumptions were introduced:

- the shaft is homogeneous and of constant diameter,
- the influence of clearance in the joints of the power steering system is neglected,
- the influence of tangential elasticity of the steering wheel and other elements in the steering system is neglected, and
- the existence of other vibrational excitations originating from the vehicle itself is neglected.

Since the partial differential equation describing the torsional vibrations of an elastic rod, which also applies to the steering shaft, is detailed in [5,6], it will not be done here, but its final form will be shown. Forced torsional vibrations of the steering shaft [5,6] are described by a partial differential equation:

$$\rho \frac{\partial^2 u}{\partial t^2} = G \frac{\partial^2 u}{\partial x^2} + f(x, t), \quad (1)$$

where: $u(x, t)$ - torsional vibrations of the shaft, x - coordinate along the length of the shaft, $f(x, t)$ - the forced torque transmitted from the steering wheel to the shaft, t - time, G - shear modulus, and ρ - material density of the shaft.

The excitation function from the moment at the steering wheel is given by the expression:

$$f(x, t) = m_s(t), \quad (2)$$

where: $m_s(t)$ - the experimentally registered torque at the steering wheel.

As known [5-7], to determine the general integral of the partial differential equation (1), it is necessary to know the boundary and initial conditions.

The torsional torque due to shaft vibrations can be expressed [5,8]:

$$M = GI_0 \frac{\partial u(x, t)}{\partial x}, \quad (3)$$

where:

- I_0 - polar moment of inertia of the cross-section of the shaft, given by the expression [8]: $I_o = \frac{\pi r^4}{2}$
- r - shaft radius.

Defining boundary conditions in the analysis of vibrations of elastic bodies, in general, represents an idealization of the real state. In this specific case, it is assumed that one end is quasi-free (subject to a steering wheel torque), and the other end is clamped. Additionally, it is assumed that torsional vibrations and their velocities are initially equal to zero, i.e.:

$$\begin{aligned} GI_o \frac{\partial u(0,t)}{\partial x} &= m_s(0,t) \\ u(0,L) &= 0 \\ u(x,L) &= 0 \\ \dot{u}(x,0) &= 0 \end{aligned} \quad , \quad (4)$$

The partial differential equation (1), with boundary and initial conditions (4), can only be solved in closed form in the case of harmonic excitation [5-7]. Attempts to solve it using Wolfram Mathematica 13.2 [7] encountered difficulties in presenting numerical data, so it was decided to solve the problem numerically using the finite difference method [9].

The author developed a program in Pascal to numerically solve the partial differential equation (1) with the excitation function (2) and boundary and initial conditions (4). It is noted that in the case of numerical solution of partial differential equations, additional boundary and initial conditions may sometimes need to be introduced [7].

Dynamic simulation was performed for a steel steering shaft structure with the following data: $G = 8 \cdot 10^4$, N/mm²; $\rho = 8 \cdot 10^{-6}$, kg/mm³; $n_x = 4086$ $h_x = 0.1$, mm; $n_t = 4096$; $h_t = 0.001$, s.

The values of the number of points and discretization steps used during the dynamic simulation ensured the reliability of the results for parameters in the x-axis direction: 0.0024 to 5, 1/mm and t: 0.244 to 500, Hz [13].

3 DYNAMIC SIMULATION

In the following text, there will be more words about the analysis of torsional vibrations of the steering shaft, using optimization methods. It should be noted that in practice, various procedures are used for these purposes, and here the method of "stochastic parametric optimization" will be applied. As is known, it is used in optimizing the oscillatory parameters of motor vehicles and is based on nonlinear programming methods. Since there are constraints on the design parameters in the optimization process, the problem is solved by introducing "external" or "internal" penalty functions [10,11].

In this specific case, the method used for selecting the diameter of the shaft is based on the Hooke Jeeves method and external penalty functions (the length was accepted from the ergonomic aspect). The optimization method is detailed in reference [11], so it will not be discussed in detail here. The block diagram of the method will be shown in Figure 3 for illustration purposes.

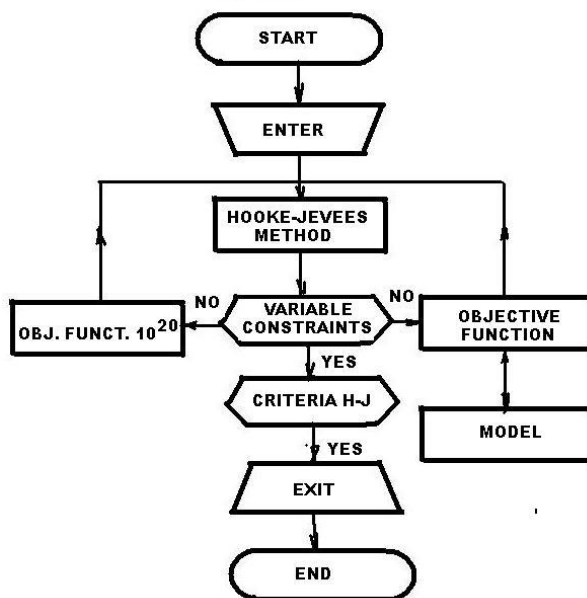


Figure 3. Flow block diagram of the optimization method

The analysis of torsional vibrations of the shaft is focused on minimizing the tangential accelerations of the steering wheel, by using the objective function.

$$Z = Ra_{RMS}, \quad (5)$$

where: RMS values of the tangential acceleration of the steering wheel due to torsional vibrations of the axle obtained by solving the partial differential equation (1), R - radius of the steering wheel.

RMS of the tangential vibrations of the steering wheel using the formula:

$$a_{RMS}^2 = \frac{1}{n_x n_t} \sum_{i=1}^{n_x} \sum_{j=1}^{n_t} a(i, j)^2, \quad (6)$$

where: $a(i, j)$ - tangential accelerations of the steering wheel due to torsional vibrations of the shaft, n_x - number of points along the x-axis, and n_t - number of points along the t-axis.

During the optimal selection process of the shaft unknown dimension, boundary values for the shaft radius were defined: $5 \leq r \leq 15$

By introducing the optimizing parameter $x[i]$, $i=1$, instead of r , with corresponding adopted boundary values $x_u[i]$, $x_l[i]$, $i=1$ (u - upper, l - lower boundary value), the objective function depends on one optimizing parameter and it has more local minima and only one global minimum [10].

Considering that, in practice, finding the global minimum is achieved by starting the optimization process with more initial values of optimizing parameters [2,10,11], it was deemed appropriate in this case to start with three initial parameter values, namely:

$$x=0.5 x_u[1] \quad x=0.5 x_u[2]$$

$$x=0.8 \ x_u[1] \quad x=0.8 \ x_u[2]$$

$$x=1.2 \ x_l[1] \quad x=1.2 \ x_l[2]$$

The optimization was performed on a Pentium 4 computer (Intel 2.4, GHz, 9, GB RAM), and the iterative process was automatically stopped when the difference between two adjacent values of the objective function was 10^{-30} . The optimization time for one combination was around 20 minutes, and the calculated parameters are shown in Table 1.

Table 1. Key parameters of the optimal selection of the steering shaft diameter

Initial values	Optimal parameter, r, mm	Objective function, Z, rads ⁻²	No of iter., N,-
0.5(x _l +x _u)	5.000	9.814976100393929E-004	574
0.8 x _u	5.000	9.814976100393929E-004	576
1.2 x _l	5.000	9.814976100393929E-004	560

4 DATA ANALYSIS

By analyzing the data from Table 1, it can be concluded that the optimal value of the shaft diameter and the objective function do not depend on the initial value of the optimizing parameter, as identical values are obtained (5, mm).

Considering that the integration of the partial differential equation was performed at 4096 points, due to Excel limitations, torsional vibrations of the steering shaft for the optimal diameter value at 256 points are shown in Figure 4.

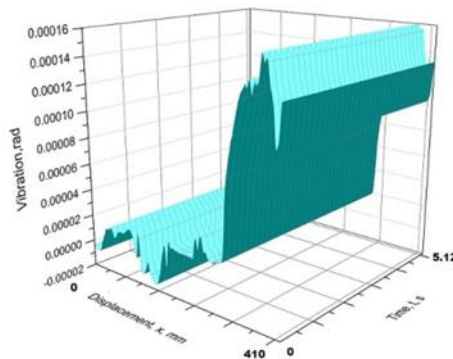


Figure 4. Torsional vibrations of the steering shaft

By analyzing the data from Figure 4, it can be determined that they stochastically change along the length of the shaft. The random nature of the vibrations can be explained by the random nature of the excitation function used, which is in agreement with [5].

It was deemed appropriate to perform a frequency analysis of torsional vibrations using 2D Fourier transform. The author developed software for calculating the parameters of 2D Fourier transform [12], but it was deemed appropriate to use commercial software Origin [13]. The calculated values of the magnitude and phase angles of the 2D Fourier transform are shown in Figures 5 and 6 (for 256 points).

By analyzing the data from Figures 5 and 6, it can be observed that the magnitude is highest at the ends of the axle, and the phase angles change stochastically along its length.

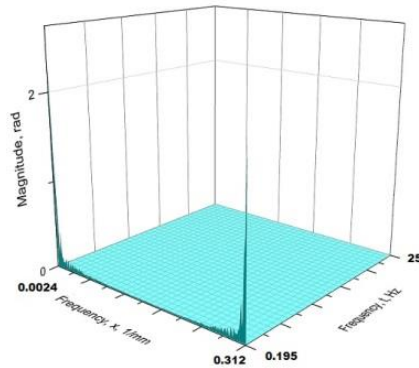


Figure 5. Spectrum magnitude of torsional vibrations of the steering shaft

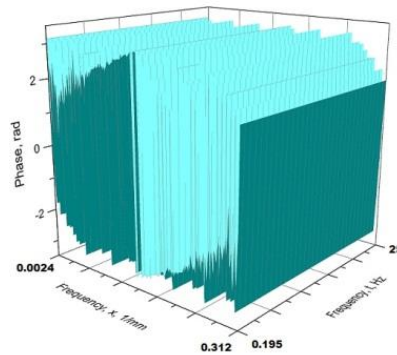


Figure 6. Phase angles of the spectrum of torsional vibrations of the steering shaft

It is noted that the optimal diameter of the steering shaft is calculated based on the conditions of minimal tangential vibrations of the steering wheel, so it can be changed during the later design phase through finite element method verification and experimentation, or the one supplied with the power steering can be adopted, which will not be discussed further here [14].

It is emphasized that based on the adopted standard dimensions, an analysis of the torsional resonance of the steering shaft must be performed and compared with the harmonic frequencies obtained by 2D Fourier transform. The goal is to avoid overlap of axle resonance and wave frequencies, which will not be discussed further here [15]...

It was deemed appropriate to compare the tangential accelerations of the steering wheel with the ISO 5349/DIS criteria [3]. Therefore, tangential accelerations of the steering wheel were calculated and a third-octave frequency analysis was performed, with the results shown in Figure 7.

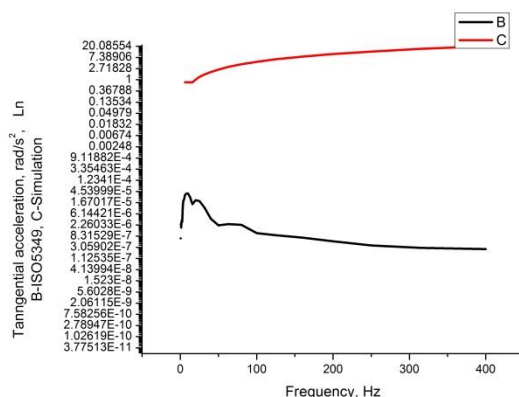


Figure 7. The comparison of ISO 5349/DIS criteria and calculated tangential accelerations (the ordinate axis is logarithmic due to small values of tangential accelerations).

By analyzing the data from Figure 7, it can be observed that the ISO 5349/DIS criterion is satisfied, so the calculated axle radius can be accepted for further analysis.

Since the obtained values of analyzed accelerations are lower than the mentioned criteria, the calculated steering shaft diameter can be used for further analysis. More precisely, it should be compared with the one on the derived steering mechanism and, as a reliable measure, a larger one should be adopted.

It is also noted that in 2D Fourier transform, there are no explicit procedures for calculating errors in spectral analysis, as in the case of 1D Fourier transform [15]. Taking this into account, and considering that this work aims to illustrate the potential application of 2D Fourier transform in the analysis of steering axle torsional vibrations, statistical errors were not calculated.

5 CONCLUSION

The developed procedure, based on the analysis of tangential accelerations of the steering wheel due to torsional vibrations of the steering shaft, allows for the definition of its diameter, which will be compared to the one supplied with the power steering, and for further findings, a larger one is adopted.

In further project development, based on the defined diameter, more detailed calculations can be approached, possibly using the finite element method.

The analyses performed have shown that the use of 2D Fourier transform is desirable for analyzing the torsional vibrations of the steering shaft, as they allow for checking the matching of the excitation frequency and the resonance of the shaft.

REFERENCES

- [1] Demić, M.: Basics of designing heavy motor vehicles (in Serbian), Faculty of Mechanical Engineering in Kragujevac, 1994.
- [2] Demić, M. Contribution to the development of a method for optimal dimensioning of the steering rod in the conceptual design phase of a commercial motor vehicle, Science Journal of Transportation, Vol. 16, No 4. 2023.

- [3] ISO/DIS 5349: Principles for the Measurement and the Evaluation of Human Exposure to Vibration transmitted to the Hand, (1979).
- [4] Minić, M. Truck steering system: theory, calculation, construction, testing, ABC Glas, Belgrade (1992), in Serbian.
- [5] Singeresy, S.R.: Vibration of continuous systems, John Wiley and Sons, Inc. New Jersey, 2007.
- [6] Sobolev, S. L.: Partial differential equations of Mathematical Physics, Pergamon Student Edition, Elsevier, 2016.
- [7] Wolfram Mathematica:
<https://Reference.Wolfram.com/language/tutorial/NDSolverPDE.html>
- [8] Timoshenko, S.: Strength of materials, Part II, Advanced Theory and Problems, Paolo Atto, California, 1941.



DEVELOPMENT AND IMPLEMENTATION OF ADVANCED ROBOTICS IN THE AUTOMOTIVE AND ELECTRO-ELECTRONIC INDUSTRY OF CHINA

IsakKarabegović^{1*}, ErminHusak², Edina Karabegović³, Mehmed Mahmić⁴

Received in July 2024

Accepted in August 2024

RESEARCH ARTICLE

ABSTRACT: It is known that in recent years there have been major changes in all branches of industry, especially in the automotive and electro-electronic industry, because new business methods are on the scene, and production processes are being transformed so that they are flexible. In the automotive and electro-electronic industry, the leading technology is robotic technology, the application of which increases the return on investment. Advanced robotics as the basic technology of Industry 4.0 in the new era of production in the automotive and electro-electronic industry plays a very important role because it enables: mobility, readiness, reliability, adaptability, transformation of production, integration with machines, increase of flexibility, improvement of quality, storage and production systems integrated as Cyber-Physical Systems, workers are freed from routine and repetitive tasks. The paper provides an overview of applied and issued patents in robotic technology, the application of robots in the World and China as the leader in the implementation of robotic technology in the world. An analysis of the implementation of industrial robots, as well as advanced robots in the automotive and electro-electronic industries of China, is given, as well as the forecast of the application in the coming years.

KEY WORDS: *Industrial robot, automotive industry, electrical/electronic industry, Industry 4.0, production processes*

© 2024 Published by University of Kragujevac, Faculty of Engineering

¹IsakKarabegović, Academy of Sciences and Arts of Bosnia and Herzegovina, Bistrik 7. 71000 Sarajevo, Bosnia and Herzegovina, address: isak1910@hotmail.com,  <https://orcid.org/0000-0001-9440-4441> (*Corresponding author)

²Ermin Husak, Univesity of Bihać, Technical faculty Bihać, IrfanaLjubijankića bb.77000 Bihać, Bosnia and Herzegovina, address, e-mail: erminhusak@yahoo.com,  <https://orcid.org/0000-0002-3488-4436>

³Edina Karabegović, Technical faculty Bihać, IrfanaLjubijankića bb.77000 Bihać, Bosnia and Herzegovina, edina-karabeg@hotmail.com,  <https://orcid.org/0000-0003-3744-8979>

⁴Mehmed Mahmić, Technical faculty Bihać, IrfanaLjubijankića bb.77000 Bihać, Bosnia and Herzegovina, mmahmic@gmail.com,  <https://orcid.org/0000-0002-7294-2844>

RAZVOJ I IMPLEMENTACIJA NAPREDNE ROBOTIKE U AUTOMOBILSKOJ I ELEKTRO-ELEKTRONSKOJ INDUSTRIJI KIN

REZIME: Poznato je da je poslednjih godina došlo do velikih promena u svim granama industrije, posebno u automobilskoj i elektro-elektronskoj industriji, jer su na sceni nove metode poslovanja, a proizvodni procesi se transformišu tako da budu fleksibilni. U automobilskoj i elektro-elektronskoj industriji vodeća tehnologija je robotska, čija primena povećava povraćaj ulaganja. Napredna robotika kao osnovna tehnologija Industrije 4.0 u novoj eri proizvodnje u automobilskoj i elektro-elektronskoj industriji igra veoma važnu ulogu jer omogućava: mobilnost, spremnost, pouzdanost, prilagodljivost, transformaciju proizvodnje, integraciju sa mašinama, povećanje fleksibilnost, poboljšanje kvaliteta, sistemi skladištenja i proizvodnje integrisani kao sajber-fizički sistemi, radnici su oslobođeni rutinskih i ponavljajućih zadataka. U radu je dat pregled primenjenih i izdatih patenata u robotskoj tehnici, primeni robota u svetu i Kini kao lideru u primeni robotske tehnologije u svetu. Data je analiza implementacije industrijskih robota, kao i naprednih robota u automobilskoj i elektro-elektronskoj industriji Kine, kao i prognoza primene u narednim godinama.

KLJUČNE REČI: *Industrijski robot, automobilska industrija, elektro/elektronska industrija, Industrija 4.0, proizvodni procesi*

DEVELOPMENT AND IMPLEMENTATION OF ADVANCED ROBOTICS IN THE AUTOMOTIVE AND ELECTRO-ELECTRONIC INDUSTRY OF CHINA

Isak Karabegović, Ermin Husak, Edina Karabegović, Mehmed Mahmić

INTRODUCTION

We are witnessing the implementation of Industry 4.0 in the automotive and electro-electronic industry in the world where we move to increasingly present mobility, bridging the digital and physical environment, using the basic technologies of Industry 4.0. This leads us in a completely new way to wide possibilities of implementation of innovations, automation, optimization by which we raise the production processes in the automotive and electro-electronic industry to a higher level [1-3]. The very concept of production through the implementation of Industry 4.0 is such a concept that goes in the direction of production in which everything is networked. In production processes, machines and devices are connected by wireless connection and sensors, and they are also connected to a system that can independently make decisions motivated by a large amount of data. The concept of Industry 4.0 itself is not yet widespread, and the implementation of this concept is expected to advance and advance all aspects and segments of human life [4-6]. In reality, Industry 4.0 is a new phase in the organization and control of the industrial value chain, which primarily relies on CPS (Cyber-Physical-Systems), and the corresponding service, most often implemented in the Cloud Computing. There are big changes in all branches of industry, as well as new business methods, transformation of production systems, consumption, delivery and transport, changes occur thanks to the implementation of Industry 4.0 technologies.

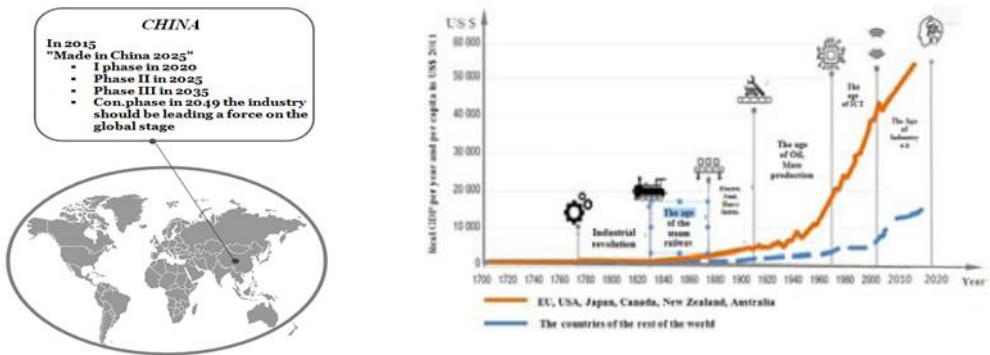
Only part of the basic technologies of Industry 4.0 are: Robotics, Internet of Things (IoT), Big Data, Smart Sensors, Additive Technologies, Virtual and Augmented Reality (AR), Artificial Intelligence (AI), Digital Twins, etc.

Companies in the automotive, electro-electronic industry mainly apply robotic technology through the implementation of the first generation of industrial robots, service robots and advanced robots in their plants to meet the growing demands of customers, as the demand for various products and services has increased, along with product redesign and customization [7-9]. The development of robotics technology and other new technologies has led to second generation industrial robots. Compared to first-generation robots, collaborative robots have a number of advantages, some of which are: increasing productivity, increasing the speed of product production, providing greater reliability, precision, for example in assembly, and therefore improving quality, using machine vision technologies that improve the perception of robots, they can improve safety, increase the accuracy of the performed task, etc., which is a motivation for companies from the automotive and electro-electronic industry to implement them [10].

1 THE TREND DEVELOPMENT AND RESEARCH OF ROBOTIC TECHNOLOGY IN THE WORLD

In the last ten years, we have witnessed an increasing demand for the implementation of robotic technology as the basic technology of Industry 4.0, which companies are hastily implementing in their production processes in order to be competitive on the global market, especially companies from the automotive and electro-electronic industries. Developed countries in the world have adopted their Industry 4.0 implementation strategies because its

implementation itself has an impact on technological changes to increase GDP as shown in Figure 1 [10-13]. Likewise, in 2015, the Government of China adopted its strategy called "Made in China 2025", whose goal is to be among the most technologically developed countries in the world by 2025, but since it cannot achieve this by 2025, they divide it into several phases: Phase I until 2020, Phase II until 2025, Phase III until 2035 and the final phase in 2049, where Chinese industry should be a leading force on the global stage in the world.



a) China's strategy

b) GDP per capita

Figure 1 Representation of the Industry 4.0 a) strategy in China and b) the impact of technological changes to increase GDP in the World

Advanced countries and developing countries invest in research and development of advanced Industry 4.0 technologies, and implement them in the production processes of companies, and the goal is for companies to conquer the global market, which is changing. Investing in research, development and implementation in the aforementioned Industry 4.0 technologies brings an increase in GDP, as shown in Figure 1.b). Technological changes and inequalities through the ages, shows the increase in real GDP per capita by the introduction of advanced technologies in production processes and the complete environment [13].

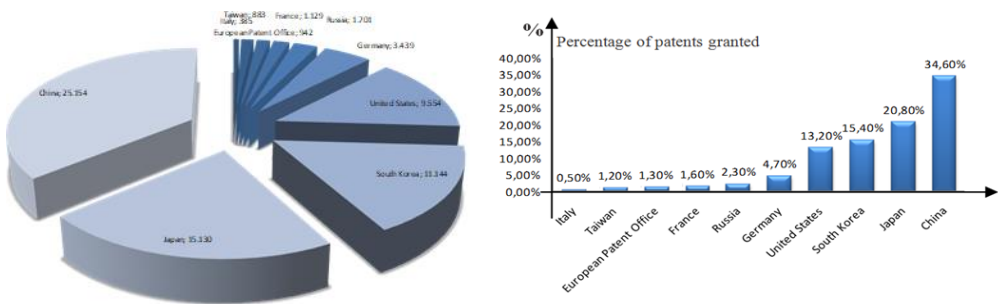


Figure 2 Approved patents in robotic technology in the World in the period 2005-2019. in ten top countries

In developed countries throughout the ages, GDP per capita has been continuously increasing (Figure 1.b), such as the countries of the European Union, USA, Australia, Canada, New Zealand and Japan, while all other countries in the World have a slight increase in GDP per capita. Year after year, the difference in GDP between developed and non-developed countries is increasing, this is what developing countries need to understand

and start investing in research and development and adopt their technological development strategies, so that their companies also start to be competitive in the global market.

The automotive industry and the electro-electrotechnical industry in many countries are the leading industries of development, and we can conclude that China is also one of the countries that develops and invests in these two industries, because China is the first country in the World in terms of vehicle production. About 30% of vehicles production is produced in China [14], and the same is the case with the electro-electronic industry. In these two industries, industrial robots are used the most in the world [15], and to create a true picture of development and research in robotic technology in the World, an analysis of the application of patents in ten top countries in the world was made and shown in Figure 2 [16-19]. In the period from 2005-2019, the top ten countries in terms of approved patents in robotic technology are: China, Japan, Republic of Korea, United States, Germany, Russia, France, European Patent Office, Taiwan and Italy. The leading country in the World is China, which in that period has 25,154 approved patents in robotics, which represents 34.6% of the total approved patents in the world for that period. In the analysis of approved patents in robotic technology, we took the year 2019 and presented it in Figure 3 [16-19].

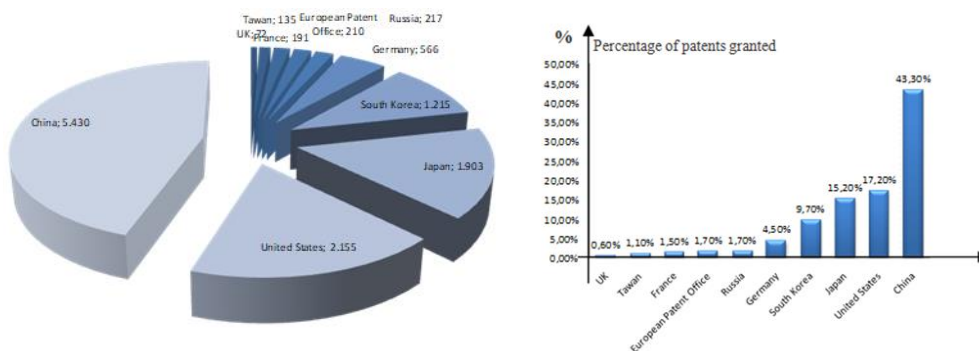


Figure 3 Approved patents in the World in 2019 from robotic technology in ten top countries

Likewise, based on the diagram shown in Figure 3, we conclude that the following countries are in the first five countries in the world in terms of the number of approved patents: China, United States, Japan, Republic of Korea, Germany. China is in first place with 5,430 approved patents in robotic technology in 2019, which represents 43.3% of the total number of patents granted in the World in robotic technology. We come to the conclusion that the leading top countries in the development and research of robotic technology are: China, the United States, Japan, the Republic of Korea and Germany. Precisely those countries in which there are the most companies from the automotive and electro-electronic industry, where industrial robots are installed in the World which we will show in the next chapter.

2 THE TREND OF IMPLEMENTATION OF INDUSTRIAL ROBOTS IN THE AUTOMOTIVE AND ELECTRO-ELECTRONICS INDUSTRY IN THE WORLD AND IN CHINA

We analyzed the trend of the implementation of industrial robots of the first and second generation in the automotive and electro-electronics industry in the World and in China based on statistical data from the International Federation of Robotics (IFR), the UN Economic Commission for Europe (UNECE) and the Organization for Economic

Cooperation and development (OECD). The trend of the implementation of industrial robots on an annual level in the world is shown in Figure 4 [20-23].

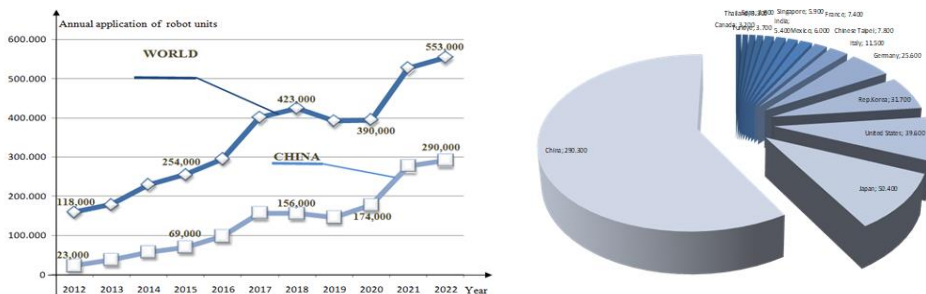


Figure 4 Annual implementation of industrial robots in the World and China for the period 2012-2022 and ten top countries in the world in 2022

Based on the Figure 4, we conclude that the use of industrial robots in the World, as well as in China, is increasing from year to year, and a small drop in use was during the CORONA-19 virus pandemic, however, there was an increase in the use trend. In the World in ten years, the application increased from 118,000 units of robots in 2013 to 553,000 units of robots in 2022. In China, in 2012, the use of industrial robots amounted to about 12,200 units, and in 2022, the use was about 100,000 units of robots. China had the biggest jump in the use of industrial robots in just ten years, increasing its use by 12.6 times. China is the leading country in the implementation of industrial robots in the world, as shown by Figure 4, which represents the implementation of robots in the top ten countries in the World in 2022. The first five countries are: China, Japan, the United States, the Republic of Korea and Germany, countries in which the automotive and electro-electronics industry has been developed or is developing, and where industrial robots are mostly used. The trend of using industrial robots in the automotive industry in the World and China in the period 2012-2022 on an annual basis is shown in Figure 5 [20-23].

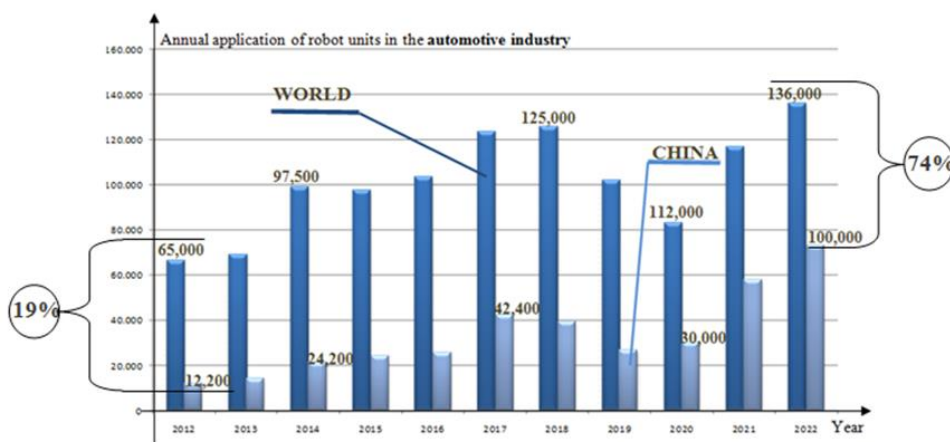


Figure 5 Annual implementation of industrial robots in the automotive industry in the World and in China in the period 2012-2022

Based on the diagram for the application of industrial robots in the automotive industry in the World and in China, Figure 5, we conclude that the trend of the application of robots in this industry is increasing both in the world and in China. In China, the growth trend of the use of robots in the automotive industry in 2012 was 19% of all robots used in this industry in the World. In ten years, China has increased its share of the use of robots in this industry to 74% in 2022 (Figure 5), where it has installed about 100,000 units of robots, which is about 35% of all industrial robots used in that year (Figure 4.) which gives us the first to conclude that China is fully automating production processes in the automotive industry. The trend of the use of robots in the electro-electronics industry in the World and in China is shown in Figure 6 for the period 2012-2022 [20-23].

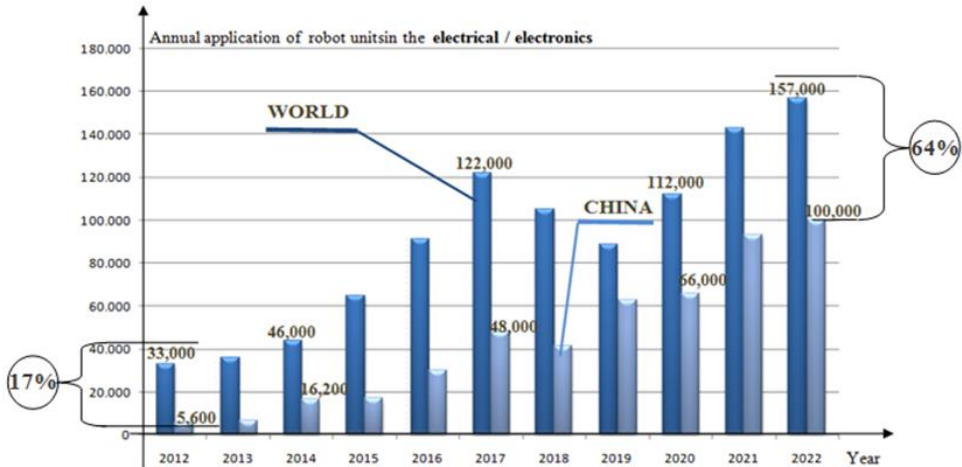


Figure 6 Annual implementation of industrial robots in electro-electronics in the World and in China in the period 2012-2022

The trend of the use of robots in the electro-electronics industry in the world and in China is shown in Figure 6. For the period 2012-2022. In the electro-electronic industry, the use of robots is increasing year by year in the world and in China, only a small drop in use was during the CORONA-19 virus pandemic. In 2012, China had 17% of the total use of industrial robots in this industry in based on application in the world. In just ten years, China has increased its participation in the electro-electronics robot industry to 64%. China is the first in the world in the application of industrial robots, and also the first in the world in the application of industrial robots in the automotive and electrical-electronics industries. The percentage share of these two industries in relation to other industries in the World and in China is shown in Figure 6 [23].

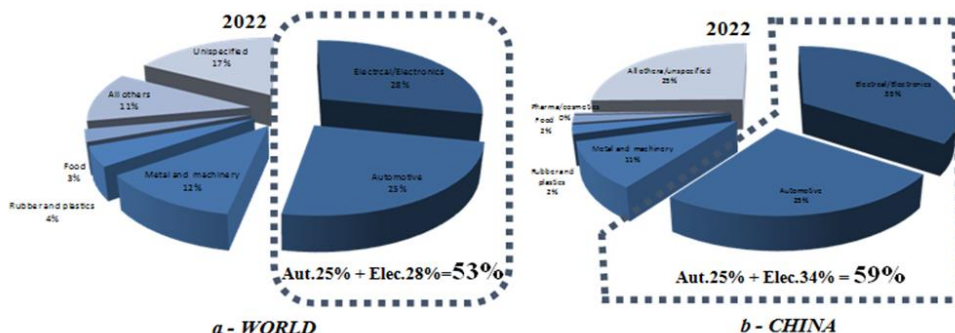


Figure 7 Annual percentage implementation of industrial robots by industry in the World and in China in 2022

By analyzing the graphs shown in Figure 7, we conclude that until today, since the very implementation of industrial robots in production processes, they have been most represented in the automotive and electro-electronics industries, so that in 2022, around 53% of all applied industrial robots have been used in the world in these two industries, but their application is starting to increase in other industries as well (Figure 7.a). In China in the same year 2022, about 59% of its total application was applied in the automotive and electro-electronics industry, and conclusion is that complete automation of production processes in the automotive and electro-electronic industry is pending in China, and reasons are:

- In China, there has been an increase in the working hours cost, and the price of industrial robots has fallen and companies are introducing robots and automating production processes,
- One of the reasons why China has adopted a strategy called "Made in China 2025" with which it wants to become the most technologically developed country in the world.
- China invests in development and research in robotics technology because it wants to increase the quality of its products, reduce production costs, and make its companies competitive on the global market.
- China is implementing Industry 4.0 in which robotic technology is the foundation of Industry 4.0 technology and without its implementation it is impossible to fully automate production processes, etc.

China is the largest producer of automobiles in the world, as well as devices and components from the electro-electronics industry, and we see that the implementation of industrial robots in law in China is the largest of these two industries.

3 THE TREND OF IMPLEMENTATION OF INDUSTRIAL ADVANCED-COLLABORATIVE ROBOTS

As we saw in the first chapter of this work, robotic technology is a key technology for the implementation of Industry 4.0, and its implementation leads us to completely smart production processes. The number of innovations and patents in robotic technology is increasing every day, and the leading country in terms of the number of registered and

approved patents in robotic technology in the World is China. Investment in development and research in robotic technology has given birth to industrial robots of the second generation, or so-called collaborative robots, which are far more advanced than the industrial robots of the first generation.

Industrial robots of the first generation had to be fenced off from workers in the production process due to worker safety, they are robust, take up a lot of work space, while collaborative robots are smaller in size, take up less work space, work together with workers and workers are safe in their environment, they are more flexible and simpler to program and manage. In recent years, their implementation has been increasing every year in production processes, as shown in Figure 8 [21-23].

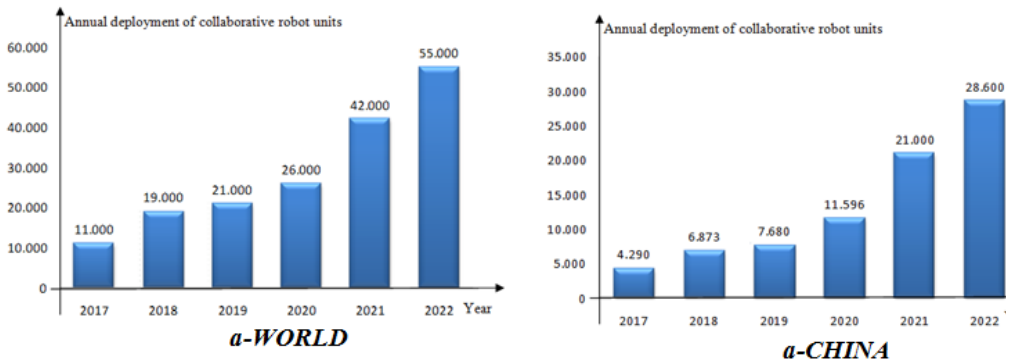


Figure 8 Annual implementation of collaborative robots in the World and China in the period 2017-2022.

In 2017, their implementation in the world amounted to about 11,000 units, while in China 4,290 units of collaborative robots were used. In just six years, its implementation has increased five times, so that in 2022 it was about 55,000 units of robots. In China, the implementation has also increased by 6.5 times in six years, as shown in Figure 8. Their implementation in production processes in industry made more flexible, and those tasks that were thought to be impossible to automate were automated. They have mostly found application in the automotive industry, especially in assembly and control, as well as in the electro-electronics industry in the assembly of printed circuit boards, testing electronic devices, etc. as Figure 9 shows [24-27].



Figure 9 Implementation of collaborative robots in the automotive and electro-electronic industry

In addition to the development of industrial robots of the second generation and their implementation in all production processes, the development and research in robotics technology has contributed to the development of service robots that are used in production

processes, and for now, service robots for logistics, which are implemented to control finished products, have the greatest application in supervision and monitoring of production processes in industry, etc. The trend of implementation of service robots for logistics is shown in Figure 10 [28].

We conclude that in recent years there has been a rapid implementation of logistics service robots in the production processes of all industrial branches, and the reason for this is the implementation of Industry 4.0, without the complete automation of warehouses, delivery of remanufactured materials, as well as the removal of finished products, where service robots for logistics are used, there is no application of Industry 4.0.

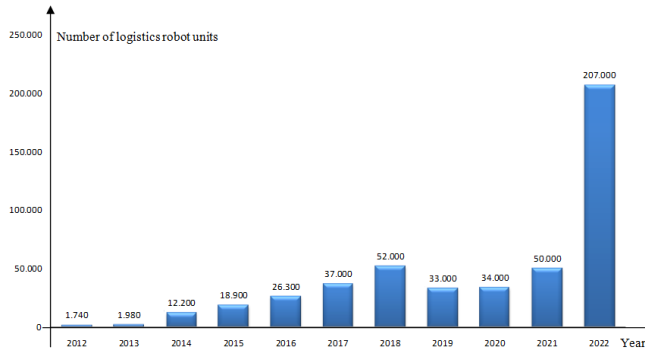


Figure 10 Implementation of service robots for logistics

Predictions are that the trend of using service robots will continue to increase in the coming years. Many companies engaged in the research, development and production of service robots have developed different constructions of service robots for logistics depending on the tasks they have to perform, and examples of their application in the automotive industry and electro-electronics industry are shown in Figure 11 [29-32].

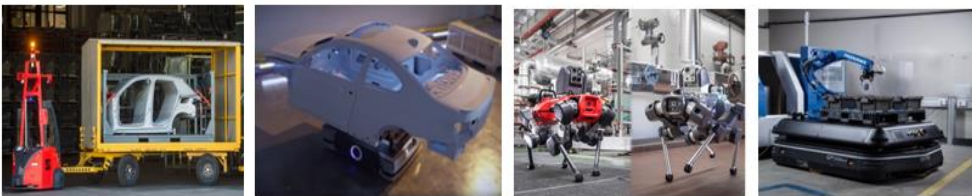


Figure 11 Implementation of service robots in the automotive and electro-electronics industry

The very implementation of advanced robots in the automotive and electro-electronic industry is necessary because global competition requires the modernization of production capacities in order to satisfy increasingly demanding customers. We are witnessing that the growing consumer markets require the expansion of production capacities, and the cooperation between man and device will open up new applications and attract new customers. Improved quality requires sophisticated high-tech robotic systems that can provide all of the above [30-32]. The implementation of advanced robotic systems in the automotive and electro-electronics industry brings a number of advantages such as:

- industrial robots help workers in various tasks,
- can maintain efficient and flexible production,

- increase productivity,
- increase in accuracy, which improves the quality of production and processes,
- support human-robot collaboration, and flexible manufacturing at a higher level,
- increasing work safety in inadequate working conditions,
- reduced production and maintenance costs,
- reducing the participation of workers in the production process,
- reduction of the workforce in the conditions of performing difficult and repetitive tasks,
- mobile manipulation with adaptable grippers will serve different production cells, and etc.

Industrial robots of the second generation and service robots as the base technology of Industry 4.0 will transform the production processes of the automotive and electro-electronics industry, the communication between the devices themselves in the production processes, a great increase in flexibility, profitability and productivity, which leads us in the direction of smart production processes. Here we must mention that the implementation of robots in production processes does not take workers' jobs, but on the contrary helps industries to increase employment because they are more competitive and they are able to enter new markets [33-36]. Workers will be freed from routine, repetitive tasks and will be focused on jobs that require judgment, common sense, creativity, problem solving, widely varying skills and dexterity. Workers with gruesome words will need new education. The development of advanced technologies will have an impact on the development of various constructions of advanced robots and their ever-increasing application in production processes, both in the automotive and electro-electronic industries, as well as in other industries, but also in the entire environment around us, because everything is moving in the direction of making everything a smart factory, houses, infrastructure, cities, etc. In other words, workers will need new education. The development of advanced technologies will have an impact on the development of various constructions of advanced robots and their ever-increasing application in production processes, both in the automotive and electro-electronic industries, as well as in other industries, but also in the entire environment around us, because everything is moving in the direction of making everything a smart factory, houses, infrastructure, cities, etc.

4 CONCLUSIONS

Based on everything presented in the paper, we conclude that China is the leading country in the world when it comes to research and development of robotic technology, because it is the country in the world with the largest number of registered and approved patents in robotic technology. China has a strategy called "Made in China 2025", which it has innovated until 2049. The year in which it wants to become the most technologically developed country in the world and one of the reasons is that it is the first country in the world for the largest implementation of industrial robots. China is the first in the world in terms of the implementation of industrial robots in the automotive and electro-electronics industry, in which in 2022 it has applied about 59% of industrial robots. China is first in the world for the production of vehicles and electronics components and devices, and it wants to increase the quality of these products to a higher level, and it can only do so by applying industrial robots in production processes. In this way it increases flexibility, productivity,

reduces energy consumption, and reduces costs production, increases product quality, satisfies increasingly demanding customers and companies from China become recognizable on the global world market. In the coming years, we can expect an increasing use of all types of robots in the production processes of the automotive, electro-electronics industry in China, but also in other industries and environments.

REFERENCES

- [1] Karabegović, I., Majstorović, V., Industry 4.0: Digital transformation is shaping the future, Society of Robotics in Bosnia and Herzegovina, ANU BiH, Bihać/Sarajevo 2024.
- [2] Schwab, K.: The Fourth Industrial Revolution, World Economic Forum, Geneva, Switzerland, 2016.
- [3] Majstorović, V., Đuričić, D., Mitrović, R.,: *Industrija 4.0: Renesansa inženjerstva*, Univerzitet u Beogradu, Mašinski fakultet Beograd, Beograd, Srbija, 2022.
- [4] Karabegović, I., Kovačević, A., Banjanović Mehmedović, L., Dašić, P.: *Integrating Industry 4.0 in Business and Manufacturing*, IGI Global, Hershey, PA, USA, 2020. <https://www.igi-global.com/book/handbook-research-integrating-industry-business/237834>
- [5] Esmaeilian, B., Behdad S., Wang, B.,: The evolution and future of manufacturing: a review, *Journal Manufacturing System*, Vol.39., pp.79-100., 2016.: <http://dx.doi.org/10.1016/j.jksy.2016.03.001>
- [6] Wang, K.: Intelligent Predictive Maintenance (IPdM) system—Industry 4.0 scenario. *WIT Transactions on Engineering Sciences*, Vol. 113, pp.259–268. 2016. www.witpress.com, doi:10.2495/IWAMA150301
- [7] Karabegović, I., Husak, E., Karabegović, E., Mahmić, M., China is the leading country in the world in the implementation of robotic technology as the basic technology of Industry 4.0, 12th International Conference – KOD 2024 „Machine and Industrial Design in Mechanical Engineering, Book of abstracts, Univerzitet u Novom Sadu, Fakultet tehničkih nauka, Novi Sad, 23-26 May 2024, godine u Hotel Marina, Balatonfüred, Hungary, ISBN 978-86-6022-339-7. COBISS.SR-ID 144621065, pp.128-129.
- [8] Muller, J.M., Buliga, O., Voigt, K.I.: Fortune favors the prepared: How SMEs approach business model innovations in Industry 4.0. *Technological Forecasting and Social Change*, Vol.132, Iss.C, pp.2–7. 2018. DOI: 10.1016/j.techfore.2017.12.019
- [9] Karabegović, I.,: Improving Innovativeness and Competitiveness in Germany, Japan and China Through the Analysis of the Application of Robotics as an Industry 4.0 Technology in the Manufacturing Industry, International Scientific Conference, Industry 4.0 in Circular Economy and Environmental Protection and Recovery, Union of Engineers and Technicians of Serbia, 15th December 2023. Beograd, Serbia, Proceedings: ISBN 978-86-82563-26-6, COBISS.SR-ID 131923977, pp. 38-51. <https://www.sits.org.rs/>
- [10] Karabegović, I., Turmanidže, R., Dašić, P., : Analysis of Patent Trends from Industry 4.0 and the Implementation of Robot Technology in the Countries of China, USA, Japan, Republic of Korea and Germany, 6th International Scientific Conference, Conference on Mechanical Engineering Technologies and Applications-COMET-a, 17th-19th November, 2022, East Sarajevo, pp.273-286., RS, Bosnia and Herzegovina.: <http://cometa.ues.rs.ba/>

- [11] Digital-Transformation-Monitor (2017) Country: Portugal “Indústria 4.0”. Technical report, European Commission. <https://ec.europa.eu/growth/toolsPosebnaizdanja> ANUBiH CCII, OTN knjiga 20, str. 49-68;
- [12] Prime-Minister’s-Office of Singapore (2016) Research, innovation and enterprise 2020 plan: winning the future through science and technology. Technical report, National Research Foundation of Singapore
- [13] Kang HS, Lee JY, Choi SS, Kim H, Park JH, Son JY, Kim BH, Noh SD (2016) Smart manufacturing past research, present findings, and future directions. *Int J PrecisEngManuf Green Technol* 3:111–128
- [14] Karabegović, I., Husak, E. Karabegović, E., Mahmić, M.,; How the Core Technologies of Industry 4.0 Are Changing the Automotive Industry in the World, With a Focus on China, IX International Congress Motor Vehicles and Motors (MVM 2022) IOP Conf. Series: Materials Science and Engineering 1271 012017; pp.1-14 ; doi:10.1088/1757-899X/1271/1/012017; <https://iopscience.iop.org/issue/1757-899X/1271/1>.
- [15] Karabegovic Edina, Karabegovic Isak, Hadzalic Edit Industrial Robot Application Trend in World’s Metal Industry *Inzinerine Ekonomika-Engineering Economics*, , 23(4), 368-378. 2012. <http://dx.doi.org/10.5755/j01.ee.23.4.2567>
- [16] World Intellectual Property Indicators 2022, <https://www.wipo.int/edocs/pubdocs/en/wipo-pub-941-2022-en-world-intellectual-property-indicators-2022.pdf>
- [17] European PatentOffice, Munich, Germany,2020, pp:7-13; <https://baa.no/en/services/ip-rights/>
- [18] UNCTAD (2018) Technology and innovation report 2021, United Nations conference on Trade and Development; based on data from Maddison Project Database, version 2018, Bolt et al. (2018), Perez (2002), and Schwab (2013).https://unctad.org/system/files/official-document/tir2020overview_en.pdf
- [19] Trademarks and patents in China: The impact of non-market factors on filing trends and IP systems.” January 2021. <https://www.uspto.gov/sites/default/files/documents/USPTOTrademarkPatentsInChina.pdf>
- [20] IFR, “World Robotics Report: ‘All-Time High’ with Half a Million Robots Installed in one Year,” IFR International Federation of Robotics.<https://ifr.org/ifr-press-releases/news/wr-report-all-time-highwith-half-a-million-robots-installed> [Accessed; June 26, 2024].
- [21] International Federation of Robotics, “Executive Summary World Robotics 2012Industrial Robots.”2012. [Online]. Available: https://ifr.org/img/worldrobotics/Executive_Summary_WR_Industrial_Robots_2012.pdf
- [22] International Federation of Robotics, “Executive Summary World Robotics 2022 Industrial Robots.”2022. [Online]. Available: https://ifr.org/img/worldrobotics/Executive_Summary_WR_Industrial_Robots_2022.pdf
- [23] Bill, M., Müller, C., Kraus, W., and Bieller, S.,: World Robotics Report 2023, Frankfurt 2023. [Online]. Available: <https://ifr.org/ifr-press-releases/news/world-robotics-2023-report-asia-ahead-of-europe-and-the-americas>

- [24] Belanger-Barretto, M., What Should be the First Collaborative Robot Application in Your Factory? 2016. <https://blog.robotiq.com/first-collaborative-robot-application-in-your-factories>; [Access: 15. Aug. 2024.]
- [25] BMW, General Motors among manufacturers using robots for efficiency, 2013 <https://www.newsday.com/classifieds/cars/bmw-general-motors-among-manufacturers-using-robots-for-efficiency-y29635>; [Access: 15. Aug. 2024.]
- [26] Figure 3 - Triple 3D Printing Production Production With Collaborative Robots <https://robotiq.com/resource-center/case-studies/triple-3d-printing-production-with-collaborative-robots>; [Access: 15. Aug. 2024.]
- [27] Figure 4 - Collaborative Robots for 3C Electronics Industry, <https://www.jakarobotics.com/industries/3c-electronics/>; [Access: 15. Aug. 2024.]
- [28] Karabegović, I.: The Role of Industrial and Service Robots in the Fourth Industrial Revolution, ACTE Technica Corviniensis-Bulletin of Engineering, University Politehnica Timisoara, Tome XI, Fascicule 2. April 2018. Hunedoara, Romania, pp. 11-16. 2018. <http://acta.fih.upt.ro/pdf/2018-2/ACTA-2018-2-01.pdf>
- [29] https://www.google.com/search?q=service+robots+for+logistics+i&tbm=isch&ved=2ahUKEwja1YjGx4v0AhVV56QKHSUnBBcQ2cCegQIABAA&oeq=service+robots+for+logistics+i&gs_lcp=CgNpbWcQDDIHCCMQ7wMQJ1AAWABgwxAHAAeACA AW OIAWOSAQExmA EAoAEBqgELZ3dzLXdpei1pbWfAAQE&sclient=img&ei=wY6KYZrxBtXmkgWlzpC4AQ&bih=757&biw=1821&rlz=1C1NHXL_hrBA708BA708#imgrc=94P-XI8uZvrhCM [Accessed: 16.7.2021]
- [30] Introducing the HD-1500. Our Strongest Mobile Robot. https://assets.omron.eu/downloads/brochure/en/v1/i854_hd-1500_leaflet_en.pdf [Accessed: 8.11.2021]
- [31] Autonomy The SqUID allows us to plan the future, <https://www.bionichive.com/> [Accessed: 15.11.2021]
- [32] Bill, M., Müller, C., Kraus, W., and Bieller, S.: World Robotics Report 2022, Frankfurt 2022. [Online]. Available: https://ifr.org/downloads/press2018/2022_WR_extended_version.pdf
- [33] Beaupre M., (2015), Collaborative Robot Technology and Applications, International Collaborative Robots, Workshop, Columbia, 7. October 2015. (https://www.robotics.org/userAssets/riaUploads/file/4-KUKA_Beaupre.pdf)
- [34] Karabegović, I., Karabegović, E., Mahmić, M., Husak E., : The Implementation of Industry 4.0 by Using Industrial and Service Robots in the Production Processes, Chapter 1. Handbook of Research on Integrating Industry 4.0 in Business and Manufacturing, IGI Global, USA, pp.1-30, 2020. DOI: 10.4018/978-1-7998-2725-2.ch001
- [35] Ostrgaard E., (2015), Collaborative Robot Technology and Applications, International Collaborative Robots, Workshop, Columbia, 7. October 2015. (www.robotics.org/robotics/international-collaborative-robots-workshop)
- [36] Karabegović, I., Karabegović, E., Mahmić, M., Husak, E.: Implementation of Industry 4.0 and Industrial Robots in Production Processes In: Isak Karabegović (eds) New Technologies, Development and Application II 2019. Lecture Notes in Networks and Systems. Springer Nature Switzerland AG 76, pp.96-102. 2020.



HANDLING AND STABILITY ANALYSIS OF AN AUTOMATED VEHICLE WITH INTEGRATED FOUR-WHEEL INDEPENDENT STEERING (4WIS)

Vasko Changoski¹, Igor Gjurkov², Vase Janushevska³

Received in July 2024

Accepted in August 2024

RESEARCH ARTICLE

ABSTRACT: The latest revisions of the UN and the European Union regulations regarding the steering system allow implementation of novel technologies in automated vehicles. Four-wheel independent steering (4WIS) system represents an upgrade of the steer-by-wire concept that enhances the capabilities of the steering system. The primary focus of this research is to enhance vehicle handling and stability performance by integration of four-wheel independent steering (4WIS) and vehicle stability control (VSC) system in an automated vehicle. A virtual vehicle equipped with 4WIS and VSC is created in ADAMS/Car. The proposed control algorithms are implemented in MATLAB/Simulink and their effect is tested in co-simulation environment. As a control method, Sliding Mode Control (SMC) is used to improve vehicle handling while maintaining vehicle stability under different driving conditions. The proposed concept is evaluated through different open-loop and path following manoeuvres to thoroughly assess its performance.

KEY WORDS: *Four-wheel independent steering (4WIS), steer-by-wire, co-simulation, vehicle handling, vehicle stability.*

© 2024 Published by University of Kragujevac, Faculty of Engineering

¹ Vasko Changoski, Ss. Cyril and Methodius University in Skopje, Faculty of Mechanical Engineering – Skopje, ul. Rugjer Boshkovikj 18, 1000 Skopje, Republic of North Macedonia,

vasko.changoski@mf.edu.mk,  <https://orcid.org/0000-0001-6148-9389> (*Corresponding author)

² Igor Gjurkov, Ss. Cyril and Methodius University in Skopje, Faculty of Mechanical Engineering – Skopje, ul. Rugjer Boshkovikj 18, 1000 Skopje, Republic of North Macedonia,

igor.gjurkov@mf.edu.mk,  <https://orcid.org/0000-0001-5887-8797>

³ Vase Janushevska, PhD., Assistant Professor, Ss. Cyril and Methodius University in Skopje, Faculty of Mechanical Engineering – Skopje, ul. Rugjer Boshkovikj 18, 1000 Skopje, Republic of North Macedonia, vase.janushevska@mf.edu.mk,  <https://orcid.org/0000-0001-5403-3447>

ANALIZA UPRAVLJANJA I STABILNOSTI AUTOMATIZOVANOG VOZILA SA INTEGRISANIM NEZAVISNIM UPRAVLJANJEM NA SVA ČETIRI TOČKA (4WIS)

REZIME: Najnovije revizije propisa UN i Evropske unije u vezi sa sistemom upravljanja omogućavaju implementaciju novih tehnologija u automatizovana vozila. Sistem nezavisnog upravljanja na četiri točka (4VIS) predstavlja nadogradnju koncepta upravljanja po žici koji poboljšava mogućnosti upravljačkog sistema. Primarni fokus ovog istraživanja je poboljšanje performansi upravljanja vozilom i stabilnosti integracijom nezavisnog upravljanja na sva četiri točka (4VIS) i sistema kontrole stabilnosti vozila (VSC) u automatizovano vozilo. Virtuelno vozilo opremljeno 4VIS i VSC je kreirano u ADAMS/Car. Predloženi kontrolni algoritmi su implementirani u MATLAB/Simulink i njihov efekat je testiran u ko-simulacionom okruženju. Kao metoda kontrole, kontrola kliznog režima (SMC) se koristi za poboljšanje upravljanja vozilom uz održavanje stabilnosti vozila u različitim uslovima vožnje. Predloženi koncept se procenjuje kroz različite manevre u otvorenom krugu i praćenju putanje kako bi se temeljno procenio njegov učinak.

KLJUČNE REČI: *Nezavisno upravljanje na četiri točka (4VIS), upravljanje po žici, kosimulacija, upravljanje vozilom, stabilnost vozila.*

HANDLING AND STABILITY ANALYSIS OF AN AUTOMATED VEHICLE WITH INTEGRATED FOUR-WHEEL INDEPENDENT STEERING (4WIS)

Vasko Changoski, Igor Gjurkov, Vase Janushevska

INTRODUCTION

Vehicle handling and stability is significantly improving with the advancement of vehicle automated systems. The introduction of active steering systems compared to the traditional front wheel steering system offers improved manoeuvrability but also can improve vehicle stability by correcting driver's commands. With the implementation of the Active Front Steering (AFS) system, a correction on the driver's input is made by adding or subtracting front wheel steering angle [22]. The AFS system could be further improved by applying steer-by-wire system. With the latest revision of the UN regulation ECE – R79 [18], a steer-by-wire concept can be implemented in the new vehicles. This would allow enhanced vehicle control and adaptability of the steering system. Steer-by-wire AFS system is analysed in [21] where a Sliding Mode Control (SMC) is applied in combination with Extreme Machine Learning that results in improved vehicle stability. Shuai et al. in [15] analyse integrated AFS steer-by-wire and direct yaw control (DYC) systems. The results are verified using co-simulation environment between MATLAB/Simulink and Carsim. AFS and DYC are used for integrated vehicle dynamic control with Sliding Mode Control (SMC) where the system demonstrates strong robustness against uncertainties but also improves the transient response of the control system [12].

Another approach in implementation of active steering system, but in this case using four wheels steering (4WS) system and integrated with DYC, is presented in [7] where a linear parameter varying (LPV) system and H_∞ optimal control theory are applied to improve vehicle stability. A comparison between vehicle equipped with vehicle stability system (VSC), vehicle with VSC and AFS and vehicle VSC and ARS systems is conducted in [1] where the 4WS vehicle shows greater vehicle stability and handling over the other vehicles. Further improvement in the steer-by-wire system represents the four-wheel independent steering (4WIS) system. Chen et al. suggest using SMC for tracking reference parameters by switching between front wheel steering, rear wheel steering and 4WIS [4]. Researchers in [3] apply Linear Quadratic Regulator (LQR) for coordinated control of 4WIS and four-wheel independent drive (4WID) vehicle for enhanced vehicle stability. Liang et al. suggest using SMC 4WID/4WIS vehicle to improve vehicle stability in high-speed conditions [11]. The authors implement SMC controllers for 4WIS system and SMC controller for yaw corrective moment in combination with phase-plane method (β - β') where a transition between the handling orientated control and stability orientated control is suggested based on the vehicle stability region. Yim and Jo compare different integration combination of AFS, ARS and ESC systems under force constraint of AFS system [20]. The systems are activated in different combination based on the tire side slip angle.

Another aspect of applying 4WIS steering is to improve vehicle path following control. Hang et al. in [6] use Model Predictive Control (MPC) for improved path following in 4WIS vehicle. The MPC controller is applied to control the four wheels steering angles and to apply corrective yaw moment. On the other hand, a combination of Linear Parameter Varying and H_∞ controllers is applied in 4WS vehicle equipped with DYC [5] to improve the trajectory following of autonomous ground vehicles. He et al. propose robust coordination control of AFS and ARS based on H_∞ controller [8]. The proposed algorithm

shows improved path tracking and stability of autonomous vehicles. A combination of SMC controller with Luenberger observer is applied in [10] in 4WID-4WIS vehicle to allow improved trajectory following. SMC control for path following manoeuvres is applied in 4WID vehicle [2] and in 4WIS vehicles [13,19].

The purpose of this research is to improve the handling and the stability of an automated vehicle with integrated 4WIS and VSC system using Sliding Mode Control. The proposed control algorithm utilizes the advantages of the 4WIS system by combining AFS and ARS systems, while maintaining Ackerman steering geometry thus enhancing the vehicle handling. When the stability of the vehicle is critically endangered then the VSC system is activated to stabilize the vehicle. The proposed control algorithm is also effective in following a predefined path trajectory while traveling at lower and higher velocities. The open-loop manoeuvres are defined using the standard ISO 7401 [17], while the path following manoeuvres are inspired by the standard ISO 3888-1 [17]. The main contribution of this study is the application of SMC controllers in steer-by-wire vehicle equipped with 4WIS and VSC, where the proposed concept can be used in both open loop and path following manoeuvres. The 4WIS system allows improvement in vehicle handling and stability while the occasional involvement of the VSC system further improves the vehicle stability. The integrated control algorithm exploits the advantages of both systems.

1 VEHICLE MODELS

Three vehicle models are used in this research: 3D virtual model created in ADAMS/Car, linear bicycle model and nonlinear bicycle model. The 3D virtual model is used to represent the real vehicle and to test the proposed control algorithm, while the bicycle models are used as reference models and for defining and executing the control algorithm.

1.1 4WIS virtual vehicle model

The 4WIS virtual vehicle model is created in the ADAMS/Car software. It consists of 4 independent steering wheels actuated by linear actuators. Two of the actuators responsible for the same axle steering wheels are positioned in one shared housing, but they are actuated individually. A steering wheel is still positioned in the vehicle through which the driver controls the vehicle's direction, but there is no mechanical linkage between the steering wheel and the steered wheels, thus achieving steer-by-wire steering system. The tested vehicle is equipped with vehicle stability control system (VSC), active front steering (AFS) and active rear steering (ARS) systems. These systems are explained in detail in the next section and this vehicle would be referred as VSC + 4WIS vehicle (figure 1).

The vehicle model represents a large crossover SUV with mass of 2150 kg. The vehicle is equipped with nonlinear tire models based on the Magic tire formula (Pacejka model 2002) and front and rear MacPherson suspension system. The vehicle parameters are presented in table 1.

Additionally to the VSC + 4WIS vehicle, two 3D vehicle models with standard front wheel steering system are created. One vehicle is without any automated system (passive vehicle) and another vehicle equipped only with VSC system implemented, referred to as VSC vehicle. These vehicles were created in order to compare the vehicle with the 4WIS system with vehicles with conventional steering system.

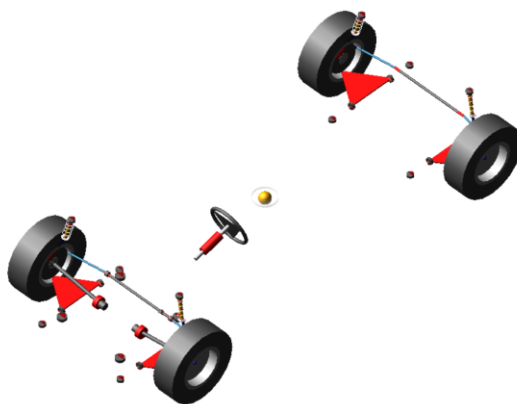


Figure 1 4WIS virtual vehicle model in ADAMS/CAR

Table 1 4WIS Virtual vehicle model - parameters

Mass (m):	2150 kg
Vehicle weight distribution (front/rear):	50/50 %
Length (L):	4635 mm
Width (W):	1890 mm
Wheelbase (l):	3000 mm
Front track width (b_f):	1508 mm
Rear track width: (b_r):	1508 mm

1.2 Linear bicycle model

Next, 2DOF linear bicycle model (figure 2) with rear wheel steering is used for the SMC controllers of the 4WIS system. Linear bicycle model is used for a simpler control algorithm for the 4WIS system and faster computation. On the other hand, the 4WIS system is mostly capable of improving the handling and stability of the vehicle in the linear region of the tires, while in terms of stability, when the vehicle is near its limits, the tires are well in the nonlinear region. In this situation the 4WIS system can help in stabilization of the vehicle, but the vehicle stability control system is more dominant. The linear bicycle model is defined using equations (1) and (2).

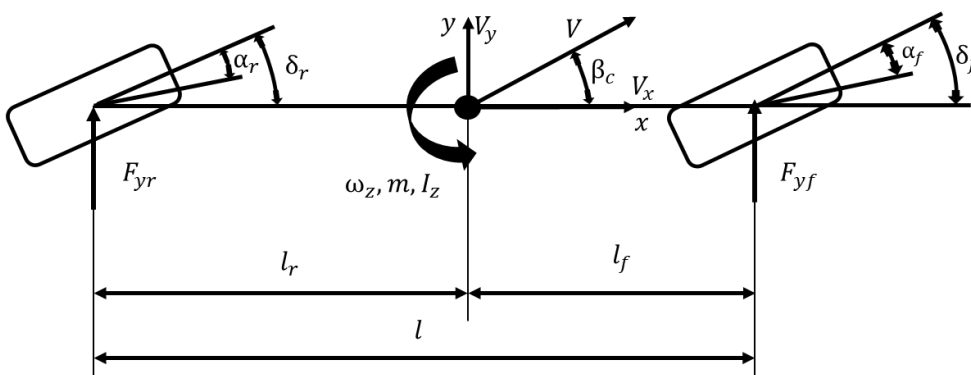


Figure 2 4WS Bicycle vehicle model

$$\dot{V}_y = \left(\frac{-C_{\alpha_f} - C_{\alpha_r}}{mV_x} \right) V_y + \left(\frac{C_{\alpha_r}l_r - C_{\alpha_f}l_f}{mV_x} - V_x \right) \omega_z + \frac{C_{\alpha_f}}{m} \delta_f + \frac{C_{\alpha_r}}{m} \delta_r, \quad (1)$$

$$\dot{\omega}_z = \left(\frac{C_{\alpha_r}l_r - C_{\alpha_f}l_f}{I_z V_x} \right) V_y + \left(\frac{-C_{\alpha_f}l_f^2 - C_{\alpha_r}l_r^2}{I_z V_x} \right) \omega_z + \frac{C_{\alpha_f}l_f}{I_z} \delta_f - \frac{C_{\alpha_r}l_r}{I_z} \delta_r, \quad (2)$$

The bicycle model is defined by its lateral velocity V_y and yaw rate ω_z . I_z defines vehicle material moment of inertia, β_c - vehicle side-slip angle, l_f and l_r define the distance from center of mass to the front and rear axle respectively. The input variables to the system are the front wheel steering angle (δ_f) and the rear wheel steering angle (δ_r). During the co-simulation the longitudinal velocity (V_x) is not constant, rather it is fed to the linear bicycle model from the current velocity of the virtual vehicle model from ADAMS/Car. In equation (3) the state-space model of the bicycle model is presented. It is used in the control algorithms.

$$\begin{bmatrix} \dot{V}_y \\ \dot{\omega}_z \end{bmatrix} = \begin{bmatrix} a_{11} & a_{12} \\ a_{21} & a_{22} \end{bmatrix} \begin{bmatrix} V_y \\ \omega_z \end{bmatrix} + \begin{bmatrix} b_{11} \\ b_{21} \end{bmatrix} \delta_f + \begin{bmatrix} b_{12} \\ b_{22} \end{bmatrix} \delta_r, \quad (3)$$

where $a_{11} = \frac{-C_{\alpha_f} - C_{\alpha_r}}{mV_x}$, $a_{12} = \frac{C_{\alpha_r}l_r - C_{\alpha_f}l_f}{mV_x} - V_x$, $a_{21} = \frac{C_{\alpha_r}l_r - C_{\alpha_f}l_f}{I_z V_x}$, $a_{22} = \frac{-C_{\alpha_f}l_f^2 - C_{\alpha_r}l_r^2}{I_z V_x}$, $b_{11} = \frac{C_{\alpha_f}}{m}$, $b_{12} = \frac{C_{\alpha_r}}{m}$, $b_{21} = \frac{C_{\alpha_f}l_f}{I_z}$, $b_{22} = -\frac{C_{\alpha_r}l_r}{I_z}$ while C_{α_f} and C_{α_r} represent the cornering stiffness of the front and rear tires, respectively.

1.3 Nonlinear bicycle model

Beside the linear bicycle model, a nonlinear vehicle bicycle model is used in the proposed concept. A 2WS nonlinear bicycle model (figure 3) is used as a reference model for the passive and the VSC vehicle, while 4WS nonlinear reference bicycle model is used for the VSC+4WS vehicle. The nonlinear bicycle model is described using equations (4) and (5). The same principle for the longitudinal velocity is applied here for the nonlinear bicycle model.

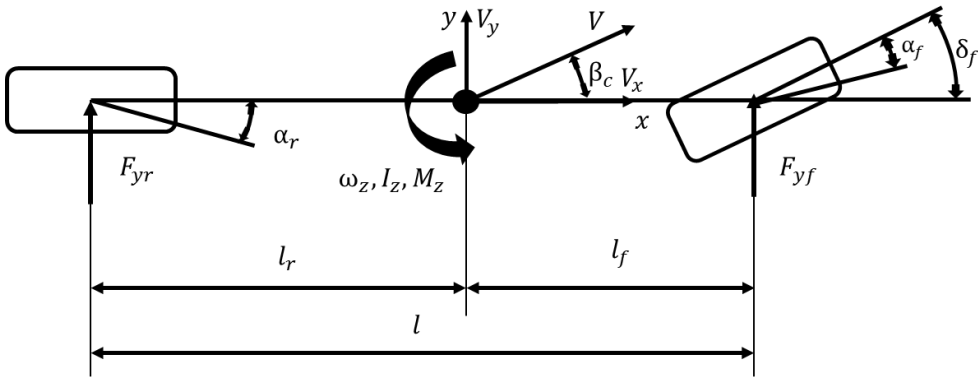


Figure 3 2WS Bicycle vehicle model

$$m(\dot{V}_y + V_x \omega_z) = F_{yf} + F_{yr}, \quad (4)$$

$$I_z \dot{\omega}_z = F_{yf} l_f - F_{yr} l_r, \quad (5)$$

The tire models are defined using the Magic Tire Formula presented in equations (6) and (7) where the front F_{yf} and rear F_{yr} tire lateral forces are defined in function to the front $\beta_f = \delta_f - \alpha_f$ and rear $\beta_r = \delta_r - \alpha_r$ tire side slip angles.

$$F_{yf} = D \sin\{C \operatorname{atan}[B\beta_f - E(B\beta_f - \operatorname{atan}(B\beta_f))]\}, \quad (6)$$

$$F_{yr} = D \sin\{C \operatorname{atan}[B\beta_r - E(B\beta_r - \operatorname{atan}(B\beta_r))]\}, \quad (7)$$

The coefficients of the Magic Tire Formula are presented in table 2 and are chosen for driving on a wet surface with $\mu=0.4$. These conditions are chosen during the co-simulation in order to test the vehicle stability and handling.

Table 2 Bicycle vehicle model and Magic Tire Formula - parameters

Front tire cornering stiffness (C_{af}):	120000 N/rad
Rear tire cornering stiffness (C_{ar}):	120000 N/rad
Inertia radius (i):	1275 mm
Pacejka tire model stiffness factor (B):	$C_{F\beta}/(CD)$
Pacejka tire model stiffness $C_{F\beta}$:	$C_a \sin\left\{2 \operatorname{atan}\left(\frac{F_n}{F_{nom}}\right)\right\}$
Pacejka tire model shape factor (C):	1.2
Pacejka tire model peak factor (D):	μF_n
Pacejka tire model curvature factor (E):	0

In table 2 the F_n parameter defines the tire vertical load. For the reference 4WS bicycle model, a linear control strategy is being used for the rear wheel steering. The control strategy is derived from equation (1) and it enables the vehicle to achieve zero value of the side-slip angle in steady and transient state. This reference model and control strategy presented in equation (8) is used because it had shown improved vehicle stability and handling in our previous research [1].

$$\delta_r = -\frac{c_{af}}{c_{ar}} \delta_f + \frac{mV_x^2 + c_{af}l_f - c_{ar}l_r}{c_{ar}V_x} \omega_z, \quad (8)$$

2 PROPOSED CONTROL ALGORITHM

The control strategy that is used in this research is based on sliding mode control theory. In equation (9) the sliding surface (s_i) is defined, where the error (e) is defined in equation (10) as a difference between the actual yaw rate (ω_z) of the 4WIS virtual model and the reference yaw rate (ω_{zref}).

$$s_i = \dot{e} + \lambda_i e \quad (9)$$

$$e = \omega_z - \omega_{zref} \quad (10)$$

To avoid destabilization of the reference model and thus destabilizing the 4WIS virtual vehicle, a limitation of the maximum yaw rate ω_{zmax} is defined using equation (11).

$$\omega_{zmax} = \left| \frac{\mu g}{V_x} \right| \quad (11)$$

The proposed control algorithm for the VSC+4WIS vehicle is presented in figure 4. The steering wheel angle applied by the driver is also used for the reference vehicle bicycle model where a steering ratio between the steering wheel and front steering wheels is assumed to be 1:16.71. A comparison between the actual yaw rate ω_z of the virtual vehicle model and the reference vehicle model ω_{zref} is made, thus defining the error (equation

(10)). The error signal is applied to the three SMC controllers. From here the 4WIS controllers output is applied to an Ackerman steering geometry to generate 4 independent steering angles, while the VSC controller output is applied to a torque distributor to generate 4 independent braking torques on each wheel. These elements and each SMC controllers are explained in detail in the next subsections.

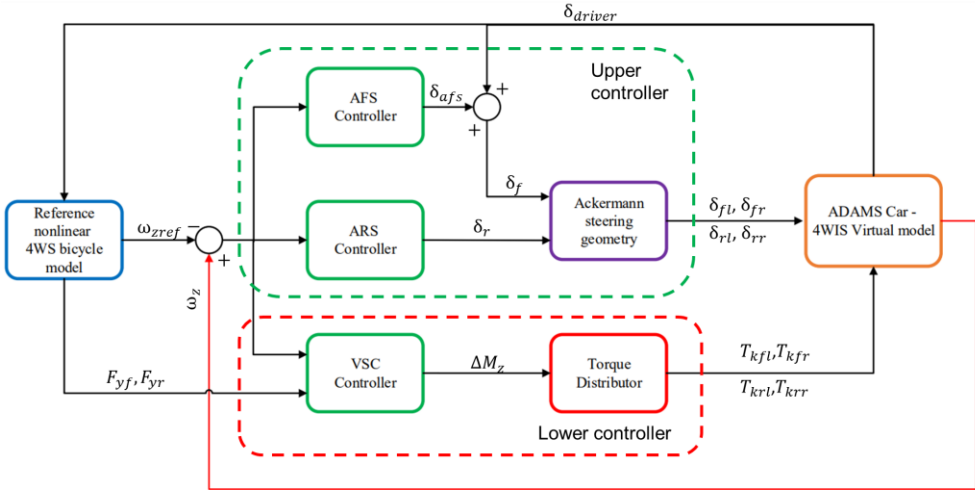


Figure 4 Proposed control algorithm diagram

2.1 4WIS control strategy

4WIS steering system control strategy is based on the linear bicycle model. As mentioned before this was adopted because the 4WIS system would have bigger impact on vehicle handling when the vehicle is not near its limits and is most effective in the linear region of the tires. Additionally, the usage of linear model allows faster computing process. The 4WIS control strategy is also named as upper controller in the system which is active continuously during the co-simulation. Although the vehicle possesses a steer-by-wire system, still the initial input to the system is defined by the driver and the steering wheel angle. The 4WIS control strategy is divided into two individual SMC controllers, one responsible for controlling the rear axle entirely and another responsible for correcting the driver's input to the front axle. In its core the 4WIS control strategy represents a combination of AFS and ARS systems.

The front wheels SMC controller is only responsible for correcting the driver's input and still the main command comes from the driver. Therefore, the front wheels steering angle is defined as combination of the driver's input (δ_{driver}) and the SMC controller output (δ_{afs}): $\delta_f = \delta_{driver} + \delta_{afs}$. If the desired error is $e = 0$, then the sliding surface would be $s = 0$. With that assumption if we combine equations (9) and (10), equation (12) is defined as:

$$\dot{e} = -\lambda_i e \quad (12)$$

By combining equation (2) and equation (12) the control law for the first SMC controller is presented in equation (13).

$$\delta_{afs} = \frac{1}{b_{21}} \left[-a_{21} V_y - a_{22} \omega_z - b_{21} \delta_{driver} - b_{22} \delta_r + \dot{\omega}_{ref} - \lambda_{afs} (\omega_z - \omega_{ref}) \right] \quad (13)$$

$$-k_{af_s} \tanh\left(\frac{s}{\phi_{af_s}}\right)$$

where the controller parameters are $\lambda_{af_s} = 3$ and $k_{af_s} = 0.087$, while sliding surface thickness is $\phi_{af_s} = 10$. The same principle is applied for the second SMC controller which is responsible for the independent steering angle of the rear wheels. In this case the SMC controller output defines the rear steering angle. The control law is presented in equation 14.

$$\delta_r = \frac{1}{b_{22}} \left[-a_{21} V_y - a_{22} \omega_z - b_{21} (\delta_{driver} + \delta_{af_s}) + \dot{\omega}_{ref} - \lambda_{ars} (\omega_z - \omega_{ref}) \right] - k_{ars} \tanh\left(\frac{s}{\phi_{ars}}\right) \quad (14)$$

where $\lambda_{ars} = 3$, $\phi_{ars} = 10$ and $k_{ars} = 0.087$. Combining equation (13) and (14) the 4WIS control law is derived. These two SMC controllers are defined as coupled control laws. The reason that coupled control laws are used instead of uncoupled is to derive more precise steered wheels angles and to achieve improved vehicle handling. On the other hand, this will result in increased demand for computation power and longer duration of the co-simulation.

2.2 Ackerman steering geometry

The output of the 4WIS SMC controllers defines the desired front and rear steering angles of the vehicle bicycle model. To define the steering angles of the four wheels, an Ackerman steering geometry is used (figure 5). Depending on the front and rear wheels steering directions, two cases are defined. The first case is when the front and rear wheels are steered in same direction and the second case when the wheels are steered in opposite direction. Based on the SMC controller outputs and the desired steering angles, equations (15.a) and (15.b) are used when the SMC controllers impose same direction steering angles and equations (16.a) and (16.b) are used when the controllers demand opposite direction steering. δ_{fi} and δ_{fo} define the front inner and outer steering wheel angle respectively, while δ_{ri} and δ_{ro} define the rear inner and outer steering wheel angle respectively.

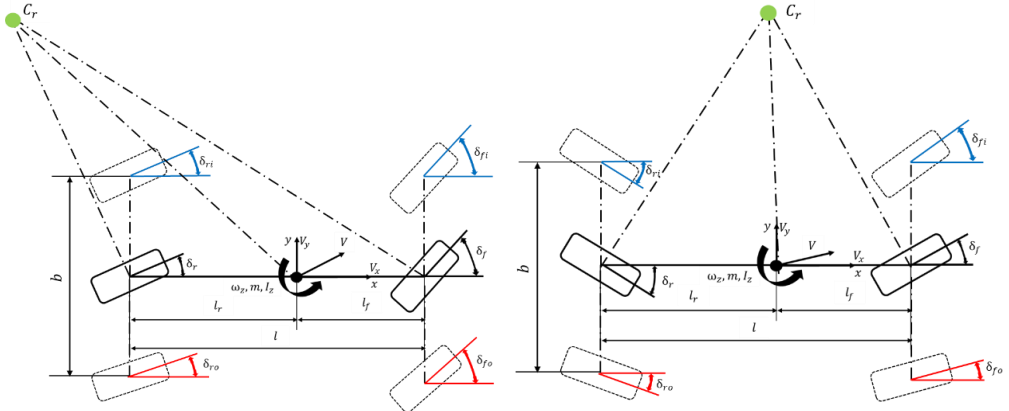


Figure 5 4WIS kinematic model, (a) Front and rear wheels are turned in the same direction, (b) Front and rear wheels are turned in the opposite direction.

$$\delta_{fi} = \operatorname{atan}\left(\frac{\tan \delta_f}{1 - \frac{b}{2l} (\tan \delta_f - \tan \delta_r)}\right), \quad \delta_{fo} = \operatorname{atan}\left(\frac{\tan \delta_f}{1 + \frac{b}{2l} (\tan \delta_f - \tan \delta_r)}\right) \quad (15.a)$$

$$\delta_{ri} = \operatorname{atan}\left(\frac{\tan \delta_r}{1 - \frac{b}{2l}(\tan \delta_f - \tan \delta_r)}\right), \delta_{ro} = \operatorname{atan}\left(\frac{\tan \delta_r}{1 + \frac{b}{2l}(\tan \delta_f - \tan \delta_r)}\right) \quad (15.b)$$

$$\delta_{fi} = \operatorname{atan}\left(\frac{\tan \delta_f}{1 - \frac{b}{2l}(\tan \delta_f + \tan \delta_r)}\right), \delta_{fo} = \operatorname{atan}\left(\frac{\tan \delta_f}{1 + \frac{b}{2l}(\tan \delta_f + \tan \delta_r)}\right) \quad (16.a)$$

$$\delta_{ri} = \operatorname{atan}\left(\frac{\tan \delta_r}{1 - \frac{b}{2l}(\tan \delta_f + \tan \delta_r)}\right), \delta_{ro} = \operatorname{atan}\left(\frac{\tan \delta_r}{1 + \frac{b}{2l}(\tan \delta_f + \tan \delta_r)}\right) \quad (16.b)$$

2.3 VSC control strategy

Unlike the 4WIS control strategy a SMC controller algorithm for the VSC system is derived based on a nonlinear vehicle bicycle model. This is because the VSC system is activated when the tires are in their nonlinear region and the vehicle is on verge of destabilization. To define the VSC controller in equation (5) the corrective yaw moment ΔM_z is added. In this case the vehicle bicycle model is presented in figure 6 with the corrective yaw moment ΔM_z and the new equation is presented in equation (17). Using the same analogy as the 4WIS controllers and equations (12) and (17), the VSC controller output is defined using the equation (18).

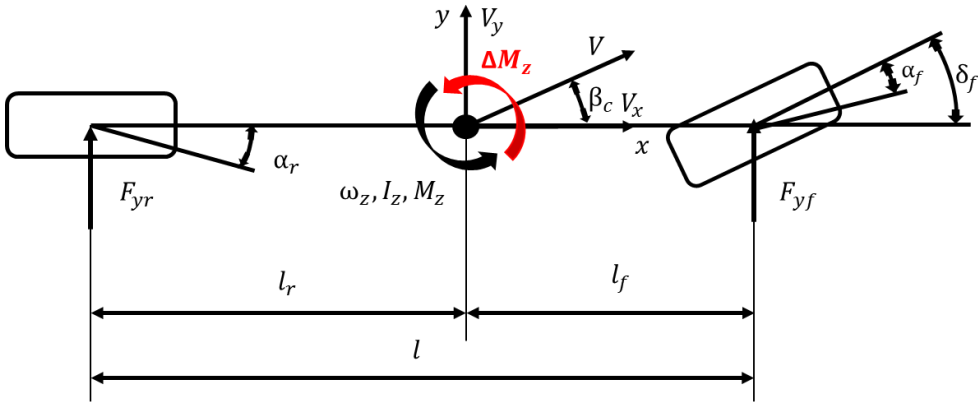


Figure 6 2WS Bicycle vehicle model with corrective yaw moment

$$I_z \dot{\omega}_z = F_{yf} l_p - F_{yr} l_z + \Delta M_z \quad (17)$$

$$\Delta M_z = -F_{yf} l_p + F_{yr} l_z - I_z \dot{\omega}_{ref} + I_z \lambda_{vsc} (\omega_z - \omega_{ref}) - k_{vsc} \tanh\left(\frac{s}{\phi_{vsc}}\right) \quad (18)$$

where $\lambda_{vsc} = 3$, $\phi_{vsc} = 3$ and $k_{vsc} = -3$. After defining the desired corrective yaw moment from the SMC controller, a braking torque distribution must be made to each wheel. The VSC system is designed to brake the wheels on same side simultaneously. If the value $\Delta M_z > 0$ then the left wheels are braked, while when $\Delta M_z < 0$ the right wheels are braked. The braking forces of each wheel in relation with the ΔM_z are presented in equation (19).

$$\Delta M_z = \frac{F_{xfl}b_f}{2} + \frac{F_{xrl}b_r}{2} - \frac{F_{xfr}b_f}{2} - \frac{F_{xrr}b_r}{2} \quad (19)$$

where F_{xij} defines the longitudinal tire force on each wheel while b_f and b_r represent vehicle front and rear track width respectively. Using equation (20) the total braking torque that should be applied to wheels is taken into consideration.

$$\begin{cases} \Delta M_z > 0 \rightarrow Tk = (F_{xfl} + F_{xrl})r_d \\ \Delta M_z < 0 \rightarrow Tk = (F_{xfr} + F_{xrr})r_d \end{cases} \quad (20)$$

where $r_d = 0.33 \text{ m}$ represents the tires rolling radius and the braking system is designed to allow 60/40 torque distribution between the front and rear wheels.

To avoid constant activation of the VSC system a phase-plane method ($\beta - \dot{\beta}$) is used. The stable region is below the value of 0.7 which is determined by testing the proposed control algorithm. This value allows activation of the VSC system to stabilize, but also the activation is not so frequent thus allowing the vehicle to perform different manoeuvres without interference in the stable region of the phase-plane method ($\beta - \dot{\beta}$).

$$|C_1\beta + C_2\dot{\beta}| \leq 0.7 \quad (19)$$

The values of $C_1 = 2.41$ and $C_2 = 9.615$ are used as suggested in [9].

2.4 4WIS control strategy for path following manoeuvres

For the path following manoeuvres a modification of the 4WIS must be made. In this case the driver is omitted and there is no input from him while the vehicle is forced to follow predefined trajectory. Therefore, the reference variables are now changed and the sliding surface and error are defined differently. Instead of the yaw rate error (equation (10)) the path deviation is defined using the lateral position y and yaw angle φ of the vehicle. The new error e_p is defined in equation (20) by combination of lateral position error $e_1 = y - y_{ref}$ and yaw angle error $e_2 = \varphi - \varphi_{ref}$.

$$e_p = y - y_{ref} + \xi(\varphi - \varphi_{ref}) \quad (20)$$

where $\xi = 1.5$ represents a weighing coefficient. The reference lateral position y_{ref} is predetermined based on the defined trajectory while the reference yaw angle φ_{ref} is defined in equation (21) [13] based on the relations described by Rajamani [14].

$$\varphi_{ref} = \text{atan} \frac{\dot{y}_{ref}}{\dot{x}_{ref}} \approx \frac{\dot{y}_{ref}}{\dot{x}_{ref}} \quad (21)$$

From here the error derivative is described using equation (22).

$$\dot{e}_p = V_x\varphi + V_y - \dot{y}_{ref} + \xi(\omega_z - \dot{\varphi}_{ref}) \quad (22)$$

After combining the equations (1), (2) and (12) with equations (20), (21) and (22) the coupled control laws for the front δ_{fp} and rear δ_{rp} wheel angles for path following are defined using equations (23) and (24).

$$\delta_{fp} = \frac{1}{b_{11}} [a_{11}V_x\varphi + \dot{V}_y - a_{12}\omega_z - b_{12}\delta_{rp} + \dot{y}_{ref} + \xi(\omega_z - \dot{\varphi}_{ref}) + \quad (23)$$

$$\lambda_{fp}(e_1 + \xi e_2)] - k_{fp} \tanh\left(\frac{s}{\phi_{fp}}\right)$$

$$\delta_{rp} = \frac{1}{b_{12}} [a_{11} V_x \varphi + \dot{V}_y - a_{12} \omega_z - b_{11} \delta_{fp} + \dot{y}_{ref} + \xi(\omega_z - \dot{\varphi}_{ref}) + \lambda_{rp}(e_1 + \xi e_2)] - k_{rp} \tanh\left(\frac{s}{\phi_{rp}}\right) \quad (24)$$

where $\lambda_{fp} = \lambda_{rp} = 3$, $\phi_{fp} = \phi_{rp} = 10$ and $k_{fp} = k_{rp} = 0.087$. The proposed control law is presented in figure 7, where it can be observed that the control law for the VSC system remains the same where a yaw rate error is used for system control, while the reference yaw rate is still obtained from the nonlinear bicycle model.

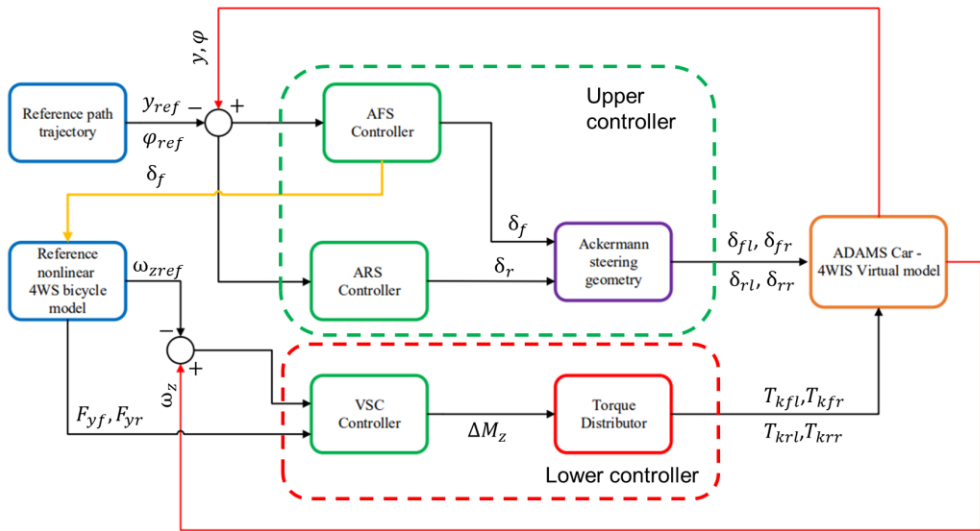


Figure 7 Proposed control algorithm diagram for path following manoeuvres

3 CO-SIMULATION RESULTS

To test the proposed control algorithm and the 4WIS steering system, a co-simulation was conducted where the virtual vehicles are tested using standardized open-loop and path following manoeuvres. The open-loop manoeuvres that were conducted are step-steer and single lane-change manoeuvre, based on the ISO 7401 standard with the vehicle travelling at 80 km/h. The velocity is not maintained during the manoeuvres, rather it decreases because of the activation of the VSC system or the destabilization of the vehicle. The open-loop manoeuvres are conducted on a wet surface with friction coefficient of $\mu=0.4$. This surface was chosen in order to test the vehicles stability and handling in worsening road conditions and to achieve lateral acceleration of 4 m/s^2 in order to fulfil the ISO 7401 standard.

3.1 Step-steer manoeuvre

According to the ISO 7401 standard, the steering wheel is turned for 0.5 s and is maintained at the maximum value during the manoeuvre. The maximum value of the steering wheel (figure 8) is determined as to achieve lateral acceleration of 4 m/s^2 in steady-state condition (figure 9). Based on the analysis in figures 10 and 11 it could be observed that the

VSC+4WIS vehicle steers the wheels in same direction and the values of the front steering wheels angles are larger than the passive and VSC vehicle. That would impose the need for slightly larger mounting space for the steering system. Figure 9 shows that the standard ISO 7401 has been fulfilled and all vehicles achieve 4 m/s^2 in steady-state condition. Also, all vehicles are at their physical limits. This can be also shown in figure 12 where the yaw rate of the passive vehicle indicates that the vehicle has started to lose its stability. On the other hand, both VSC and VSC+4WIS vehicles remain stable. This can be seen in figure 13 where the side-slip angle of the passive vehicle starts to rise exponentially. On the other hand, the VSC+4WIS vehicle has a near zero value of the side-slip angle, thus significantly improving the driver's awareness of the vehicle traveling direction. VSC+4WIS vehicle also shows lowest velocity decrease, while completing the manoeuvre successfully (figure 14). Figure 15 presents the trajectory of all the vehicles, and they are very similar. If the simulation time is prolonged, than a destabilization of the passive vehicle would be also shown on the trajectory diagram. It is also worth noting that the VSC system activates only the left wheel brakes (the vehicle turns to the left) indicating that the vehicles had shown understeer characteristics, but the activation of the brakes in VSC+4WIS vehicle is shorter (figure 16).

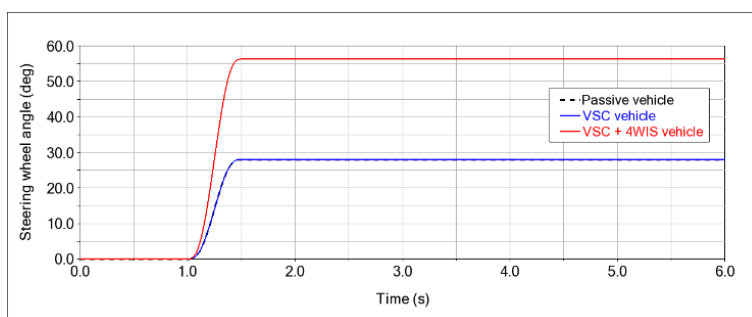


Figure 8 Steering wheel angle

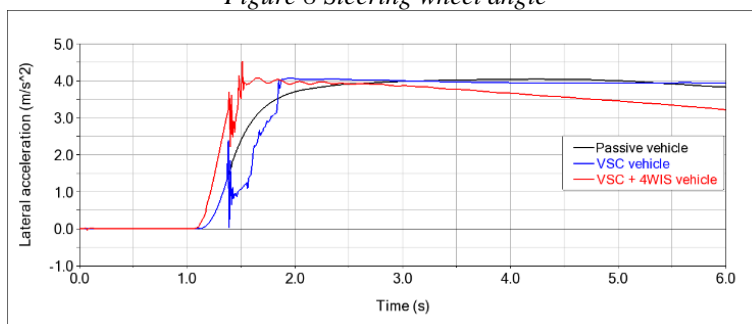


Figure 9 Lateral acceleration

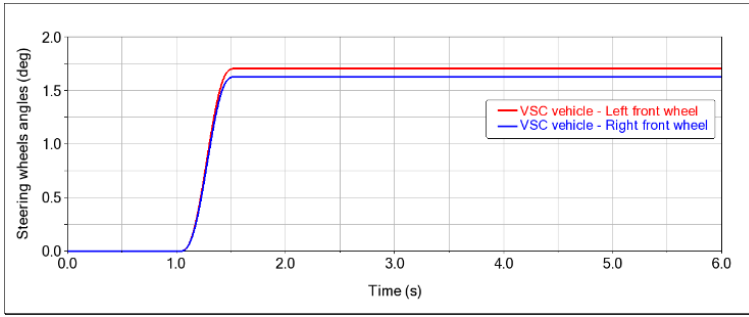


Figure 10 VSC vehicle - front and rear steering wheels angle

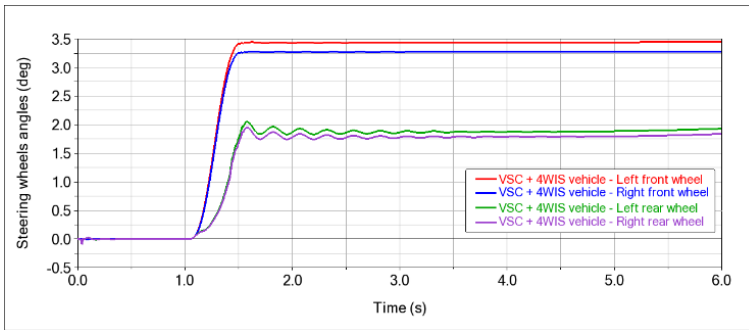


Figure 11 VSC + 4WIS vehicle - front and rear steering wheels angle

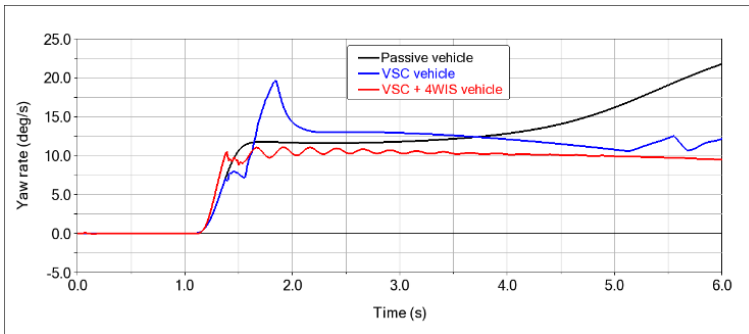


Figure 12 Yaw rate

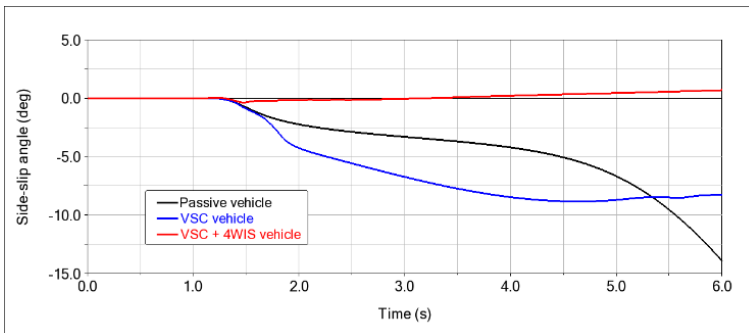


Figure 13 Side-slip angle

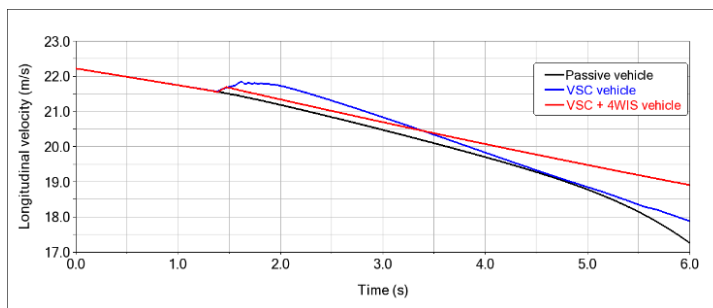


Figure 14 Longitudinal velocity

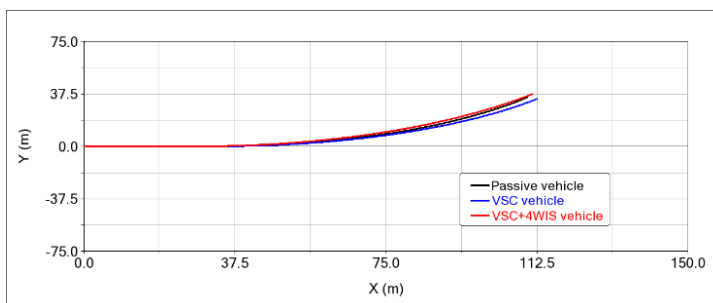


Figure 15 Trajectories

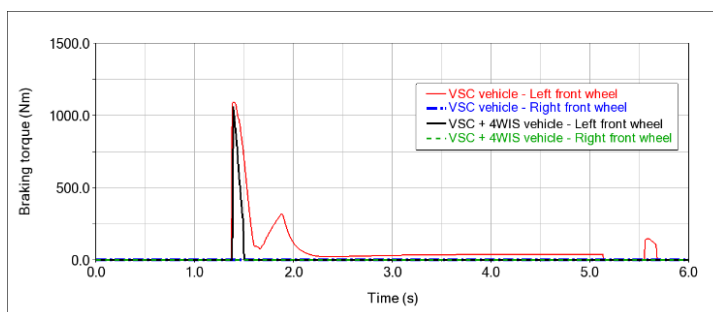


Figure 16 Braking torque – VSC and VSC + 4WIS vehicle

3.2 Single lane-change manoeuvre

Beside the step-steer manoeuvre, a single lane-change manoeuvre was conducted. The input signal from the driver is defined as one full period sinus function with frequency of 0.5 Hz (figure 17). According to the standard, the initial velocity of the vehicles is 80 km/h and the steering wheel angles are determined by the request for the vehicles to achieve lateral acceleration of 4 m/s^2 in the first peak value (figure 18). The conclusions are similar to the previous manoeuvre, but in this scenario the difference between the vehicles is larger. Figures 19 and 20 represents the steering wheel angles where the VSC+4WIS vehicle requires larger values. The first considerable difference could be observed in figure 18 where the passive vehicle loses its stability and fails to complete the manoeuvre. Also, the reaction time and the settling time of the VSC+4WIS vehicle is shorter than the VSC vehicle. The same conclusions can be derived from figure 21. The smoother transition of

VSC+4WIS and shorter settling time implies that the VSC+4WIS vehicle possesses improved handling and stability. This conclusion can be confirmed in figures 22 and 23 where the values of the side-slip angle of the VSC+4WIS are more than 2.5 times smaller than the VSC vehicle. In figures 22 and 25 it is once again shown that the passive vehicle loses its stability. Figure 25 also shows that the VSC+4WIS needs narrower road to complete the manoeuvre. During the manoeuvring of the vehicles with automated system, their velocity is decreased insignificantly compared to the passive vehicle that swerves out (figure 24). The superiority of the 4WIS system is more noticeable in this manoeuvre where the 4WIS manages to stabilize the vehicle while the VSC system is activated only in short time interval and with smaller braking torque values (figure. 26). On the other hand, the VSC system of the VSC vehicle is activated more often and with bigger intensity, but still the VSC vehicle shows reduced stability and handling characteristics compared to the VSC+4WIS vehicle.

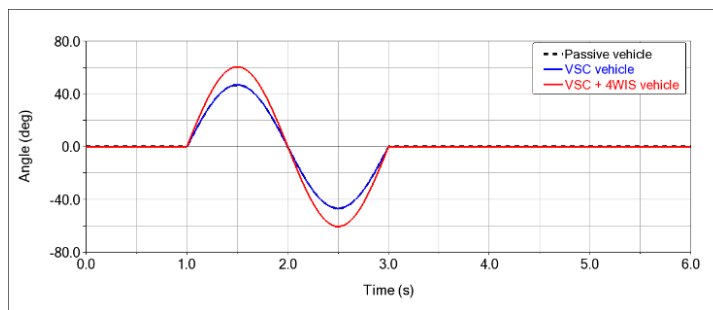


Figure 17 Steering wheel angle

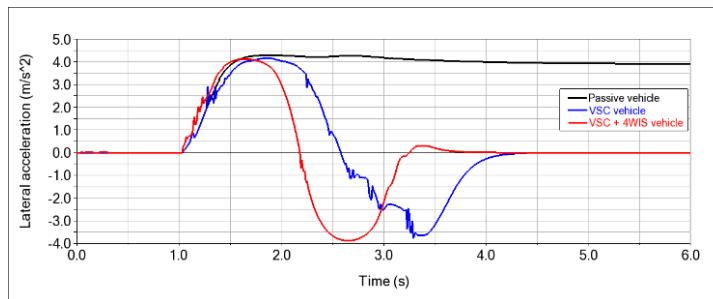


Figure 18 Lateral acceleration

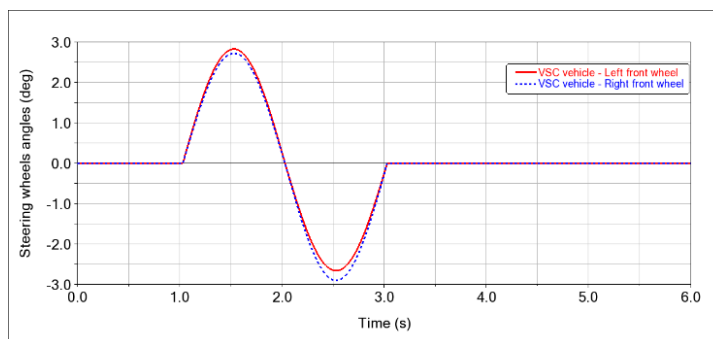


Figure 19 VSC vehicle - front and rear steering wheels angle

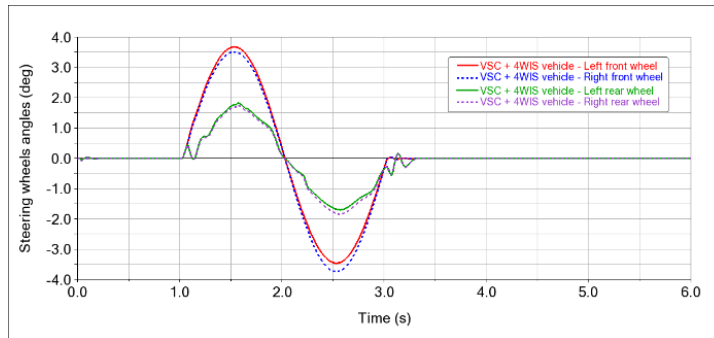


Figure 20 VSC + 4WIS vehicle - front and rear steering wheels angle

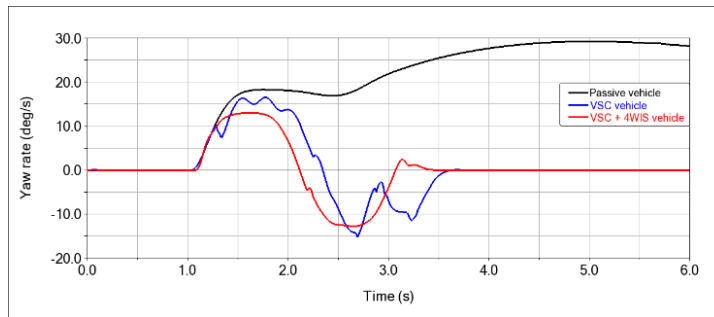


Figure 21 Yaw rate

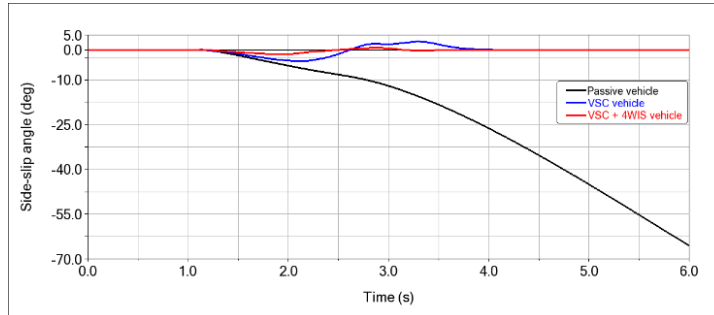


Figure 22 Side-slip angle

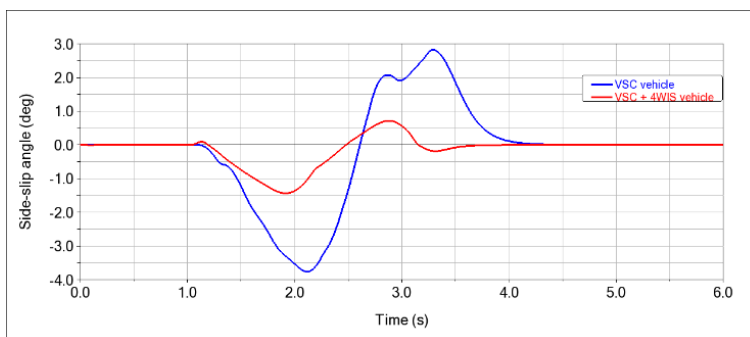


Figure 23 Side-slip angle of the alternative vehicles

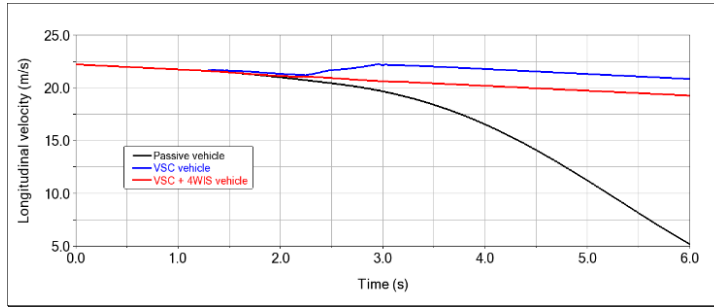


Figure 24 Longitudinal velocity

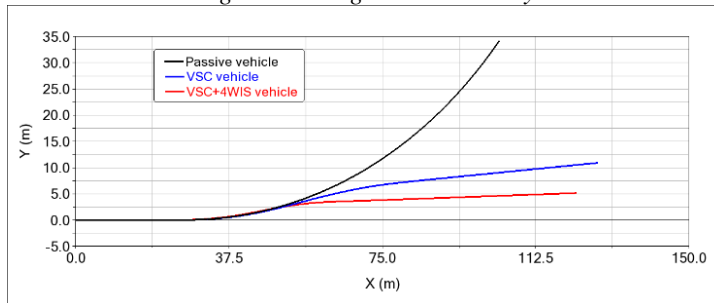


Figure 25 Trajectories

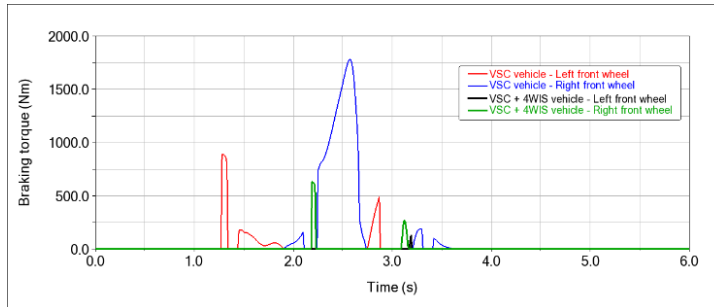


Figure 26 Braking torque – VSC and VSC + 4WIS vehicle

3.3 Path-following manoeuvres

The path-following manoeuvres are inspired by the ISO 3888 standard [16] where the trajectory dimensions and its boundaries are defined according to it. The trajectory's boundaries are presented in figure 27, where the blue line represents the reference central line that the vehicle should follow. In order to make the trajectory smoother, a combination of step and cosine function is defined. These manoeuvres are conducted in order to test the proposed control algorithm of the VSC+4WIS vehicle and its capabilities to follow a desired trajectory. The co-simulation is conducted only on the VSC+4WIS vehicle because the other vehicles do not possess automated steering system. One simulation is performed where the vehicle is traveling at 50 km/h, a city cruising speed, and one simulation is conducted according to the standard where the vehicle is traveling at 80 km/h. The tests are conducted on dry surface with friction coefficient $\mu=0.9$.

The first set of results represents a co-simulation when the vehicle is traveling with 50 km/h. In figure 27 it could be observed that the vehicle is following the reference trajectory within

the boundaries of the vehicles. The offset of the reference trajectory can be result on several parameters such as the fact that the reference trajectory is purely kinematic and could be further optimized, the inertia of the vehicle itself, lack of longitudinal controller and lack of prediction horizon. Figure 28 shows the steering wheel angles, while from figures 29, 30 and 31 it can be concluded that the vehicle is stable during the manoeuvring process and the values are within the desired limits. Figure 32 presents the longitudinal velocity of the vehicle where it can be seen that the vehicle completes the manoeuvre successfully with the predefined velocity. Beside the 4WIS, the activation of the VSC system maintains the stability of the vehicle (figure 33).

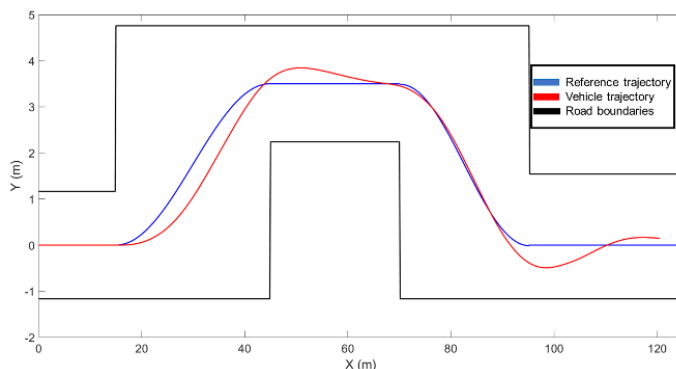


Figure 27 Trajectory – 50 km/h

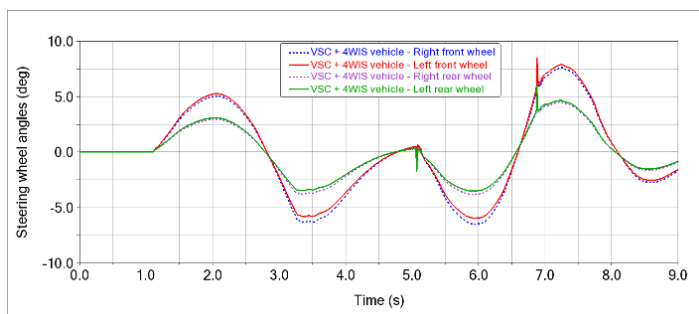


Figure 28 Front and rear steering wheels angle– 50 km/h

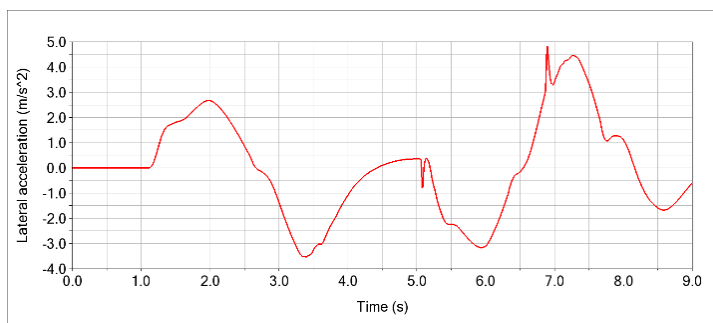


Figure 29 Lateral acceleration – 50 km/h

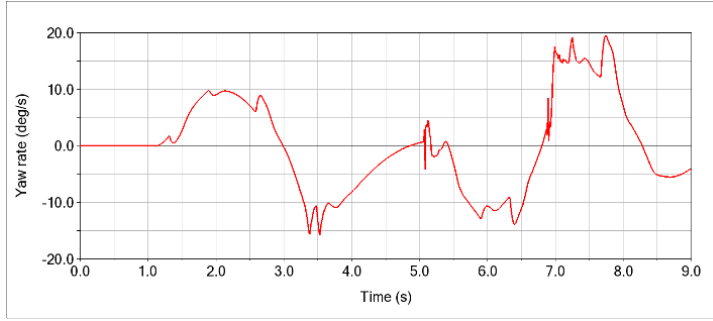


Figure 30 Yaw rate – 50 km/h

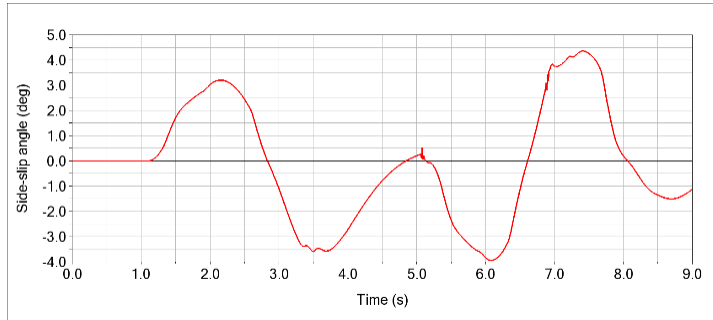


Figure 31 Side-slip angle – 50 km/h

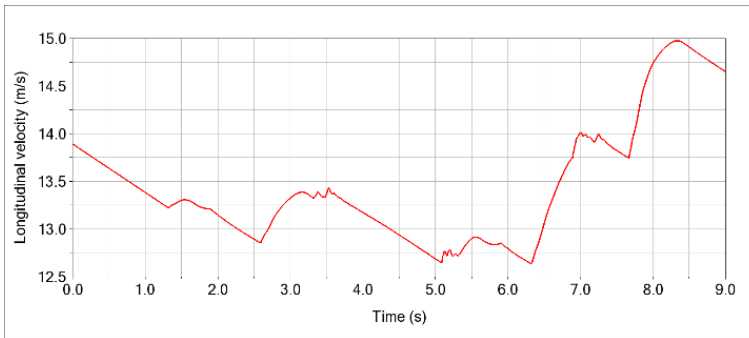


Figure 32 Longitudinal velocity – 50 km/h

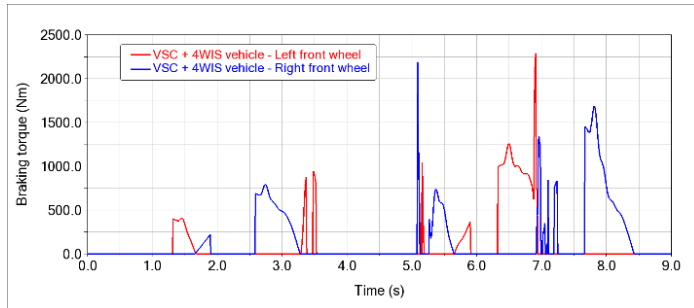


Figure 33 Braking torque – 50 km/h

In order to test path-following capability of the proposed control algorithm of the VSC+4WIS vehicle the manoeuvre was repeated in a scenario where the vehicle is traveling at 80 km/h. From figure 34 it can be concluded that the vehicle passes the manoeuvre successfully, while maintaining its stability, at 60 meters longitudinally the vehicle shows larger offset of the reference trajectory. This may lead to small collision between the side of the vehicle and the road boundary. Figure 35 presents the steering wheel angle. Figures 36, 37 and 38 present the lateral acceleration, yaw rate and the side-slip angle where it can be observed that the vehicle maintains its stability, but due to the larger values compared to the previous manoeuvre it is obvious that the vehicle is on its limits. This could be also observed in figure 40 where the VSC system is activated more frequently and with higher intensity. During the manoeuvre the vehicle almost maintains the desired velocity (figure 39).

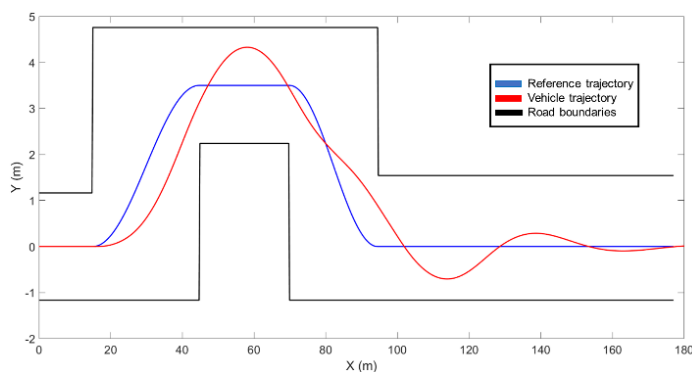


Figure 34 Trajectory – 80 km/h

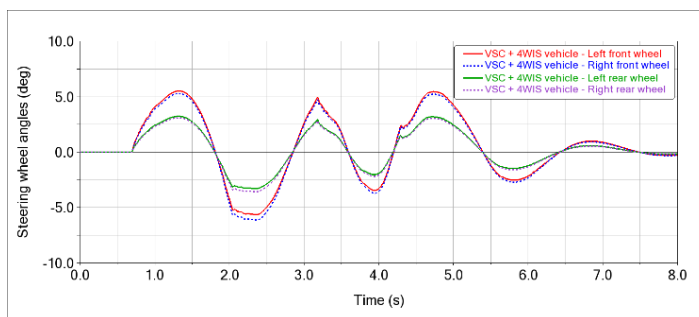


Figure 35 Front and rear steering wheels angle – 80 km/h

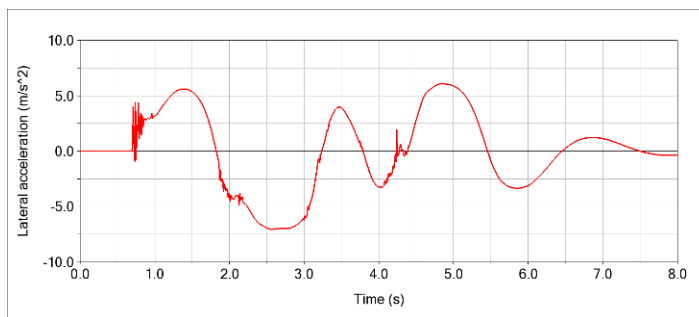


Figure 36 Lateral acceleration – 80 km/h

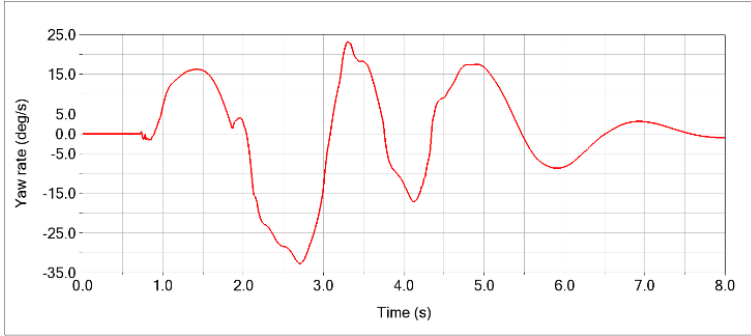


Figure 37 Yaw rate – 80 km/h

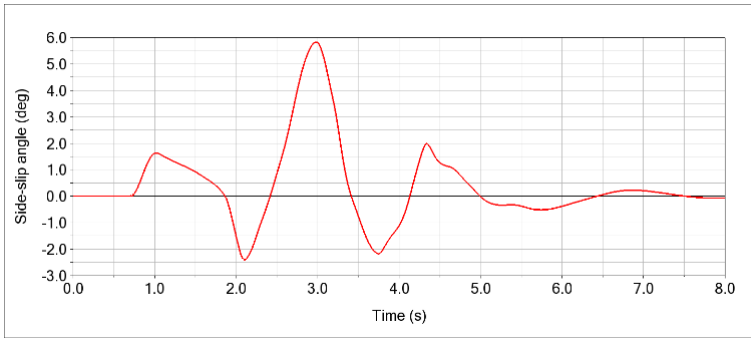


Figure 38 Side-slip angle – 80 km/h

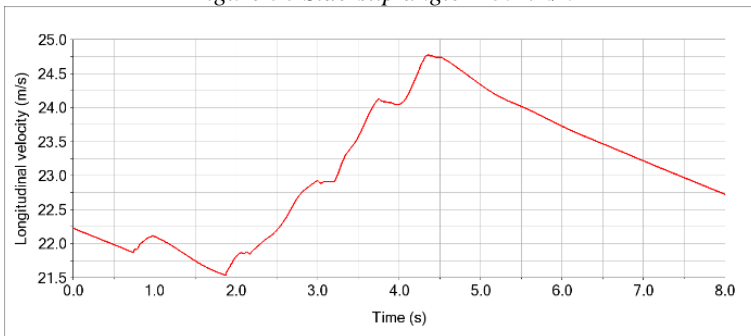


Figure 39 Longitudinal velocity– 80 km/h

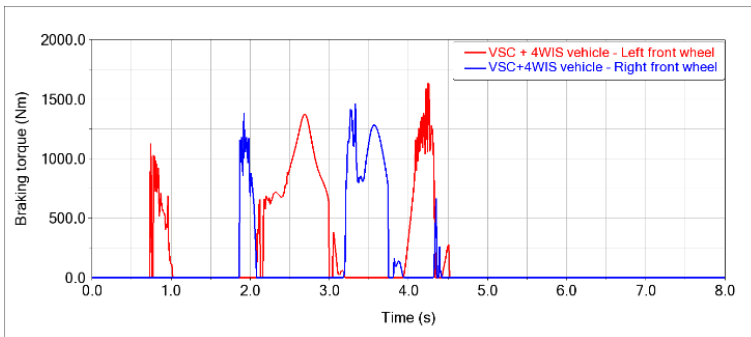


Figure 40 Braking torque – 80 km/h

4 CONCLUSIONS

The implementation of 4WIS steering system as a steer-by-wire system would improve the vehicle handling and stability of the vehicle as shown in this research. The VSC+4WIS has shown that the 4WIS system is responsible for improving vehicle handling and stability while the tires are in their linear region, but when combined with the VSC system the vehicle has improved stability in the tires nonlinear region. This can be confirmed with the fact that the VSC system is activated less frequently and with smaller intensity compared to the VSC vehicle. Also, lower vehicle side-slip angle values of the VSC+4WIS result in improved drivers handling feel during manoeuvring.

Beside the open loop manoeuvres, the proposed control algorithm with small modification could be implemented in path-following manoeuvre resulting in improved autonomous vehicle handling and stability. Further improvement in the control algorithm could be applied by adding longitudinal controller which would mostly improve the vehicle path-following capabilities.

REFERENCES

- [1] Changoski, V., Gjurkov, I., Jordanoska, V.: "Improving vehicle dynamics employing individual and coordinated sliding mode control in vehicle stability, active front wheel steering and active rear wheel steering systems in co-simulation environment", In IOP Conference Series: Materials Science and Engineering, Vol. 1271, No. 1, 2022, p. 012026.
- [2] Chen, J., Shuai, Z., Zhang, H., Zhao, W.: "Path following control of autonomous four-wheel-independent-drive electric vehicles via second-order sliding mode and nonlinear disturbance observer techniques", IEEE Transactions on Industrial Electronics, Vol. 68, No. 3, 2020, pp.2460-2469.
- [3] Chen, X., Han, Y., Hang, P.: "Researches on 4WIS-4WID stability with LQR coordinated 4WS and DYC", In The IAVSD International Symposium on Dynamics of Vehicles on Roads and Tracks, 2019, pp. 1508-1516.
- [4] Chen, X., Luo, F., Hang, P. Luo, J.: "Steering Mode Switch Control of Four-Wheel-Independent-Steering Electric Vehicle", In Proceedings of the 19th Asia Pacific Automotive Engineering Conference & SAE-China Congress 2017: Selected Papers, 2019, pp. 437-453.
- [5] Hang, P., Chen, X., Luo, F.: "LPV/H ∞ controller design for path tracking of autonomous ground vehicles through four-wheel steering and direct yaw-moment control", International Journal of Automotive Technology, Vol. 20, 2019, pp.679-691.
- [6] Hang, P., Luo, F., Fang, S., Chen, X.: "Path tracking control of a four-wheel-independent-steering electric vehicle based on model predictive control", In 2017 36th Chinese control conference (CCC), 2017, pp. 9360-9366.
- [7] Hang, P., Xia, X., Chen, X.: "Handling stability advancement with 4WS and DYC coordinated control: A gain-scheduled robust control approach", IEEE Transactions on Vehicular Technology, Vol. 70, No. 4, 2021, pp.3164-3174.
- [8] He, X., Liu, Y., Yang, K., Wu, J., Ji, X.: "Robust coordination control of AFS and ARS for autonomous vehicle path tracking and stability", In 2018 IEEE International Conference on Mechatronics and Automation (ICMA), 2018, pp. 924-929.
- [9] Jin, L., Xie, X., Shen, C., Wang, F., Wang, F., Ji, S., Guan, X., Xu, J.: "Study on electronic stability program control strategy based on the fuzzy logical and genetic

- optimization method”, *Advances in Mechanical Engineering*, Vol. 9, No. 5, 2017, p.1687814017699351.
- [10] Lei, Y.L., Wen, G., Fu, Y., Li, X., Hou, B., Geng, X.: “Trajectory-following of a 4WID-4WIS vehicle via feedforward-backstepping sliding-mode control”, *Proceedings of the Institution of Mechanical Engineers, Part D: Journal of Automobile Engineering*, Vol. 236, No. 2-3, 2022, pp.322-333.
- [11] Liang, Y., Li, Y., Yu, Y., Zheng, L.: “Integrated lateral control for 4WID/4WIS vehicle in high-speed condition considering the magnitude of steering”, *Vehicle System Dynamics*, Vol. 58, No. 11, 2020, pp.1711-1735.
- [12] Mousavinejad, E., Han, Q.L., Yang, F., Zhu, Y., Vlacic, L.: “Integrated control of ground vehicles dynamics via advanced terminal sliding mode control”, *Vehicle System Dynamics*, Vol. 55, No. 2, 2017, pp.268-294.
- [13] Norouzi, A., Adibi-Asl, H., Kazemi, R. Hafshejani, P.F.: “Adaptive sliding mode control of a four-wheel-steering autonomous vehicle with uncertainty using parallel orientation and position control”, *International Journal of Heavy Vehicle Systems*, Vol. 27, No. 4, 2020, pp.499-518.
- [14] Rajamani, R.: “Vehicle dynamics and control”, Springer Science & Business Media, 2011.
- [15] Shuai, Z., Zhang, H., Wang, J., Li, J., Ouyang, M.: “Combined AFS and DYC control of four-wheel-independent-drive electric vehicles over CAN network with time-varying delays”, *IEEE Transactions on vehicular technology*, Vol. 63, No. 2, pp.2013, 591-602.
- [16] Standard ISO 3888-1:2018 - <https://www.iso.org/standard/67973.html>
- [17] Standard ISO 7401:2011 <https://www.iso.org/standard/54144.html> 1
- [18] UN Regulation No. 79 - <https://unece.org/transport/documents/2023/10/working-documents/un-regulation-no-79-revision-5>
- [19] Wang, R., Yin, G., Jin, X.: “Robust adaptive sliding mode control for nonlinear four-wheel steering autonomous Vehicles path tracking systems”, In 2016 IEEE 8th international power electronics and motion control conference (IPEMC-ECCE Asia), 2016, pp. 2999-3006.
- [20] Yim, S., Jo, Y.H.: “Integrated chassis control with AFS, ARS and ESC under lateral force constraint on AFS”, *JMST Advances*, Vol.1, 2019, pp.13-21.
- [21] Zhang, J., Wang, H., Ma, M., Yu, M., Yazdani, A., Chen, L.: “Active front steering-based electronic stability control for steer-by-wire vehicles via terminal sliding mode and extreme learning machine”, *IEEE Transactions on Vehicular Technology*, Vol. 69, No. 12, 2020, pp.14713-14726.
- [22] Zheng, B., Anwar, S.: "Yaw stability control of a steer-by-wire equipped vehicle via active front wheel steering." *Mechatronics*, Vol. 19, No. 6, 2009, pp.799-804.



TOWARDS AN ENERGY EFFICIENT OPERATION OF A
SUPERCAPACITOR ELECTRIC BUS

Miloš Maljković^{1*}, Ivan Blagojević², Branko Miličić³, Dragan Stamenković⁴

Received in July 2024

Accepted in August 2024

RESEARCH ARTICLE

ABSTRACT: Energy efficiency and reliable range prediction are important for all vehicles, especially for public transport vehicles such as a supercapacitor electric city buses. This research was conducted experimentally and has shown that most energy can be saved by adequate acceleration and coasting (i.e. deceleration without braking) between two stops. For this particular vehicle the most efficient acceleration is achieved when the driver presses the accelerator pedal for the full travel (100%) until reaching the required speed, then coast-down. Speed oscillation and unnecessary “hesitation” to fully depress the pedal during acceleration are highly undesirable. Coasting was found out to be most effective in energy recuperation, but other constant low intensity deceleration modes have also positive effects. Proposed driving style can lower the energy consumption by around 28%, extending the driving range and reducing the need for recharging. For the fleet of 4 buses, the total annual energy saving could amount to around 86.8 MWh.

KEY WORDS: *eco-driving, electric bus, energy efficiency, public transport, supercapacitor*

© 2024 Published by University of Kragujevac, Faculty of Engineering

¹ Miloš Maljković, University of Belgrade, Faculty of Mechanical Engineering, Kraljice Marije 16, 11120 Belgrade, Serbia, mmaljkovic@mas.bg.ac.rs, -, *Corresponding Author

² Ivan Blagojević, University of Belgrade, Faculty of Mechanical Engineering, Kraljice Marije 16, 11120 Belgrade, Serbia, iblagojevic@mas.bg.ac.rs, <https://orcid.org/0000-0002-5776-5990>

³ Branko Miličić, University of Belgrade, Faculty of Mechanical Engineering, Kraljice Marije 16, 11120 Belgrade, Serbia, bmilicic@mas.bg.ac.rs, <https://orcid.org/0000-0003-2297-524X>

⁴ Dragan Stamenković, University of Belgrade, Faculty of Mechanical Engineering, Kraljice Marije 16, 11120 Belgrade, Serbia, dstamenkovic@mas.bg.ac.rs, -

KA ENERGETSKI EFIKASNOM RADU SUPERKANDACITORSKOG ELEKTRIČNOG AUTOBUSA

REZIME: Energetska efikasnost i pouzdano predviđanje dometa su važni za sva vozila, posebno za vozila javnog prevoza kao što su superkondenzatorski električni gradski autobusi. Ovo istraživanje je sprovedeno eksperimentalno i pokazalo je da se većina energije može uštedeti adekvatnim ubrzanjem i kretanjem (tj. usporavanjem bez kočenja) između dva zaustavljanja. Za ovo konkretno vozilo najefikasnije ubrzanje se postiže kada vozač pritisne papučicu gasa za puni hod (100%) dok ne postigne potrebnu brzinu, a zatim spusti. Oscilacije brzine i nepotrebno „oklevanje“ da se pedala potpuno pritisne tokom ubrzanja su veoma nepoželjni. Utvrđeno je da je kočenje najefikasnije u rekuperaciji energije, ali i drugi režimi usporavanja konstantnog niskog intenziteta takođe imaju pozitivne efekte. Predloženi stil vožnje može smanjiti potrošnju energije za oko 28%, produžavajući domet vožnje i smanjujući potrebu za punjenjem. Za vozni park od 4 autobusa, ukupna godišnja ušteda energije mogla bi da iznosi oko 86,8 MWh.

KLJUČNE REČI: *eko-vožnja, električni autobus, energetska efikasnost, javni prevoz, superkondenzator*

TOWARDS AN ENERGY EFFICIENT OPERATION OF A SUPERCAPACITOR ELECTRIC BUS

Miloš Maljković, Ivan Blagojević, Branko Miličić, Dragan Stamenković

INTRODUCTION

Belgrade, the capital of Serbia has long tradition in using electric vehicles in public transport, with the first electric tram launched in 1892 and the first trolleybus in 1947. Recently, the city has been looking at new alternatives, hydrogen fuel cell, battery and supercapacitor as a source of energy for the propulsion of city buses. In 2015 the city acquired five supercapacitor Higer buses, with the aim to operate four full time on a specific route and keep one as a backup. Although initial experience was very positive, some problems were experienced with the driving range and the research presented here was focused on understanding the energy requirements for vehicle propulsion and looking at the ways of making the operation more energy efficient, primarily in extending the driving range, but also in saving the energy and reducing the associated costs.

In the last decade, a considerable experience has been accumulated with electric passenger vehicles using batteries. Much less information is available about commercial vehicles and even less on using supercapacitors as energy source.

Typically, the advantages of electric vehicles in urban driving conditions are not only related to their zero emission, but to the fact that they are more energy efficient due to the lower speeds and more frequent recuperation of electrical energy [1]. There is no doubt that in urban driving the range is not often a critical issue, due to low speeds and inevitably shorter distances covered. The advantages of regenerative braking cannot materialise when the battery temperature and/or the state of charge are high [2]. The authors of [3] concluded that increased vehicle mass and payload have not so detrimental effect on energy consumption as electric propulsion is more efficient than IC engines at higher loads and a “by-product” of higher mass is an increase of the recuperated energy. Results of the simulation conducted in [4] showed that the impact of the passenger load in an electric bus is more pronounced in urban driving conditions, characterised by lower average speed and higher number of stops. Furthermore, the impact is pronounced when the driver is driving more aggressively.

The results of the simulations showed that coasting with no energy recuperation is always more efficient than braking with energy recuperation, even in case it could be 100% energy efficient [5]. Furthermore, aggressive driving can increase energy consumption by around 30% compared to the economical driving style [6]. Even the most efficient energy recuperation is no match for good driving.

Similarly to the research conducted in [6], research [7] concludes, by performing simulation in MATLAB/Simulink, based on a modified NEDC test cycle, that economical driving leads to a 32% longer range compared to aggressive driving, for a battery electric vehicle with energy recuperation.

There are three main factors affecting the energy efficiency of electric vehicles (not related to the vehicle design) – ambient temperature, traffic conditions and driving style [8]. Research [9] showed that impact of ambient temperature on electric bus range can be significant (increased usage of heating or air conditioning system), while the usage of heating system during winter has the most negative impact on vehicle range. The fact that electric vehicles are more economical in urban driving conditions, primarily due to the

frequent braking with energy recuperation, is advantageous for public transportation. Research [10] comes to the similar conclusion, stating that drivers should avoid excessive speeds, accelerate moderately, drive in an anticipatory manner, minimise the auxiliary loads, and use advantages of energy recuperation during braking and coasting as much as possible. Likewise, research [11] investigating energy-saving driving style for electric bus, recommends vehicle speed interval and acceleration modes. It was shown that, for the considered electric bus, speed range from 30 to 35 km/h gives the best results in terms of energy efficiency, but the recommended speed range is extended to 40 km/h to follow the traffic flow. It suggested that the curve that represents speed versus time during acceleration should have a convex shape in order to minimise energy consumption. Developed energy-saving driving strategy reduced energy consumption during short sections of acceleration between 12.3% and 18.7%, while about 2.5% of energy was saved on entire electric bus route. Another research developed a model for determination of a specific driving style from collected data during real-world driving. It was shown that the model can successfully recognise different driving styles [12].

1 AIMS AND OBJECTIVES OF THE RESEARCH

The aim of this research is to evaluate an electric supercapacitor bus and develop the most energy efficient driving style. This research concentrates particularly on:

- Evaluating the supercapacitor electric bus and operating route characteristics.
- Defining the electric bus operating parameters to be recorded and the method of their measurement.
- Defining the driving cycles and vehicle payload for trial tests and giving the appropriate recommendations for energy efficient electric bus operation.
- Implementation and verification of a driving style in passenger service for the most energy efficient operation on the specific route.

2 THE VEHICLE

Higer KLQ6125GEV3 bus is an electric vehicle that uses supercapacitors as an energy source and two inter-connected motors for propulsion. Maximum permissible mass of the vehicle is 19,000 kg, while maximum passenger capacity is 90. The vehicle can reach maximum speed of 70 km/h and is configured as a 2 axle single deck bus with 3 doors. It is propelled by two permanently coupled Siemens 1PV5135-4WS28 electric motors [13], having maximum power of 90 kW and torque of 360 Nm each. Motor supply and control is provided via Siemens DC-DC/IGBT Mono inverter drive, drawing current from 20 kWh Aowei supercapacitor.

Supercapacitor charging can be accomplished by connecting to a standard electric grid as well by a pantograph, while the vehicle is at a bus stop or in a garage equipped with a fast charger. There are two 150 kW fast chargers located on each end of service route, where the electric bus charging is accomplished by a pantograph.

3 BUS OPERATING ROUTE

The bus operates on a city route (divided in directions A and B for the purpose of presentation in this research), characterised by high traffic frequency, numerous junctions and traffic lights. The route is 7 km long in direction A and 8 km in direction B. There are

16 bus stops and 26 intersections regulated by traffic lights in direction A and 17 bus stops and 29 intersections regulated by traffic lights in direction B. Bus dedicated lane is present only on a smaller part of the route. The change in elevation is about 60 meters, between starting and finishing point of the route.

As mentioned earlier on, the traffic is very dense on the operating route. To illustrate that, a typical speed profile in service conditions (with passengers) in direction A of the operating route is shown in Figure 1. The speed of 40 km/h is drastically exceeded only on the straight part of the route, in the bus dedicated lane and with no stations or traffic lights.

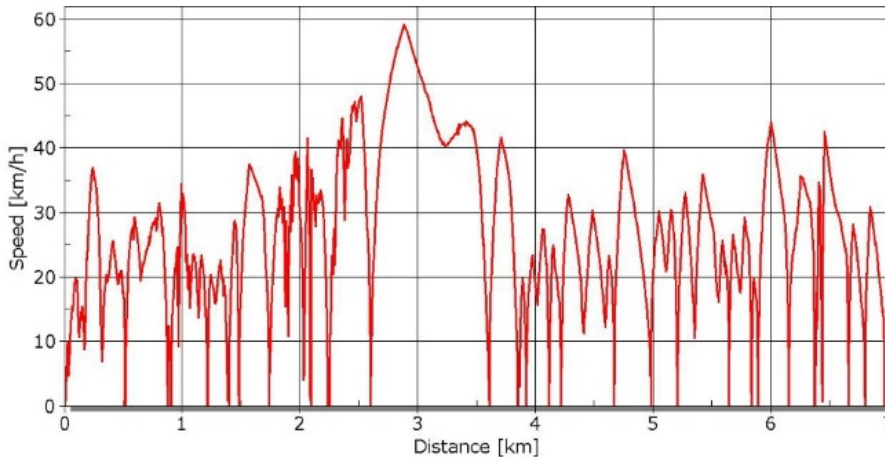


Figure 1 Typical speed profile in passenger service for direction A

4 INSTRUMENTATION USED AND BASIC DRIVING MODES

4.1 Instrumentation used

Bus operating parameters were monitored and recorded both in test trials and passenger service.

These included:

- Vehicle speed (v) [km/h].
- Vehicle position on the route (and driving direction, A or B).
- Accelerator pedal position (APP) [%].
- Brake pedal position (BPP) [%].
- Supercapacitor current (I_{uc} and I_{recup}) [A].
- Supercapacitor voltage (U_{uc}) [V].
- Supercapacitor state of charge (SoC) [%].
- Electric motor torque (T , T_{recup}) [Nm] and speed (ω) [min^{-1}].
- Ambient temperature [$^{\circ}\text{C}$].

Some parameters were measured directly (e.g. supercapacitor voltage and current), with the values of others obtained through CAN bus. Some cross-checks were also performed. For

example, in order to check the accuracy of vehicle speed acquired through CAN bus, Racelogic speed sensor was used. By comparing the data, it was concluded that CAN bus values are of a lower accuracy. Data acquisition was done with the help of HBM QuantumX, while sampling rate was set to 50 Hz. During testing, heating and air conditioning systems were turned off as their power is considerable (26 and 32 kW respectively), which would make final results difficult to correctly interpret.

4.2 Vehicle loading and test drivers

For this particular bus and the route studied, an average in-service payload was 50% of the maximum payload, which is identical to the value defined by UITP PROJECT “SORT”, used to determine and compare energy consumption of different buses [14]. Consequently, such a payload was used in all tests, which was achieved by evenly distributed bags of sand with a total mass of 3,060 kg, corresponding to 45 passengers of 68 kg each. Furthermore, there were also seven examiners in the vehicle, adding 490 kg and bringing the total loading to 3,550 kg and the mass of the bus to 16,100 kg.

All driving during testing was conducted by 2 experienced bus drivers, each having more than 10 years of experience with diesel-powered buses and about 4 years with this electric bus operating on this very route. Consequently, when the reference was made to “usual driving” that is how they used to normally drive prior to this research and the establishment of a more energy efficient, economical driving style.

4.3 Acceleration modes

Considering that vehicle speed can rarely exceed 40 km/h, all acceleration trials were performed up to that speed, for both constant and variable accelerator pedal positions. To overcome the subjectivity problem, a guidance for the driver was implemented. Several acceleration curves were established, each representing speed versus time spent to reach the same maximum speed value, defined by equation (1), following the research [11]:

$$v = v_0 + (v_f - v_0) \left(\frac{t - t_0}{t_f - t_0} \right)^\beta \quad (1)$$

where v is vehicle speed, t is time, the subscripts 0 and f relate to: 0 – initial; f – final, β is a parameter defining the intensity of acceleration, with typical values between 0.2 and 4.0.

The driver was following a curve with the prescribed acceleration parameter β displayed on a tablet computer mounted in front of him (Figure 2). Accelerator and brake pedal position and speed values were also shown. Maximal acceleration achieved during testing was slightly below 1.2 m/s^2 , which is acceptable from the aspects of traffic safety and passenger comfort. This was within a range of comfortable longitudinal accelerations and decelerations from 0.9 to 1.47 m/s^2 [15]. During the tests, it was found that curves defined by $\beta < 0.7$ could not be achieved due to the limits of powertrain dynamic characteristics of the bus. Furthermore, it was concluded that when the β coefficient is equal or greater than 2, the bus needed at least 10 s to reach the speed of 10 km/h, which is considered to be too slow.

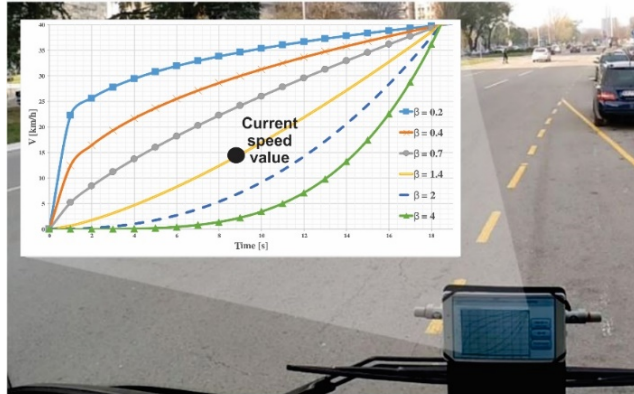


Figure 2 Target acceleration curves and tablet computer installed in the bus Deceleration modes

Trials with different deceleration rates were performed in order to determine the most energy efficient driving mode and the amount of recuperated energy for different brake pedal positions and vehicle speeds. The bus is set up in such a way that regenerative braking is provided as soon as the driver releases acceleration pedal, even when not pressing the brake pedal. This “free rolling” (coasting) mode provides gentle deceleration. When the driver presses brake pedal, in the first portion regenerative braking is gradually increased, and when pressing further friction braking is being activated.

4.4 Determination of consumed and recuperated energy

Power (P) and energy (E) during acceleration and deceleration are governed by the well-known relationships (Equation (2)):

$$P = U_{uc} I_{uc} \quad (2)$$

where U_{uc} and I_{uc} represent supercapacitor voltage and current, respectively.

Consequently, the energy equals (Equation (3)):

$$E = \int_0^t P dt \quad (3)$$

The consumed energy can be calculated from the measured current and voltage supplied from the supercapacitor through the inverter to the electric motors during acceleration. The recuperated energy can be calculated from the measured current and voltage recharging the supercapacitor, during coasting and braking periods.

5 VEHICLE TEST TRIALS

Unfortunately, it was not possible to experimentally study acceleration and deceleration driving modes on a dedicated test track, hence a suitable street section was used, having wide, smooth and horizontal surfaces, with little traffic and availability of the fast charger. The route consisted of 3 distinctive sections named “P”, “M” and “B” for more convenient presentation of the results. The mean altitude is around 80 m and various driving cycles

were completed consecutively on each of the sections with several repetitions. The ambient temperature during tests was between 12°C and 16°C and there was no precipitation during tests (the road was dry).

5.1 Acceleration and deceleration cycles

Starting from the beginning of section “P” driving cycles were conducted, which consisted of an acceleration, followed by a deceleration, for each section “P”, “M” and “B”, until a full circle (“lap”) was completed. After that, at the end of section “B”, the supercapacitor was recharged using fast charger. That was to ensure equal state of charge for all tests. In total, over 100 driving cycles were completed, varying acceleration and deceleration parameters, but repeating the same cycles multiple times.

The results presented here will relate to accelerating to the speed of 40 km/h, for different acceleration rates, defined by the values of β coefficient (see Figure 2). The driver was achieving this by controlling the accelerator pedal position APP [%]. As soon as the speed was reached and stabilized, a chosen deceleration mode followed. The deceleration was also conducted with different intensity BPP [%], from gentle coasting, prolonged light braking, short heavy braking and various combinations. The goal was to determine which deceleration mode leads to the most efficient energy recuperation, still ensuring smooth and safe driving.

The procedure used and the results obtained will be explained here on an example, test cycle 8/M, conducted on section “M”. Figure 3 shows the test cycle 8/M. The driver is pressing the accelerator pedal to around 50% (APP) from the very start, but hesitantly increasing and even slightly decreasing the pressure on the pedal until 15 seconds into the cycle, when he depressed the pedal fully (APP = 100%). Vehicle speed (v) is increasing relatively linearly to 40 km/h at about 22 seconds into the cycle. At this point the driver is releasing the accelerator pedal (APP dropping to 0). The total (cumulative) energy E consumed during acceleration is increasing relatively gently for the first 10 seconds, with the increase at a higher rate in later stages of acceleration. As soon as the desired speed of 40 km/h is reached and the driver releases accelerator pedal, the total energy consumed reduces due to recuperation which start instantly when the acceleration pedal is released.

Approximately one second after releasing the accelerator pedal, the driver presses the brake pedal relatively gently to about BPP = 20% over around 3 seconds and then keeps it in that position. The recuperation current I_{recup} rises sharply to around - 140 A (negative value), holding at that value for several seconds and dropping to 0 when the vehicle comes to a stop. The recuperation torque T_{recup} increases to about - 60 Nm, staying approximately constant throughout the deceleration period. The total energy consumed drops throughout the braking period, though the drop is modest in the last 3 seconds.

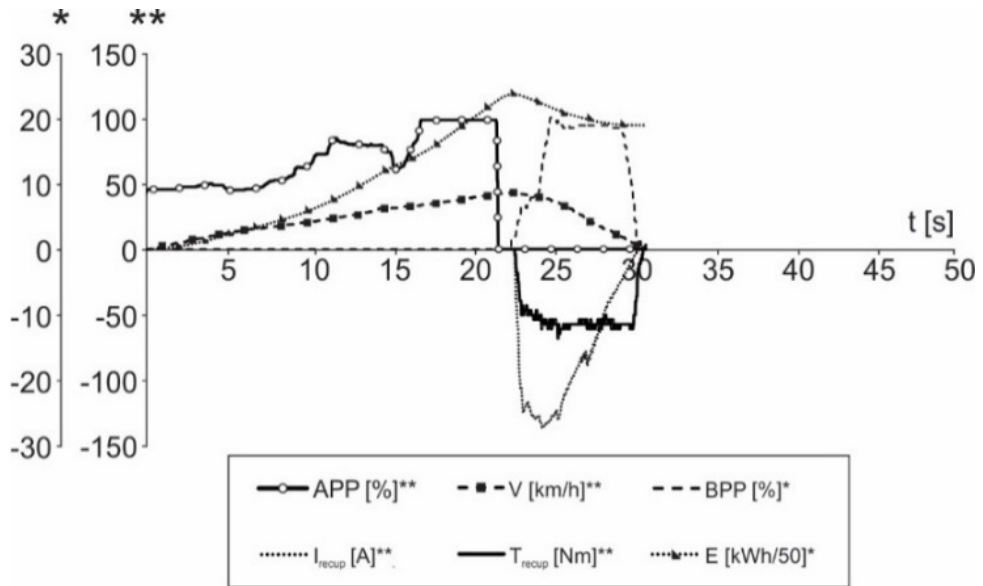


Figure 3 Test cycle 8/M

The actual values obtained for test 8/M are included in Table 1, together with test results for 5 more characteristic driving cycles which have been chosen for the comparison.

The energy efficiency of each driving cycle should be evaluated based on energy consumed during acceleration - acceleration rates were predefined (as said before), while decelerations were performed randomly and covered variety of scenarios (coasting, heavy and light braking, combined coasting and braking, etc.). Consequently, each acceleration can be combined with any deceleration scenario and should be regarded separately.

Table 1 Drive cycle results

Cycle number/section	Energy consumed to reach 40 km/h [kWh]	Accel. par. β [-]	Energy recuperated during braking [kWh]	BPP[%]	Cycletime [s]	Supercap. voltage: start / end of cycle [V]
8/M	0.399	≈ 0.85	0.095	≈ 20	30	554 / 533
26/M	0.381	≈ 0.7	0.045	≈ 2	45	542 / 523
9/B	0.389	≈ 0.85	0.094	≈ 18	32	546 / 526
27/B	0.367	≈ 0.7	0.139	≈ 7	36	535 / 516
13/P	0.410	var.	0.093	≈ 4	42	576 / 560
25/P	0.376	≈ 0.7	0.094	≈ 17	28	545 / 527

Starting with cycle 8/M, Table 1 shows that the energy consumed to reach 40 km/h was 0.399 kWh, with the driver following acceleration parameter $\beta \approx 0.85$. Only 0.095 kWh was recuperated during braking which was conducted keeping the brake pedal relatively steady at approximately BPP = 20%. Supercapacitor voltage remains high, dropping only by 21V, from 554 to 533 V at the end of the cycle.

The analysis of other cycles (presented in Table 1) leads to some interesting conclusions:

- overall, the least energy during acceleration was consumed with $\beta \approx 0.7$, which corresponds to the maximum displacement of accelerator pedal (APP = 100%). The

cycles with $\beta \approx 0.85$ were least energy efficient. However, in reality by far the worst possible manner of acceleration, from the consumed energy point of view, is oscillating (variable) increase/decrease in accelerator pedal displacement.

- when decelerating, the most energy was recuperated in the cycle 27/B - 0.139 kWh. However, it should be pointed out that when operating a vehicle, the energy used over a distance should be minimised. From this point of view, coasting is the most energy efficient method. Practically, the driver should accelerate “hard” and then release the accelerator without applying the brake pedal, when road and operating conditions permits. City buses have to stop regularly at bus stops, but often other traffic conditions (traffic lights, traffic jams etc.) also require more frequent stopping.
- the manufacturer of the bus recommends that the brake pedal should be depressed not further than 28% of the full displacement, which ensures best energy recuperation of the electric motor acting as a generator. During testing, for a partly loaded bus (as said earlier on) brake pedal position (BPP) did not exceed 20% - even this level of brake pedal position lead to a deceleration exceeding 2 m/s^2 , which is becoming uncomfortable and even unsafe for standing passengers.

5.2 Energy efficiency maps

Research [16] established energy efficiency maps for this vehicle powertrain by testing the motor-inverter combination on a powertrain dynamometer. The contour lines (Figure 4 and Figure 5) indicate an overall efficiency between 0.5 to 0.92. Following vast amount of tests and processed data it was necessary to be selective in presenting the most interesting findings, which in this case relates to the driving cycles performed in sections “B” and “P”. Acceleration modes are particularly important in determining powertrain efficiency, so this driving condition was used here. The torque versus engine speed points were entered into a map for section “B” in Figure 4 and for section “P” in Figure 5.

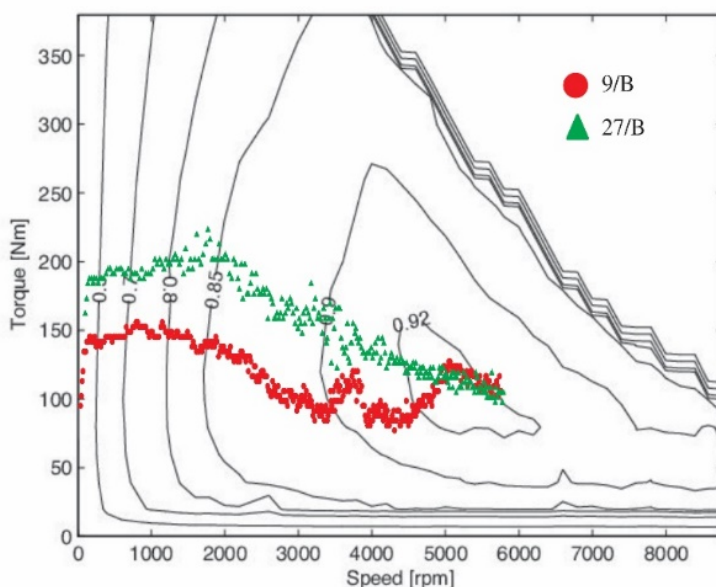


Figure 4 Energy efficiency map for driving cycles on section “B”

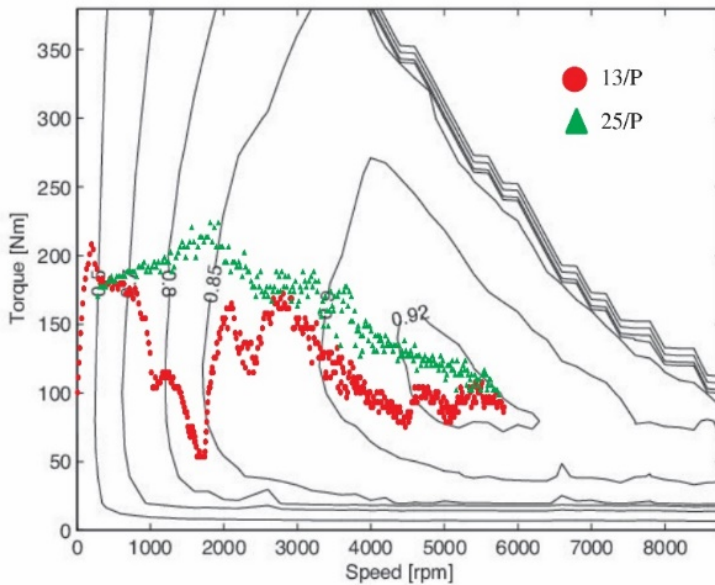


Figure 5 Energy efficiency map for driving cycles on section “P”

With intense acceleration (see Table 1) the path made of torque versus engine speed points follows the shortest possible distance to the area of highest energy efficiency (0.92) and the higher number of points will concentrate in this area for cycles 27/B and 25/P, as shown in Figures 4 and 5. In contrast, cycles 9/B and 13/P, which features oscillating displacement of accelerator pedal, show lower efficiencies on Figures 4 and 5, which is more pronounced in cycle 13/P.

6 IMPLEMENTATION IN OPTIMISING THE DRIVING ON THE BUS ROUTE

Following the measurements and analyses presented, a strategy was developed to implement the findings, in order to achieve more energy efficient bus operation. Acceleration and deceleration habits of the drivers needed to be improved. Consequently, the results were obtained for the newly developed “economical” driving alongside the “usual” driving prior to the implementation of the new techniques and the corresponding driver training. All driving has been conducted in the normal passenger service, in the same time of the day and similar vehicle loading, traffic and climatic conditions.

A selection of the results obtained are presented in Table 2, concentrating specifically on:

- Energy aspects (consumed, recuperated and net energy used).
- Total travel time and the time the vehicle was in motion.
- The average speed when the vehicle was in motion.
- Braking portion in total route time.
- Coasting portion in total route time and distance.

Table 2 Comparison of economical and usual driving styles

Parameter	Route direction and driving style			
	A to B		B to A	
	Usual	Economical	Usual	Economical
Consumed energy [kWh]	11.766	9.559	16.907	12.944
Recuperated energy [kWh]	2.890	2.789	2.453	2.258
Net energy used [kWh]	8.876	6.770	14.454	10.736
Difference [kWh]	-	- 2.106	-	- 3.718
Relative difference [%]	-	- 26.9	-	- 29.5
Trip duration [min:sec]	27:30	30:23	35:48	34:20
Time difference [min:sec]	-	+ 2:53	-	- 1:28
Relative time difference [%]	-	+ 9.5	-	- 4.3
Time in motion [min:sec]	17:37	20:17	20:37	24:52
Braking time portion [%]	17.4	11.4	13.5	6.3
Coasting time portion [%]	12.4	27.4	9.3	32.2
Coasting distance as a percentage of route [%]	21.5	49.7	17.9	50.0
Average speed [km/h] (when in motion)	24.17	20.67	24.41	19.96

By analysing the data presented in Table 2, some fundamental conclusions can be drawn:

- When driving economically, the average saving in used energy is around 28% (26.9% in direction A to B and 29.5% in opposite direction).
- The above reduction is the result of lower consumed energy, with the recuperated energy being actually lower in economical driving (by 3.5% A to B and 8.3% B to A).
- Economical driving leads to about 10% longer average driving times when travelling from A to B, but 4% shorter when driving in opposite direction. Generally, it can be concluded that an overall average increase in driving time is around 5%.
- Time that the electric bus spends in motion is longer for around 15% while driving economically. At the same time, braking time portion is lower for around 6.5% on average, while the time share of coasting is higher for 15% to 22.9%.
- It can be seen that while driving economically, the electric bus can cover around 50% of the route distance by coasting, compared to around 20% while driving as usual.
- The average speed is decreased for around 18% while driving economically, but without a significant impact on a trip duration.

The fundamental difference between the usual and newly developed economical driving style can be best explained by a speed vs. time graph shown in Figure 6. Even without the need to change the acceleration or deceleration rates or vehicle speed, the drivers had a habit of varying the speed (usual driving on Figure 6) which led to unnecessary increase in energy usage. Brake pedal should be used only gently, but again constantly (steeper speed decline at around 49 seconds in Figure 6) bringing the vehicle to a stop, with friction brakes applied only at the very end. Obviously, this is somewhat simplified scenario, but essentially shows how the driving needs to be improved.

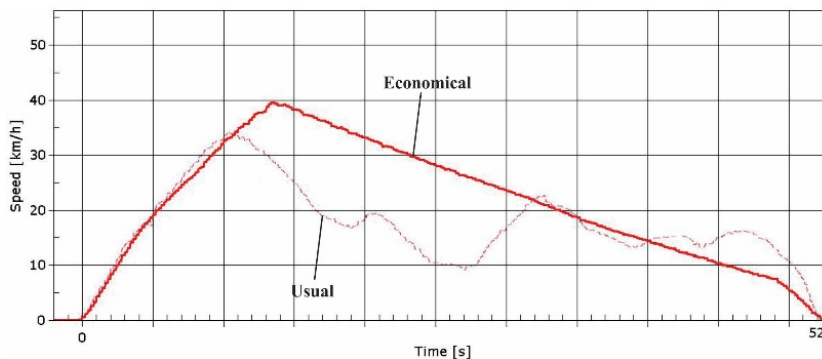


Figure 6 Speed profile between two stops recorded for “economical” and “usual” driving style in passenger service conditions

7 CONCLUSIONS

Indeed, for any propulsion system, energy efficient driving assumes diligent traffic observation, timely anticipation and use of vehicle momentum, avoiding unnecessary acceleration and braking whenever possible. However, the research presented here clearly demonstrates the most efficient acceleration and deceleration modes, followed by driver training to develop an appropriate driving style, different to the one they got used to when driving diesel powered buses.

In particular, the research showed that acceleration modes (defined by accelerator pedal position) have a major impact on energy efficiency of the electric bus. For this particular vehicle the simplest and most energy efficient manner of acceleration is by pressing fully the acceleration pedal. This is by no means causing excessive acceleration or any discomfort or danger to the passengers.

The vehicle needs to be brought to a required speed with constant acceleration (preferably APP=100%) and let to coast-down to a stop, at the next bus stop or traffic light. Brake pedal should be only used when necessary, depressed to a certain position and kept there, ensuring constant deceleration. Such driving is not only more economical, but is also safer for all road users and in particular for standing passengers. It is more comfortable too.

Proposed driving style lowered the net energy used on this route for 26.9% and 29.5%, depending on the direction (A or B). This reduction is practically between 2.1 and 3.7 kWh per direction, which represents considerable total saving of 5.8 kWh. Consequently, it is possible for the electric bus to complete the entire route (in both directions) without charging, as with economical driving the net energy used is 17.5 kWh and the supercapacitor capacity 20 kWh.

Charging at the end of the route will depend on other parameters too, but such a saving is more than welcomed in urban transport when the vehicle may need to make an immediate return, without waiting at the end of the route (turning point). Even if needed, the recharge can be shorter. When driven as recommended, tested electric bus can save about 65 kWh per day. For the fleet of 4 electric buses operating on this route, total saving is about 260 kWh per day, which accounts to about 86.8 MWh per year. And this is one of the “lighter” routes in Belgrade bus public transport.

This research and presentation focused on energy usage for propulsion of the bus. The bus uses around 10 kWh per direction or around 20 kWh for the entire round-trip route, which

actually equals the capacity of the supercapacitor. However, HVAC systems can present heavier load on the energy demand. The heating system is rated at 26 kW and air conditioning (A/C) at 32 kW. Obviously, both systems will not be used simultaneously (although this is possible) and not be used at full power all the time. If any of the systems is used 50% of the time in one direction, with travel times of about 30 minutes, that amounts to about 8 kWh, which is approximately equal to the energy used for bus propulsion (also in one direction). Advanced control in using these systems and driver notification would need to be developed. This particularly relates to the use of A/C for heating which can be more energy efficient than using the resistor heaters in suitable atmospheric conditions.

Furthermore, more advanced driver information system would be beneficial, in terms of energy status, energy usage, route traffic, timetable and perceived passenger numbers. Driver training and suitable incentives and awards for energy efficient driving and punctuality would need to be also established. Looking to the future, this opens a unique line of potential research looking into how traffic variables (road lengths, traffic lights and congestion) can be taken into account for the provision of driver instructions. These recommendations could be applicable for different road sections, such as those between two points (bus stops, traffic lights) and distance to the vehicle in front, allowing for informed, dynamic speed control.

REFERENCES

- [1] Wu, X., Freese, D., Cabrera, A., Kitch, W.A.: "Electric Vehicle's Energy Consumption Measurement and Estimation", *Transportation Research Part D: Transport and Environment*, 34 (2015), pp. 52-67,
- [2] Varocky, B.J.: "Benchmarking of Regenerative Braking for a Fully Electric Car", Report No. D&C 2011.002, TNO Automotive, Helmond & Eindhoven University of Technology, Netherlands, 2011,
- [3] Fiori, C., Ahn, K., Rakha, H.A.: "Power-Based Electric Vehicle Energy Consumption Model: Model Development and Validation", *Applied Energy*, 168 (2016), pp. 257-268,
- [4] Lajunen, A., Tammi, K.: "Evaluation of Energy Consumption and Carbon Dioxide Emissions of Electric City Buses, Electric Commercial Vehicles (ECV): Final Report", VTT Technology, Finland, 2019,
- [5] Mruzek, M., Gajdáč, I., Kučera, L., Barta, D.: "Analysis of parameters influencing electric vehicle range", *Procedia engineering*, 134 (2016), pp. 165-174,
- [6] Bingham, C., Walsh, C., Carroll, S.: "Impact of driving characteristics on electric vehicle energy consumption and range", *IET Intelligent Transport Systems*, 6 (2012), 1, pp. 29-35,
- [7] Alvarez, R., López, A., De la Torre, N.: "Evaluating the effect of a driver's behavior on the range of a battery electric vehicle", *Proceedings of the Institution of Mechanical Engineers, Part D: Journal of Automobile Engineering*, 229 (2015), 10, pp. 1379-1391,
- [8] Maljković, M., Stamenković, D., Blagojević, I. and Popović, V.: "The Analysis of Available Data on Energy Efficiency of Electric Vehicles to be Used for Eco-Driving Project Development", *Science and Technique*, 18 (2019), 6, pp. 504-508,
- [9] Mišanović, S., Glišović, J., Blagojević, I., Taranović, D.: "Influencing factors on electricity consumption of electric bus in real operating conditions", *Thermal Science*, 27 (2023), 1B, pp. 767-784,

- [10] Neumann, I., Franke, T., Cocron, P., Bühler, F., Krems, F.J.: “Eco-Driving Strategies in Battery Electric Vehicle Use - How Do Drivers Adapt Over Time?”, *IET Intelligent Transport Systems*, 9 (2015), 7, pp. 746-753,
- [11] Zhang, Y., Yuan, W., Fu, R., Wang, C.: “Design of an Energy-saving Driving Strategy for Electric Buses”, *IEEE Access*, 7 (2019), pp. 157693-157706,
- [12] Geqi, Q., Jianping, W., Yang, Z., Yiman, D., Yuhan, J., Hounsell, N., Stanton, N.: “Recognizing driving styles based on topic models, *Transportation Research Part D: Transport and Environment*”, 66 (2019), pp. 13-22,
- [13] Higer KLQ6125GEV3 technical documentation, Higer Bus Company Limited. (Unpublished internal company document), 2016,
- [14] UITP PROJECT “SORT”. Standardised on-road Test cycles. International Association of Public Transport, 2014,
- [15] Il, B., Jaeyoung, M., Jeongseok, S.: “Toward a Comfortable Driving Experience for a Self-Driving Shuttle Bus”, *Electronics*, 8 (2019), pp. 1-13,
- [16] Hentunen, A., Suomela, J., Leivo, A., Liukkonen, M., Sainio, P.: “Full-Scale Hardware-In-The-Loop Verification environment for Heavy-Duty Hybrid Electric Vehicles”, *World Electric Vehicle Journal*, 4 (2010), pp. 119-127.

MVM – International Journal for Vehicle Mechanics, Engines and Transportation Systems
NOTIFICATION TO AUTHORS

The Journal MVM publishes original papers which have not been previously published in other journals. This is responsibility of the author. The authors agree that the copyright for their article is transferred to the publisher when the article is accepted for publication.

The language of the Journal is English.

Journal *Mobility & Vehicles Mechanics* is at the SSCI list.

All submitted manuscripts will be reviewed. Entire correspondence will be performed with the first-named author.

Authors will be notified of acceptance of their manuscripts, if their manuscripts are adopted.

INSTRUCTIONS TO AUTHORS AS REGARDS THE TECHNICAL ARRANGEMENTS OF MANUSCRIPTS:

Abstract is a separate Word document, “*First author family name_ABSTRACT.doc*”. Native authors should write the abstract in both languages (Serbian and English). The abstracts of foreign authors will be translated in Serbian.

This document should include the following: 1) author’s name, affiliation and title, the first named author’s address and e-mail – for correspondence, 2) working title of the paper, 3) abstract containing no more than 100 words, 4) abstract containing no more than 5 key words.

The manuscript is the separate file, „*First author family name_Paper.doc*“ which includes appendices and figures involved within the text. At the end of the paper, a reference list and eventual acknowledgements should be given. References to published literature should be quoted in the text brackets and grouped together at the end of the paper in numerical order.

Paper size: Max 16 pages of B5 format, excluding abstract

Text processor: Microsoft Word

Margins: left/right: mirror margin, inside: 2.5 cm, outside: 2 cm, top: 2.5 cm, bottom: 2 cm

Font: Times New Roman, 10 pt

Paper title: Uppercase, bold, 11 pt

Chapter title: Uppercase, bold, 10 pt

Subchapter title: Lowercase, bold, 10 pt

Table and chart width: max 125 mm

Figure and table title: Figure _ (Table _): Times New Roman, italic 10 pt

Manuscript submission: application should be sent to the following e-mail:

mvm@kg.ac.rs ; lukicj@kg.ac.rs

or posted to address of the Journal:

University of Kragujevac – Faculty of Engineering

International Journal M V M

Sestre Janjić 6, 34000 Kragujevac, Serbia

The Journal editorial board will send to the first-named author a copy of the Journal offprint.

OBAVEŠTENJE AUTORIMA

Časopis MVM objavljuje originalne radove koji nisu prethodno objavljivani u drugim časopisima, što je odgovornost autora. Za rad koji je prihvaćen za štampu, prava umnožavanja pripadaju izdavaču.

Časopis se izdaje na engleskom jeziku.

Časopis *Mobility & Vehicles Mechanics* se nalazi na SSCI listi.

Svi prispeli radovi se recenziraju. Sva komunikacija se obavlja sa prvim autorom.

UPUTSTVO AUTORIMA ZA TEHNIČKU PRIPREMU RADOVA

Rezime je poseban Word dokument, „*First author family name_ABSTRACT.doc*“. Za domaće autore je dvojezičan (srpski i engleski). Inostranim autorima rezime se prevodi na srpski jezik. Ovaj dokument treba da sadrži: 1) ime autora, zanimanje i zvanje, adresu prvog autora preko koje se obavlja sva potrebna korespondencija; 2) naslov rada; 3) kratak sažetak, do 100 reči, 4) do 5 ključnih reči.

Rad je poseban fajl, „*First author family name_Paper.doc*“ koji sadrži priloge i slike uključene u tekst. Na kraju rada nalazi se spisak literature i eventualno zahvalnost. Numeraciju korišćenih referenci treba navesti u srednjim zagradama i grupisati ih na kraju rada po rastućem redosledu.

Dužina rada: Najviše 16 stranica B5 formata, ne uključujući rezime

Tekst procesor: Microsoft Word

Margine: levo/desno: mirror margine; unurašnja: 2.5 cm; spoljna: 2 cm, gore: 2.5 cm, dole: 2 cm

Font: Times New Roman, 10 pt

Naslov rada: Velika slova, bold, 11 pt

Naslov poglavlja: Velika slova, bold, 10 pt

Naslov potpoglavlja: Mala slova, bold, 10 pt

Širina tabela, dijagrama: max 125 mm

Nazivi slika, tabela: Figure __ (Table __): Times New Roman, italic 10 pt

Dostavljanje rada elektronski na E-mail: mvm@kg.ac.rs ; lukicj@kg.ac.rs

ili poštom na adresu Časopisa
Redakcija časopisa M V M
Fakultet inženjerskih nauka
Sestre Janjić 6, 34000 Kragujevac, Srbija

Po objavljivanju rada, Redakcija časopisa šalje prvom autoru jedan primerak časopisa.

MVM Editorial Board
University of Kragujevac
Faculty of Engineering
Sestre Janjić 6, 34000 Kragujevac, Serbia
Tel.: +381/34/335990; Fax: + 381/34/333192
www.mvm.fink.rs